ANALYSING THE POSTERIOR PREDICTIVE CAPABILITY OF LANDSLIDE SUSCEPTIBILITY MAPS

TANUJ PAREEK
August, 2022

SUPERVISORS:
Prof. Dr. Cees J. van Westen
Assistant Prof. Dr. Luigi Lombardo

ANALYSING THE POSTERIOR PREDICTIVE CAPABILITY LANDSLIDE SUSCEPTIBILITY MAPS

TANUJ PAREEK
Enschede, The Netherlands, August, 2022

Thesis submitted to the Faculty of Geo-Information Science and Earth Observation of the University of Twente in partial fulfilment of the requirements for the degree of Master of Science in Geo-information Science and Earth Observation.
Specialization: Natural Hazards and Disaster Risk Reduction

SUPERVISORS:
Prof. Dr. Cees J. van Westen
Assistant Prof. Dr. Luigi Lombardo

THESIS ASSESSMENT BOARD:
Prof. Dr. V.G. Jetten (Chair)
Dr. A.C. Seijmonsbergen, University of Amsterdam (External examiner)
Prof. Dr. Cees J. van Westen
Assistant Prof. Dr. Luigi Lombardo

ADVISORS:
Dr. Muhammad Aufaristama

ABSTRACT

Landslide susceptibility maps serve as the basis for hazard and risk assessment, as well as risk-informed landuse planning at various spatial scales. These maps are intended for a variety of purposes, including infrastructure planning and restrictive landuse zoning, by potential end-users such as spatial decision-makers and urban planners. These applications require accurate map information and specific map legends, as decisions based on these maps have the potential to cost lives and cause infrastructure damage. The usability of the maps depends on whether they provide the required information and whether that information is accurate enough to be utilised for the intended purpose. Therefore, assessing the usability and predictive accuracy of landslide susceptibility maps is of paramount importance. Typically, the accuracy of the maps is evaluated using the same landslide inventory that was used to create the map, which does not actually test the predictive ability of the maps in future situations. To address these issues, we evaluated three landslide susceptibility maps for an area in Kerala (India) that were generated in the past years by utilising a new landslide inventory created after the maps were generated. This research presents a method for evaluating classified maps intended for use in decision-making and planning. We assessed (1) the usability of the landslide susceptibility maps by conducting a literature analysis and conducting interviews with the map producers and users in Kerala. The assessment indicated the requirements for a map to be utilised for the intended purpose. We (2) generated a robust (new) landslide inventory using a MsaU-Net deep learning (DL) model, which was (3) used to evaluate the landslide susceptibility maps generated in the past years. We designed a method for evaluating classified maps, with a focus on evaluating and comparing in different scenarios. A major accomplishment of the research was to generate Unique Conditions Units (UCUs), which were utilised to evaluate classified maps. We propose that these units can also be used to generate landslide susceptibility maps and provide a reasonable topographic representation. Our study has huge significance, particularly in (1) investigating the usability of landslide susceptibility maps and attempting to direct the focus of map producers toward more user-oriented landslide susceptibility mapping, (2) generating landslide inventory of small-sized landslides utilizing open source datasets, (3) designing a method to assess the classified landslide susceptibility maps in multiple evaluation scenarios, and (4) providing a method to generate Unique Conditions Units (UCUs) for evaluation as well as mapping purposes, (5) highlighting the challenges of analysing the importance of landuse and landcover changes on the validity of the landslide susceptibility maps. We conclude that, although the volume of literature on the best methods for landslide susceptibility assessment is enormous, there is an urgent need to focus more on the forward predictive capability and usability by end-users.

Keywords: Map purpose, Map usability, Map reliability, Landslide detection, Predictive capability evaluation, Unique Condition Units, Land use land cover changes

ACKNOWLEDGEMENTS

ITC has been a roller coaster ride, but it was a worthwhile adventure! ITC's master's program had a profound effect on my personality, intelligence, and capacity for new learning. I would like to thank the Faculty of ITC, the University of Twente, for this opportunity and for providing me with the ITC excellence scholarship, which allowed me to embark on this journey.

My heartfelt thanks to Prof. Dr Cees van Westen and Asst. Prof. Luigi Lombardo for their unwavering support, advice, feedback, and thought-provoking questions that shaped this research. I would like to thank them for instilling critical thinking and logical argumentation skills in me. Without their consistent cooperation and encouragement, I would have lost track of my research. I thank my thesis advisor, Dr Muhammad Aufaristama, for his helpful suggestions and advice throughout the process. My sincere thanks to Asst. Prof. Dr Hakan Tanyas for his insightful ideas, discussions, and assitance during the course of research.

A special thanks to Kushanav Bhuyan for assisting me in delving deeper into the world of Deep Learning and for insightful discussions on my research. Thank you, Lorenzo Nava, for making my stay in Italy pleasant. Prof. Filippo Catani, thank you for providing me with an internship opportunity at UniPD in Italy. Special thanks to Belinda Jaarsma for her amazing support in figuring a way out of my difficult times.

I would like to thank Asst. Prof. Sajinkumar KS for his assistance during my fieldwork and for providing valuable insights into Kerala landslide geology. Special thanks to Mr Rajaneesh A. for accompanying me during the fieldwork, assisting me in surviving on the complex terrain of the Munnar region, and sharing the amazing scenery of Munnar's tea gardens. I would like to thank Dr Sekhar Kuriakose and Mr Ajin from KSDMA for their assistance and support during my fieldwork in Kerala, where I interviewed various map producers and end-users. Thank you for sharing your knowledge and everyday life experience with Kerala's landslides. My heartfelt thanks to Dr Saibal Ghosh from GSI for his invaluable insights and assistance during my field visit to Kerala.

A special thanks to Pranav Bhati, a dear friend who has helped me think objectively in my life. I would like to thank my ITC friends, Sonam, Salar, Mahek, Geethanjali, and especially *The Bag Guys* - Amanda, Carolina, Devanshi, Roberto, and Xuetong, with whom I grew up in every way over the last two years.

Last but not least, I thank my grandparents and parents for believing in me and being a constant source of inspiration as well as a strong support system. I would like to thank my beloved sister (didi), Pooja, whose unwavering care and support helped me achieve my objectives.

TABLE OF CONTENTS

LIST OF FIGURES

LIST OF TABLES

1. INTRODUCTION

This chapter introduces the research on analysing how landslide susceptibility maps are validated and used and provides the literature review which motivates the research in terms of the existing gaps. The chapter includes the (1) background, (2) research problem and scientific significance, (3) research objectives, and questions, (4) research design, and (5) literature review.

1.1. Background

Landsliding is a common phenomenon in mountainous areas, capable of causing loss of life and severe damage to infrastructure(Kjekstad and Highland, 2009). An area of around 3.7 million km^2 of the earth's surface is susceptible to landslides, home to nearly 300 million people, or 5% of the world population (Dilley et al., 2005). The impacts of landslides include human death or injury, damage to the built environment, agricultural and forest productivity loss, reduced water quality, falling real estate values, etc. (Kjekstad and Highland, 2009). Risk reduction strategies, such as better landuse planning, restrictive zoning, vegetation control, slope stabilization, landslide early warning systems, etc., can be used to minimize the impacts (Lacasse et al., 2009). However, implementing these strategies requires quantification of the landslide hazard and risks to allocate the resources and reduce the risk. The first step toward obtaining quantitative risk maps is to conduct a susceptibility and, when possible, a hazard assessment (van Westen et al., 2006a). Often, investigators confuse the term 'susceptibility' with 'hazard.' However, these are two different but related terms. Landslide susceptibility is defined as "*the relative propensity of slopes to generate landslides in a given area*" (Varnes, 1984; Brabb, 1985; Aleotti and Chowdhury, 1999), whereas landslide hazard is the probability of landslide occurrence of a given potentially damaging event with a given intensity in a given area, within a specific time period (Guzzetti et al., 1999).

Landslide susceptibility maps serve as the foundation for hazard and risk assessment, as well as risk-informed landuse planning at various scales. These maps are intended to be used for a variety of purposes, including road and infrastructure planning, risk-informed master plans, restrictive landuse zoning by potential end-users such as spatial decision-makers, urban planners, administrators, real estate agents, transport and logistics agencies, agriculture and forest managers etc. Contrary to popular belief, landslide susceptibility has not been used extensively in planning and spatial decision-making (Guzzetti et al., 2000; Chacó et al., 2006; Reichenbach et al., 2018), which could be attributed to numerous problems encountered by end-users. Based on the existing literature, the challenges can be summarized in two major categories: purpose fulfilment and reliability.

1.1.1. Purpose fulfilment:

The usefulness of a landslide susceptibility map may be evaluated by how well it serves its intended purpose. The maps can be generated for various purposes such as information, advisory, statutory[1], and design (Fell et al., 2008). Local-scale maps (1:5,000-1:25,000), for example, can be utilized for statutory purposes, although regional (1:25,000-1:250,000) or national scale (<1:250,000) maps may not be appropriate for the same (Soeters and van Westen, 1996). The local scale is the most commonly used reference scale for planning and implementing urban developments, warning systems, and emergency plans. However, because local scale landslide susceptibility maps are often unavailable, their implementation in large-scale urban planning is often not feasible.

Apart from scale, another issue is the specific information required for different purposes. For example, infrastructure planning necessitates information on the regions that may be damaged by landslides, but most susceptibility maps only consider where landslides may initiate, which may be insufficient for the purpose. Another concern is the varying interpretation of the classification of different susceptibility maps because it is often unclear

[1] Statutory purposes are those in which the maps are used with a legal implication

what landslide impact can be expected in each susceptibility class. Non-specialists may not understand the maps very well, thus hindering the optimal utilization of the map for a particular purpose (Huabin et al., 2005). The primary goal of all maps is to convey the spatial information required for the intended purpose to different end-users. If the required information is not given, the susceptibility map may not be applicable in the planning process, especially in a legislative framework. Therefore, it is critical to involve the relevant stakeholders to understand their requirements clearly and generate the map based on the purpose defined.

Once the map is generated, the map producer should indicate the conditions under which the map can be used and, more importantly, cannot be used (Hearn and Hart, 2019). More than an indication, the map producer should rather illustrate a practical application of the landslide susceptibility map for the purpose it was created, demonstrating how the map can be used and highlighting the circumstances in which it cannot be used. Hence, a collaborative approach in the preparation of landslide susceptibility maps is necessary to meet the end-user requirements and gain acceptance in the planning and decision-making process.

1.1.2. Reliability:

Reliability is defined as the "*quality of being able to be trusted to do what somebody wants or needs*" (Oxford dictionary, n.d.). In the context of landslide susceptibility, the map should be trusted by the end-user for its intended purpose. Map reliability comes from model accuracy and robustness[2], transparency, and objectivity, which leads to the acceptance of these maps into the planning and decision-making process (Guzzetti et al., 2006; Fleuchaus et al., 2021). This enables end-users to make well-informed decisions based on maps with associated technological explanations to them.

Transparency of the methods used in producing maps is vital for making these maps more reliable for the end-user. Here, transparency is referred to as the communication of the map uncertainty and usability constraints to the intended end-user. The end-users must be aware of the inherent uncertainty in landslide susceptibility maps which is inevitable due to the quality of the spatial input datasets (van Westen et al., 2008), missing knowledge of the landslide controlling factors (Carrara et al., 1999), and limitations of the technique itself (Guzzetti et al., 2006). However, the model uncertainty is rarely assessed (Reichenbach et al., 2018) and communicated to the end-users. End-users are often also not interested in knowing the map uncertainties (Petschko et al., 2014). Uncertainties should be considered in planning and preparedness, but they must be based on scientific evidence in order to produce the most rigorous assessments of the relationship between map uncertainty and its potentially disastrous repercussions (UNISDR, 2015).

Most importantly, the maps must be evaluated to ensure the reliable application of landslide susceptibility maps for risk management and land-use planning (Hearn and Hart, 2019). Accurate hazard information is required to develop economically viable mitigation options. This is important in developed countries, but especially in developing countries like India, with limited financial means combined with a large population and huge administrative areas. Robust hazard information is required in such countries to effectively manage disaster risks. The lack of such hazard information, and the inclusion of inaccuracies may have direct and indirect economic consequences such as clean-up/repair costs, search and rescue costs, infrastructure disruption, and, most importantly, loss of life (Winter et al., 2018), even in areas designated as "safe or low susceptible", giving a false sense of security. As a result, assessing the quality of the susceptibility maps/information generated is critical.

The most rational way of quality evaluation of a model (map) is accuracy assessment, which is performed by comparing the model results with observed data, also known as map validation. Typically, map validation is performed in two ways, (1) *model fit*, which is the model's ability to explain or 'mimic' the known distribution of landslides by comparing the resulting landslide susceptibility map to the same landslide inventory used to train the model (Reichenbach et al., 2018), and (2) *model prediction,* which is the model's ability to predict landslides, which is performed by comparing the output map with independent landslide occurrences not used in the construction of the model (Chung and Fabbri, 2003; Remondo et al., 2003). A landslide inventory can be considered independent when the landslides occurred in a different time period than those used in developing a susceptibility map. Acquiring an independent landslide inventory can be difficult, which makes the assessment of the predictive capabilities of a landslide susceptibility map a challenging task.

[2] Model robustness is the sensitivity of the model to small changes in parameters or inputs.

1.2. Problem statement

Since the future landslide occurrences are unknown at the time of analysis, the model can only be tested against the past landslide occurrences. Therefore, investigators attempt to create a pseudo-independent landslide inventory set to test the model prediction performance by splitting the dataset over time and space. Researchers generally use one of the four methods listed below to obtain an independent landslide dataset for model prediction performance assessment (Jaiswal, 2011; Remondo et al., 2003):

1. Dividing the available landslide inventory into two random sets and using one for calibration and the other for validation.
2. Dividing the landslide dataset into several subsets (k) and performing k-fold validation.
3. Modelling is done in one part of the study region, extrapolating the model to another portion of the region and validating the whole model with landslides from the other region.
4. Modelling is done with landslides from a specific time period, and validation is done using landslides from different time periods.

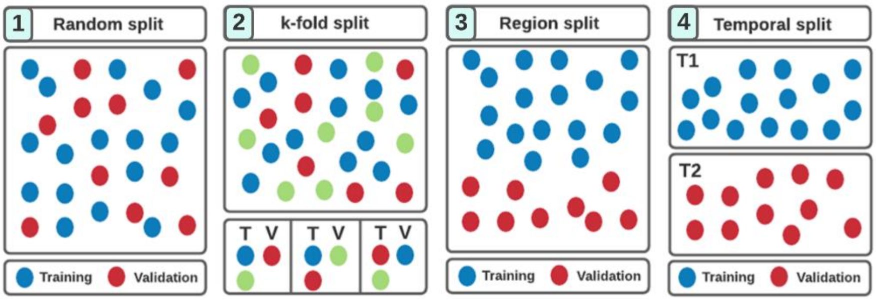

Figure 1.1: Splitting techniques to obtain an independent landslide inventory

The above methods 1 and 2 randomly split the dataset into a defined ratio of, for example, 30-70%, 25-75%, or k=10 number of partitions for calibration and validation (*Figure 1.1*). However, the landslide inventory belongs to the same time and triggering conditions; thus, it mimics the landslide occurrences rather than predicting new ones (Remondo et al., 2003). Method 3 splits the region into two parts; one for calibration and the other for validation. According to Guzzetti et al. (2006), this technique presupposes that the causal factors remain constant in the training and validation regions. In addition, it is also assumed that the combined contribution of variables to define the existing distribution of landslides remains the same geographically (Guzzetti et al., 2006). Method 4 splits the data temporally; however, the validation dataset still contributes to the generation of the landslide susceptibility maps.

Hence, the actual prediction assessment of landslide susceptibility maps is not possible using these methods, as these are more oriented towards model fit than model prediction. Although this is the case when the map is generated for future occurrences, logically, independent landslide inventory datasets cannot be available. But once these maps were created in the past a posterior[3] predictive performance assessment can be done using the new landslide occurrences (Chung and Fabbri, 2003; Remondo et al., 2003; Petschko et al., 2014; Fleuchaus et al., 2021). However, this does not directly solve the problem of model prediction assessment for real-time map generation. Still, it indicates how well the landslide susceptibility maps created in the past predicted future occurrences. Nevertheless, this assessment allows us to get more insights into the limitations and uncertainties of the maps and further improvements that can be made to these maps.

Fleuchaus et al. (2021) tested the predictive performance of statistical models retrospectively (posterior). They revealed that high validation scores achieved during model calibration (e.g. 80%) do not necessarily mean that the model will predict well. In terms of advantages, the posterior prediction assessment provides a high level of objectivity, and the reliability of the map can be demonstrated in a more reasonable manner, which helps to gain acceptance of the landslide susceptibility maps in decision-making and planning (Fleuchaus et al., 2021). A very few researches have carried out a posterior assessment of the predictive performance of these maps.

[3] Looking back in time

A complicating factor in the posterior validation of landslide susceptibility maps is that the conditions that were prevalent before the map was made may have changed. Recent investigations have challenged the concept of 'fixed' or 'time-invariant' susceptibility in an area for a few years to some decades (Guzzetti et al., 2005; Reichenbach et al., 2014). After creating the landslide susceptibility maps, landcover change may also influence the causal factors for the landslide susceptibility of the region. Samia et al. (2018) found out that old landslide occurrences affect the newly occurring landslides, also known as 'landslide path dependency', causing an increase in susceptibility over around ten years. It is a matter of further research on how the susceptibility may evolve over a period of time, considering the effects of old occurrences or change in other influencing factors such as climate (e.g., extreme rainfall events), lithology, landcover, etc.

Chen et al. (2019) investigated the effect of landcover change on landslide susceptibility. The study revealed that the susceptibility is not affected directly by landcover change but the alteration in slope conditions due to these landcover changes. Thus, landslide susceptibility maps generated at a specified time may not predict future occurrences well if there have been significant changes in the slope conditions. Therefore, while evaluating the predictive performance of landslide susceptibility, considering landcover changes is essential. Here, we assume that landcover change influences susceptibility the most, and there is no combined effect of other influencing factors on the change of susceptibility. In this thesis, we will focus on the effects of landcover changes on susceptibility, which are primarily caused by human activities and are comparatively easier to capture using remote sensing and GIS tools than other influencing factors such as climate.

1.3. Research objectives & questions

The main objective of the research is to evaluate the usage of existing landslide susceptibility maps by end-users and to analyse their posterior predictive performance using independent landslide inventories. In order to attain this goal, the following sub-objectives and research questions were considered.

1. **Sub-objective 1:** To evaluate existing landslide susceptibility maps based on their purpose and usability in a case study in Kerala, India.
    a. What are the proposed purposes of landslide susceptibility maps indicated by map producers, and to what extent do they serve these purposes?
    b. What information do end-users require from landslide susceptibility maps, and what are the operational problems in using landslide susceptibility maps in planning and decision making?
2. **Sub-objective 2:** To develop new landslide inventories using deep learning (DL) methods for posterior landslide susceptibility map evaluation
    a. Which of the many deep learning models is best suitable for landslide detection?
    b. What data combination of optical and topographical datasets is optimal for mapping landslides?
    c. How accurately can landslides be mapped using the DL model?
3. **Sub-objective 3:** To assess the predictive performances of landslide susceptibility maps using an independent landslide inventory
    a. What are the quantitative and qualitative evaluation metrics and evaluation units suitable for the predictive performance assessment of past landslide susceptibility maps?
    b. How do susceptibility maps, generated using heuristic, statistical and physically-based methods, compare in terms of their classification and predictive performance?
4. **Sub-objective 4:** To analyse how changes in landslide controlling factors, such as land cover, influence the predictive performance of landslide susceptibility maps
    a. How can landcover changes be mapped, specifically influencing the landslide occurrences?
    b. Is it possible to establish a relation between the landcover changes and landslide occurrences? Can this relation influence the predictive performance of the lanslide susceptibility maps?

The research questions will now be mentioned in conjunction with the sub-objectives. (For example, 2(a) for Question 1 of Sub-objective 2).

1.4. Research design & conceptualization

Figure 1.2 depicts the overall framework of the research to achieve the objectives and answer the linked research questions indicated in the preceding section. The research will start with the analysis of the purpose and applicability of the landslide susceptibility maps in landuse planning and decision making (sub-objective 1). To do this, two approaches were used: literature review and interviews with end-users and map producers in the southern state of Kerala, India. To address sub-objective 2**,** a landslide inventory map for the Devikolam area in Kerala was generated using deep learning (DL) methods followed by manual cleaning of the inventory. The landslide inventory generated in sub-objective 2 was used to analyse the posterior predictive performance (sub-objective 3)of the three landslide susceptibility maps for the Devikolam area in Kerala, generated by three organisations using different methods. For the assessment, a combination of quantitative and qualitative metrics was used. After the predictive performance assessment of the landslide susceptibility maps, the maps were analysed with respect to landcover changes. This objective aimed at finding out the influence of landcover changes on the predictive performance of the respective landslide susceptibility map.

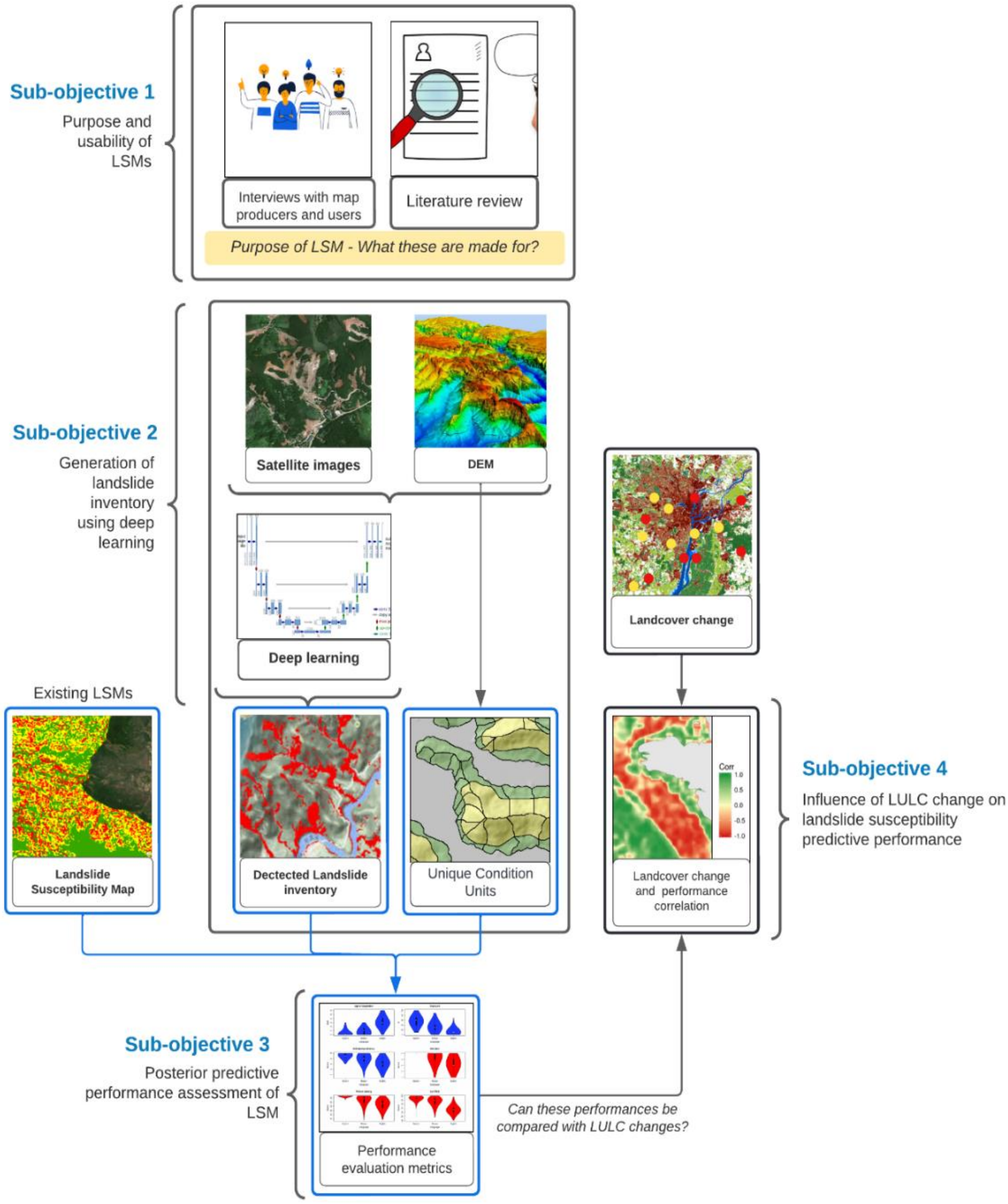

Figure 1.2: Research design

2. RESEARCH METHODOLOGY, STUDY AREA, AND DATA

This chapter includes (1) the study area description and its rationale, (2) the research methodology, and (3) the dataset acquisition and its description.

2.1. Study area

Landslides threaten 0.42 million square kilometers of India's total land area, excluding snow-covered areas (GSI, 2022). The Western Ghats and Konkan hills located on the south-western coast of India account for 0.09 million square kilometers of the total landslide prone area in India, which constituents states such as Tamil Nadu, **Kerala**, Karnataka, Goa, and Maharashtra)(GSI, 2022). The Geological Survey of India (GSI), the nodal agency for the generating and updating of national geoscientific information and mineral resource assessment, constantly monitors and maps the landslide areas. In the context of hazard management, National and State Disaster Management Authorities (NDMA & SDMA) and National Disaster Response Force (NDRF), established under the disaster management act (2005), play a key role in prevention, mitigation, preparedness and response in every part of India.

Figure 2.1: NDRF team rescuing people during the event (Source: NDRF Website)

In the state of Kerala, a catastrophic landslide and flood event in 2018 triggered 516 debris flows, 683 landslips, 62 soil slide, 22 shallow planar failure and other types of landslides (Premlet, 2019). A rapid mapping of the event was carried out by National Remote Sensing Centre using semiautomated landslide detection and GSI carried out field investigation for immediate response. The event killed nearly 534 people and an estimated million people were evacuated from various districts (*Figure 2.1*)(Premlet, 2019).

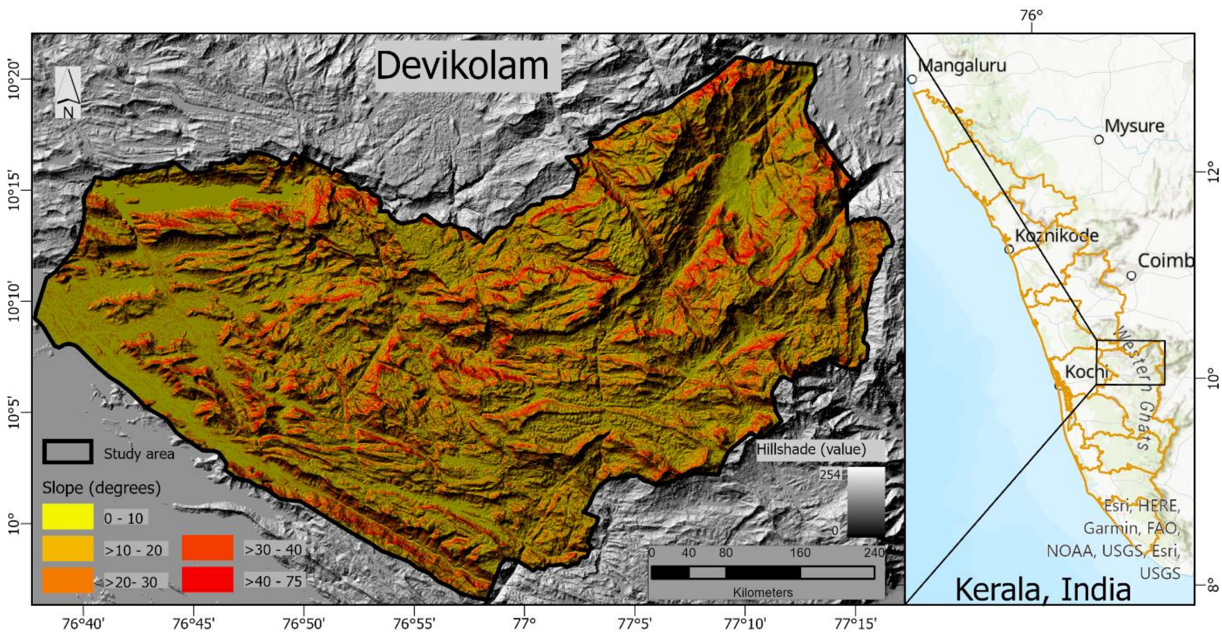

Figure 2.2: Study area

Kerala State Management Authority (KSDMA) and the National Disaster Response Force rescued 535 people, evacuated 24690 people, and relocated 119 livestock to safer locations (NDRF, 2018).

The research was conducted in Devikolam taluk of Idukki district in the state of Kerala (*Figure 2.2*). Located along the mountains of Western Ghats, Kerala is one of the most landslide-prone regions in India (Sreekumar, 2009), with historical evidence of landslide occurrences dating back to the 13th century A.D. (Kuriakose et al., 2009). With a total area of 38,863 km^2, it is the third most densely populated (860 people/km^2) state in the country (Census of India 2001). All 13 of the 14 districts of Kerala except the coastal district of Alappuzha are prone to landslides. In India, landslides are primarily triggered by rainfall in the monsoon season. The occurrence of catastrophic landslides along the leeward slope of the Kerala's western ghats during torrential rainfall is a result of the region's distinctive topography and climate. Puthumala and Kavalappara landslides killed 81 people in 2019 (Wadhawan et al., 2020), and the Pettimudi landslide killed 66 people working in a tea estate in 2020 (Achu et al., 2021). Strong bedrock weathering due to tropical climate and a heavy downpour during monsoon are the leading causes of landslides (Sajinkumar et al., 2011). In addition, anthropogenic activities like deforestation, slope modification for horticulture, road cuttings, and construction works are the main factors speeding up the weathering process.

Due to its high population density, long history of landslides, colossal death toll due to landslides, and elevated weathering process resulting from natural and human causes, Kerala is obligated to take significant steps toward disaster mitigation and adaptation strategies.

The Kerala State Disaster Management Authority (KSDMA) was the first state disaster management authority in India to provide GIS-based landslide and flood susceptibility maps of Kerala available for public use (Kuriakose, 2019). The National Center for Earth Science Studies generated a landslide susceptibility map in the year 2010, which was legalised in the year 2016 under the Disasater Management Act (2005). The map have been used for statutory purposes, specifically for landuse restrictive zoning and implementing regulations for slope alteration, e.g., a ban on mining with heavy machinery (KSDMA, 2016; Premlet, 2019). Prior to approving any infrastructure development projects, the implementing department must follow checklists for risk assessment laid out in the State Disaster Management Plan that specify restrictions in hazard zones (Kuriakose, 2019). This establishes the map as a techno-legal document; consequently, landslide susceptibility/hazard zones are not merely classes but have associated costs and restrictions. As a result, it also decreases land prices in regions designated as high susceptibility zones. Therefore, evaluating the accuracy and precision of such a map and determining the extent to which it can be utilized are of paramount importance.

2.2. Research methodology

The evaluation of existing landslide susceptibility maps necessitates a thorough understanding of their purpose and applicability, the datasets and methodologies used, and intrinsic uncertainties. This insight was gained by a systematic literature review and interviews with map producers and users. The map evaluation requires landslide susceptibility maps generated in the past years aiming to predict landslide events in the future. Another criterion is that there have been a sufficient number of landslides in the area for which the maps are available. More importantly, these landslides need to be mapped accurately and precisely so that errors and uncertainty in the landslide inventory do not hamper the evaluation process. Once a robust inventory is prepared, it can be utilized to assess the predictive capability of the landslide susceptibility maps. The evaluation results are then compared with landcover changes to establish a relationship, if any.

Keeping these aspects into consideration, the research methodology consisted of the following steps to fulfil the respective sub-objectives (*Figure 2.3*):

Sub-objective – 1

1) **Literature analysis** on the specific aims of landslide susceptibility maps. A systematic literature review was conducted to gain (Chapter 3)
2) **Interview with map producers and users** to investigate the purpose and applicability of the landslide susceptibility maps (Chapter 3)

a) Investigating the map producers' perspective on the intended use and the end-user of the map, end-users requirements and interpretation of the landslide susceptibility classes in terms of expected losses or landslide numbers.
b) Examining map users' perspectives on usability in terms of operational issues encountered when using landslide susceptibility maps. The interview was conducted in order to gain a better understanding of the specific purposes for which the maps are required, as well as the limitations of the map currently in use to meet those needs.

Sub-objective – 2

3) **Generation of landslide inventory map** using a deep learning model, which was used to evaluate the three landslide susceptibility maps. To do that, we acquired satellite images and prepared training labels, which were fed into a deep learning model. A number of model experimentations and hyperparameter tuning were performed to obtain an optimal model to finally detect landslides. (Chapter 4)

Sub-objective – 3

4) **Generation of Unique Condition Units (UCUs)** by using a Digital Elevation Model (DEM). The DEM was used to create a slope unit map as well as a generalised slope class map. These two maps were intersected to generate UCUs, which were then used to calculate landslide number and area density for map evaluation. (Chapter 5)
5) **Evaluation of the landslide susceptibility maps** was done by using newly generated landslide inventory. For the evaluation, the maps were acquired from three organisations – **1)** GSI, **2)** KU&MTU, and **3)** NCESS. Three evaluation scenarios were used to evaluate the maps – **1)** Overall, 2) Evaluation based on UCUs, and 3) Comparative evaluation. For overall evaluation, landslide densities were examined in landslide susceptibility classes of the different maps. For UCU-based evaluation, landslide densities were calculated in the UCUs and related to susceptibility classes of the maps. Comparative evaluation was performed by comparing three maps using correlation and covariance matrics and pixel-by-pixel comparison. (Chapter 5)

Sub-objective – 4

6) **The influence of LULC changes on the predictive performance of the landslide susceptibility maps** was investigated by field observations and literature review. An attempt was made to map LULC changes specifically influencing the landslide occurrences. Finally, the challenges of establishing a relation between LULC changes and predictive performances were highlighted. (Chapter 6)

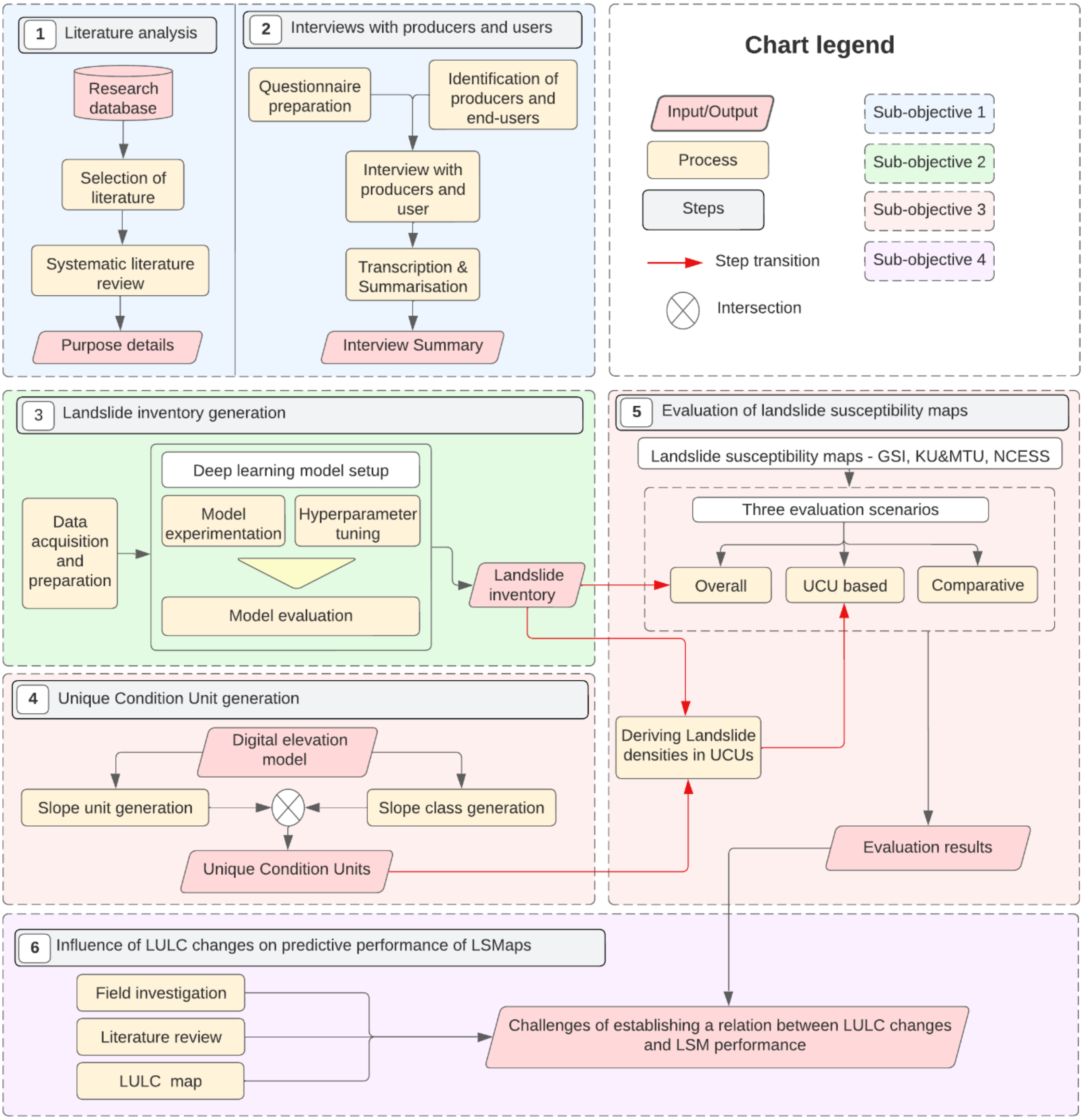

Figure 2.3: Overall methodology of the research

2.3. Data acquisition

Table 2.1 provides an overview of the datasets used for each sub-objective. Sub-objective-1 required literature on existing landslide susceptibility maps, which were acquired from WoS and Google scholar. Sub-objective-2 was to generate landslide inventory using optical satellite images, Digital Elevation Model, and label datasets from existing inventories. Sub-objective-3 required landslide susceptibility maps generated pre-2018 monsoon and landslide inventories post-2018 monsoon for evaluation. In the end, land cover changes were captured from high-resolution Google Earth images.

SN	Sub-objectives	Datasets	Type	Source (s)	Remarks	Purpose in thesis
1	To investigate the purpose and applicability of landslide susceptibility maps	Research articles	Document	Web of Science, Google Scholar	100 research articles based on a selection criteria	Used for literature analysis and extraction of information on the purpose of LSMaps
2	Landslide inventory generation using deep learning	Satellite imagery	Raster	Planet	High-resolution images (3m)	Used for training the model for landslide detection
		DEM	Raster	Alaska Satellite Facility	Digital elevation model (12.5m)	Used as complementary topographic information
		Landslide training labels	Polygon	NRSC	OBIA[4]-based inventory using 5.8 m satellite imageries	Helpful for generating label datasets
			Point	Bhukosh-GSI	Inventory generated based on field surveys & Google Earth	
			Point	Lina Hao et al. (2020)	Refined inventory of GSI & NRSC inventory	
3	To evaluate the performance of landslide susceptibility maps	Three landslide susceptibility maps	Raster/ Vector	GSI, KU&MTU, NCESS	More details are given in the next section	Maps that were evaluated using the inventory generated in sub-objective 2
4	To relate results from SO - 3 with landcover changes	Google Earth images	Raster	Google Earth Pro	High spatial and low temporal resolution	To delineate landcover changes after the creation of landslide susceptibility maps

Table 2.1: Datasets used for each subjective

2.3.1. Description of landslide susceptibility maps

Landslide susceptibility maps were acquired from three different organizations : (1) Geological Survey of India (GSI), (2) Kerala & Michigan Technological University (KU&MTU), and (3) National Centre for Earth Science Studies (NCESS). The abbreviations listed in brackets next to each organization will be used as map names from now on. *Table 2.2* contains a basic description of the maps.

Description	GSI Map	KU&MTU Map	NCESS Map
Scale of mapping	1:50,000	1:50,000	1:50,000
Data format (Resolution)	Raster (50m)	Raster (30 m)	Vector (Rasterized to 50m)
Map values[5] (available)	Classified map (discrete)	Unclassified map (continuous)	Classified map (discrete)

[4] Object-based Image Analysis – An image classification technique
[5] Whether the available raster map is already classified or has continuous susceptibility values.

Susceptibility classes	Low Medium High	Low (FS[6]<1.25) Medium(1.25<FS<1.75) High (FS >1.75) No susceptibility	Low Medium High (+Very high) No susceptibility
Method	Analytical Hierarchy Process	Infinite slope stability analysis	Index-based method
Parameters/factor maps	Slope, aspect, curvature, geomorphology, slope forming material, regolith depth, structure (fault/lineament), structure (regional thrusts/faults), land use/cover, geo-hydrology	Slope, Soil cohesion, friction angle, groundwater condition (assumed saturated), vegetation, landuse/cover, soil thickness	Slope map, landform, soil thickness, soil material, landuse, drainage density, drainage pattern, proximity to lineaments, man-made slope alterations (toe cuts etc.)
Source/author	Bhukosh (Geological Survey of India)	Dr. Sajinkumar KS, Dr. Thomas Oommen	Developed by NCESS, provided by KSDMA[7]

Table 2.2: Description of landslide susceptibility maps

The description of the map generation processes is based on published literature and interviews with map authors/producers to gain a deeper understanding of the decisions made while generating the map. Note that these maps were created for the entire state of Kerala (India), whereas this thesis is limited to the Devikolam taluk (refer to section 2.1 Study area).

(1) GSI Map:

The Geological Survery of India (referred as GSI) generated lanslide susceptibility map as part of the National Landslide Susceptibility Mapping (NLSM) program. The map for the study area was completed during the program's priority-1 phase, which ended in 2016-2017. To prepare the map, the following steps were taken:

a) Landslide inventory preparation using satellite imagery and fieldwork (routine landslide mapping).
b) GIS-based factor maps (see *Table **2.2***) are based on multiple input data preparation stages: Pre-fieldwork, fieldwork, and post-fieldwork. In the pre-field stage, factor maps such as landcover/landuse, geomorphology, and so on are created using Google Earth images. In the fieldwork stage, a 42-point detailed geo-parametric attribute table is used to collect data on the ground. These collected data are then used in the post-field stage to update/alter the factor maps generated in the pre-field stage.
c) Spatial association analysis of the various geo-factors with the landslide inventory to determine factor class ratings and geofactor theme weights.
d) Knowledge-driven estimation of ratings of the factor classes and weights of the geo-factor themes using Analytical Hierarchy Process (AHP)
e) GIS-based modelling for integrating selected and weighted geo-factor maps in order to generate landslide susceptibility scores, and
f) The use of a success rate curve to classify landslide susceptibility score maps into qualitative maps displaying varying degrees of landslide susceptibility.

Uncertainties:

Large-scale collection of regolith depth data is difficult; therefore, it was known from road and channel cuts and occasionally from newly constructed borewells, as people could easily discern the depth at which rock debris began to appear.

[6] Factor of Safety
[7] Kerala State Disaster Management Authority, India

(2) KU&MTU Map:

The Kerala Univeristy (India) and Michigan Technological University (USA) generated a landslide susceptibility map for the state of Kerala, referred as KU&MTU map in this research. *Figure 2.4* shows the three landslide susceptibility maps used in this study.

The map was produced and published in the 'Landslide atlas of Kerala' in the year 2017 (Sajinkumar and Oommen, 2017). The map was generated using the infinite slope stability model (Hammond, 1992), a physically-based method. The stability of a slope is described by its factor of safety (FS) using the infinite slope model. The FS is the ratio between the resisting forces to destabilizing forces acting on the slope. When FS > 1, the slope is stable; when FS < 1, the slope is unstable; and when FS = 1, the slope is at equilibrium. The infinite slope stability model is best suited for the analysis of shallow landslides with planar failure surfaces, which are present in the study area, because it assumes that landslides are infinitely long but have a small landslide depth in comparison to their length and width. Soil (cohesion and internal friction angle) and weight characteristics (saturated and unsaturated), as well as the local terrain slope and soil depth, are all taken into account by the infinite slope models. For the KU&MTU map, the model was applied in a GIS framework using 'A GIS tool for infinite slope stability analysis (GIS-TISSA)' (Sanders, 2017; Escobar-Wolf et al., 2021).

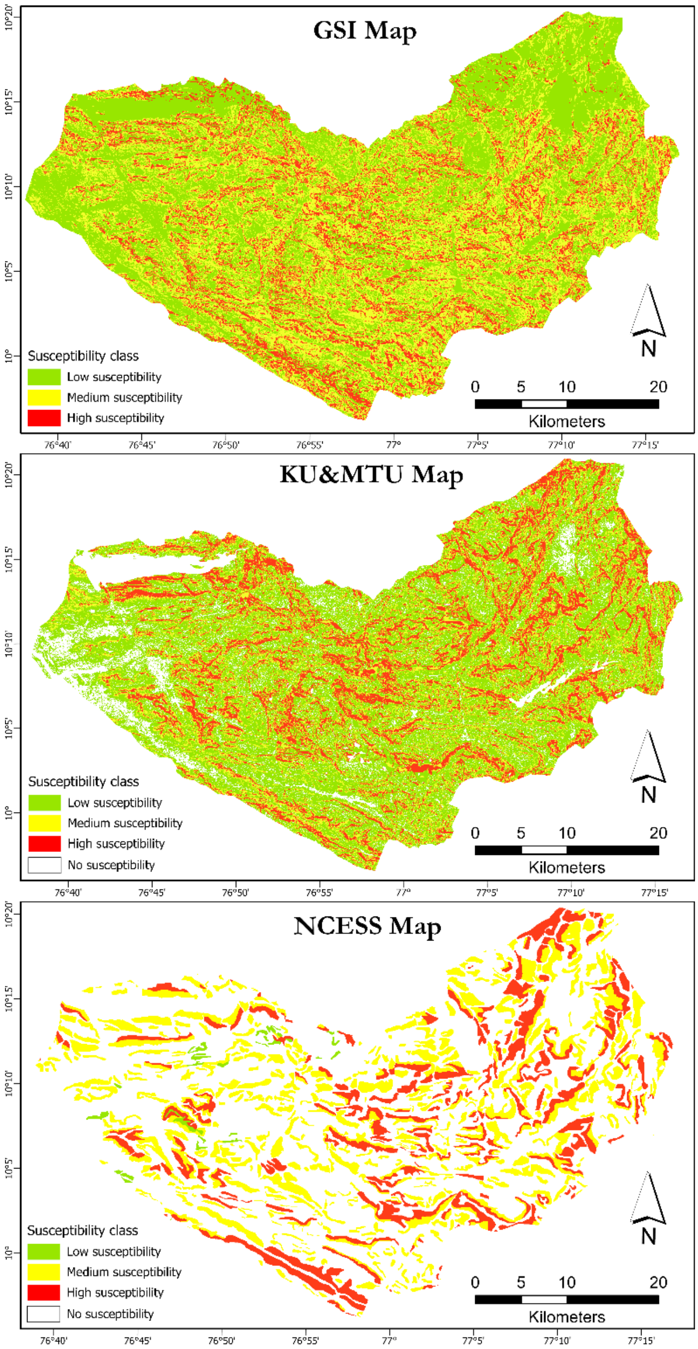

Figure 2.4: Landslide susceptibility maps used in the study

The following major decisions and steps were taken to prepare the map:

a) Preparation of the factor/input maps (see *Table 2.2*)

b) Because soil is a much more influential factor than rocks, soil geotechnical properties were taken into account. The study area contained four major soil units: well-drained sandy soil, poorly-drained clayey soil, gravelly clay, and gravelly loam.

c) The range of soil cohesion values extends from cohesionless sand (0 N/m^2) to highly cohesive gravelly clay (32,364 N/m^2). The thickness of the soil ranges between 1 m and 5.5 m, and the angle of internal friction differs between 24 and 34.5 degrees. These values were based on different studies carried out in similar terrain conditions.

d) Root cohesion and tree surcharge values were calculated from Normalised Difference Vegetation Index (NDVI) having majorly two classes: Non-vegetation (bare soil), and vegetation (Bushy vegetation, plantation and dense forest). Root cohesion and surcharge values were set to 0 in bare soil and other classes such as bushy vegetation, plantation, and dense forest were given a consant root cohesion values (Minimum-(mean)-maximum) of 4762-(4762)-25000 pa and surcharge values of 238-(1190)-1905 pa.

e) Once all of the factor maps were completed, they were processed in GIS-TISSA. The FS values were classified as follows: low susceptible (FS < 1.25), medium susceptible (1.25 > FS < 1.75), and high susceptible (FS > 1.75). Typically, FS > 1 is considered safe, but 0.25 FS was added as a margin of safety to account for uncertainties.

Uncertainties:

It was assumed that the conditions of the groundwater were saturated, which may not be entirely accurate, but the lack of data makes it difficult to make such decisions. Soil geotechnical properties and shear strength were estimated using the National Bureau of Soil Survey's (NBSS) five-class soil map, which may not be sufficient for precise estimation. As mentioned previously, root cohesion and tree surcharge values were also based on a very general classification, which may have introduced uncertainty.

(3) NCESS Map:

The map was produced in the year 2010 by National Centre for Earth Science Studies, referred as NCESS map in this research. The purpose of the map was to provide a macro-zonation of the area, which can support the government in decision-making. The map was generated using an index-based method that employs a simple ranking and rating technique for zonation of landslide susceptibility. The following steps were taken to generate the map:

a) Local studies were carried out at different sites in Kerala to establish a relation between landslides with different causal factors such as slope, soil material & thickness, landform nature, vegetation cover, and so on.
b) The factor maps (see *Table* ***2.2***) with a grid size of 250x250 m and refined with the survey of India toposheets at a scale of 1:50,000
c) Soil thickness and material types were estimated from the landform classes
d) Rating and ranking values for various factor maps and their classes were determined based on local studies and other available literature. The slope was given the highest weightage.
e) These ranking and ratings were aggregated into 250x250 m grids, which were then classified into four major classes: Low, Medium, High, and, Very High and many unclassified areas. Note that only the first three classes are present in the study area with a lot of unclassified areas. These map grids were later revised by NCESS and KSDMA and converted into KML polygon format.

Uncertainties:

Initially, the map was generated using 250 x 250 m grids as mapping units, aggregating causal factors in these large mapping units. Therefore, substantial generalization of the causal factors may have caused discrepancies in the predictions. A further issue is that field-level datasets were only collected for landslide locations; other landslide-prone areas with varying geology and slope conditions were not taken into account, which may have introduced bias into the map. Some causal maps were derived from other existing maps, such as soil material and thickness, which were derived from general landform classes such as plateau platform, plateau margins, etc. Consequently, a high degree of uncertainty is inherent in such a derivation; however, the absence of datasets necessitates such decisions.

3. ON THE PURPOSE AND USABILITY OF LANDSLIDE SUSCEPTIBILITY MAPS

This chapter addresses the first objective of the thesis by investigating the purposes and usability of landslide susceptibility maps from the perspective of map producers and end-users.

3.1. The rationale of the investigation

A collaboration of the map producer and end-user is critical for map preparation in terms of dataset collection, the scale of analysis, and the outcome relevant for the purpose it is required by the user. On the other hand, in order to use a map properly, it requires that the end-users have an understanding of the uncertainties and limitations of the map in terms of the type and detail of information provided. These should be known from the map producer. Therefore, this chapter aims to capture both producers' and end-users' perspectives on the purpose of the landslide susceptibility maps.

3.2. Map producers' perspective

As previously noted, the usability of landslide susceptibility maps can be measured by the extent to which they fulfil the desired purpose. The purpose for which the map is made determines the scale of analysis, the method used, the detail and type of input data used, and the outcome (Corominas et al., 2014). Many thousands of landslide susceptibility maps have been created and reported in the literature, but the question is, first and foremost, *'Do they have a purpose defined?'* and, secondly, if they have, *'What are the purposes these maps are made for?'*. Such maps are unlikely to be useful for end-users if the map producers did not properly consider the objective for which they make the map and the way the end-user should use it. To understand this better, two investigations were carried out to understand the map producers' perspectives on the purpose and possible use of the landslide susceptibility maps: 1) literature review and 2) interviews with producers.

3.2.1. Literature analysis

Figure 3.1 presents the workflow of the analysis carried out.

3.2.1.1. Literature search and selection:

A systematic manual search of the literature on landslide susceptibility mapping was carried out using Web of Science (WoS) and Google Scholar databases to randomly select 100 research papers. Given time limitations and scope this research we only chose 100 research papers. The research papers that presented methods and results of landslide susceptibility mapping were considered as the candidates. To find the literature, the following search term combinations were used (*Table 3.1*).

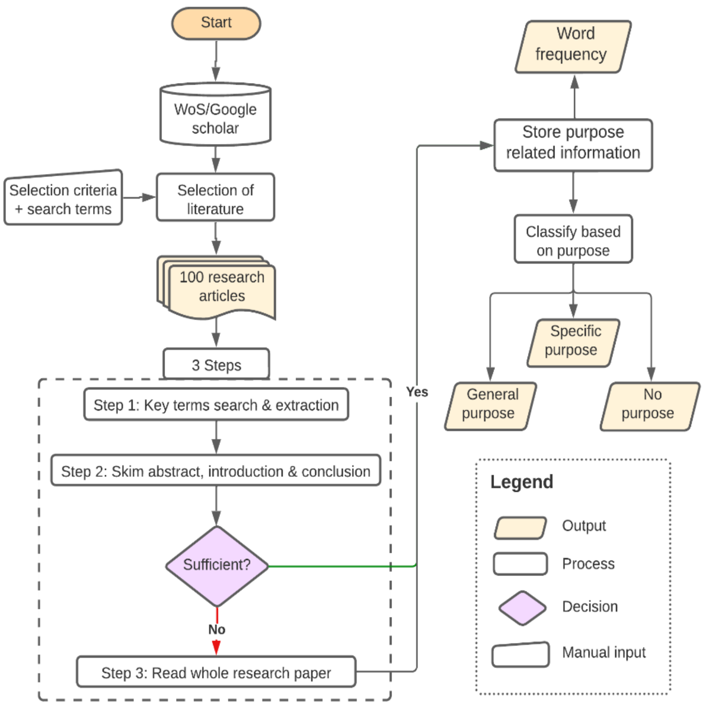

Figure 3.1: Literature analysis workflow

Nos.	Search term combinations
1	("landslide" AND "susceptibility" AND "mapping")
2	(("landslide" OR "debris flow" OR "rockfall") AND "susceptibility" AND "mapping")
3	("landslide" AND "susceptibility" AND "mapping" AND ("physically-based" OR "statistical" OR "heuristic"))

Table 3.1: Search term combinations

Around 250 research papers were chosen at random from the search results, which were narrowed down to 100 after scanning the abstract. List of these research papers is provided in **Annexure-1**. Comparative studies, including literature demonstrating the comparison of methods, metrics, and datasets, were not considered during the selection process because their primary purpose is to compare rather than to perform susceptibility mapping. Comparative studies comprised a significant portion of the literature that was omitted, which is an intriguing fact. It is important to note that terms related to potential purposes of the susceptibility maps, such as "planning", "decision-making", and so on, were not used for searching the literature because they had to be analysed after the research paper had already been chosen. Selected literature was stored, managed, and reviewed in *Zotero* (2016) software.

3.2.1.2. Systematic literature review:

This review analysis sought to answer two questions, 1) Whether the papers that report on landslide susceptibility maps have a purpose defined?, if they have, 2) What are the purposes these maps are made for?
Literature review analysis of 100 research papers can be laborious and time-taking. Therefore, three steps were taken to conduct a quick scan of the selected literature in order to extract the information pertaining to the map's purpose.
Step 1: 10 key terms were searched within the document using the basic search function (Ctrl + F). These terms include "*planning*", "*purpose*", "*objective*", "*decision*", "*government*", "*urban*", "*management*", "*reduction*", "*road*", and "*land-use*" as all of these terms relate to the potential purposes of the maps. Information around and near these key terms was extracted.
Step 2: We assume that authors can mention purpose-related information in the abstract, introduction and conclusion of the paper, so we read these three sections. If the map's purpose remains unclear or insufficient, we proceed to **Step 3**, where we read the entire paper to clear up any remaining issues (*Figure 3.1*). All of this information was stored in text format, which was then used to derive the most frequently used words to define the purpose of the maps. This gives us an insight into the focus of the map producers' perspective on the purpose of these maps. In addition, the research papers were divided into three groups according to how precisely they defined the map's purpose: *General purpose*, *No purpose*, and *Specific purpose* class.

We observed that many research papers commonly used sentences like "*This landslide susceptibility map generated using this method can be used for decision-making and landuse planning.*" but did not explain how. These research papers were assigned to the *General purpose* class. The *No purpose* class was assigned to research papers that did not include a description of the map's purpose. Research papers that defined the purpose of the map specifically (e.g., Critical road infrastructure planning) and, ideally, followed an appropriate scale of analysis, method, and presented outcome fulfilling the defined purpose, were classified in the *Specific purpose* class. Finally, a list of the specific purposes defined in these research papers is provided, together with a remark on their mapping approach.

3.2.2. Interview with map producers:

The map producers of GSI, KU&MTU, and NCESS were interviewed with the aim of understanding the purpose and possible use of landslide susceptibility maps generated by them. *Table 3.2* presents a summary of the questions asked during the interview. A consent was taken from the people interviewed before the interview of map producers and users. The complete questionnaire and consent form are attached in the **Annexure-2**.

Nos.	Questions
1	Who is intended to use this map?
2	What was the purpose of the generation of this landslide susceptibility map? (e.g., information, statutory, engineering, etc.)

3	Did you discuss with the end-users on their requirements (required information, use, detailing) with respect to the output map? If yes, what did the end-user indicate what was required?
4	What could one expect in these classes of the landslide susceptibility map that you made, in terms of landslide numbers or damage etc.?

Table 3.2: Questions asked to map producers

3.3. Map users' perspective

The counterparts of the map producers are the end-users, who should use these maps for various purposes and applications. The requirements of landslide susceptibility maps may vary depending on the aim of the potential end-users, such as urban planners, disaster risk managers, land revenue departments, geology and mining departments. For example, critical road infrastructure planning may necessitate information on the road with the greatest potential for damage as well as alternative safe roads, whereas landuse restrictive zoning necessitates information on each land parcel and the type of activity that can be carried out on it. Even within the same type of application (e.g., urban planning), the requirements can vary depending on the application (e.g., gas pipeline planning or drainage network planning). As a result, it is critical to comprehend the various purposes of maps, as well as the type and level of detail required for the same, from the perspective of map users.

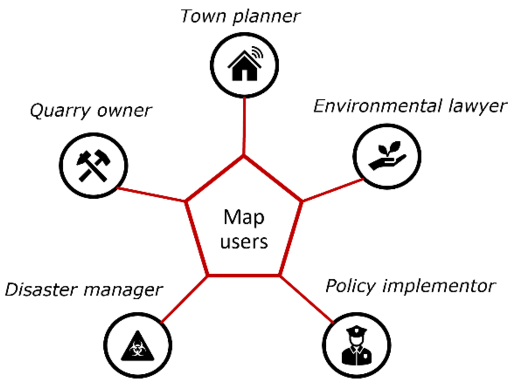

Figure 3.2: Map end-users considered in Kerala

In order to achieve that, five map end-users were selected with the help of KSDMA (*Figure 3.2*), namely: a senior town planner, an environmental lawyer, a disaster management policy implementor, a disaster manager and a quarry owner and interviewed The identity of the interviewees has been kept anonymous for privacy reasons. It is noteworthy that searching for the end-users was a difficult task. Even though we were in contact with KSDMA which has an extensive network and is a state authority, it was difficult to find people who actually use these landslide susceptibility maps. This also highlights the issue of the low popularity of these maps. All these end-users were interviewed with the following questions (*Table **3.3***) (The questionnaire is attached in the **Annexure 2**):

Nos.	Questions
1	What are the purposes do you require these landslide susceptibility maps for?
2	What information do you require to fulfil the purposes?
3	Does the map you use is applicable for your purpose?
4	What are the operational problems do you face when using these maps?

Table 3.3: Questions asked from end-users

3.4. Results and discussion

As described in section 3.2.1, a systematic review of 100 research papers was done to understand the purpose and usability of landslide susceptibility maps. As explained earlier, the literature was classified into three classes, and those that reported on specific purposes were listed together with a remark on their mapping approach. Simultaneously, the most frequently used words to describe the purposes of these maps are also presented.

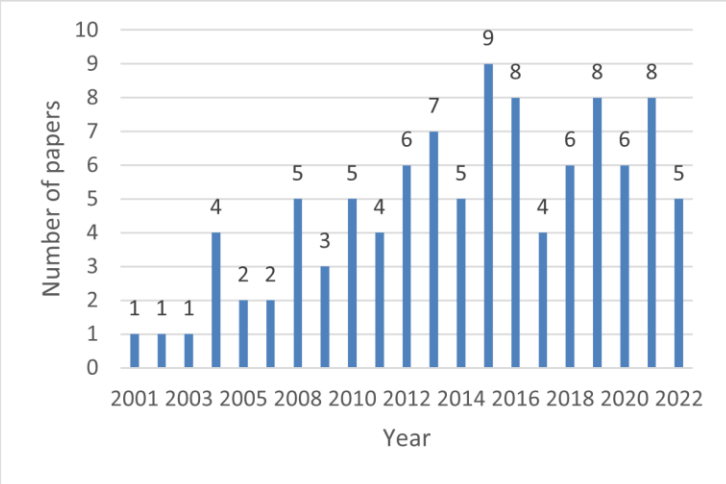

Figure 3.3: Number of papers by year

3.4.1. Distribution of literature by method and publication year

Figure 3.3 shows the distribution of the selected research papers by year. The selected research papers were classified by the method utilized, which highlights the variety in the selected literature and indicates the most frequently used methods (*Figure 3.4*). According to the classification, logistic regression was used in 22 research papers, followed by Weight-of-evidence, Fuzzy approach, and Frequency ratio. Six of the most popular methods are data-driven, while the number of physically-based methods was significantly lower.

3.4.2. Literature review and classification

Figure 3.5 displays the literature review findings, indicating the number of research papers based on the level of detail used to describe the purpose. Interestingly, the majority (62) of the 100 research papers considered, only describe the purpose of generating the landslide susceptibility map in general terms. It was discovered that research papers conduct the entire analysis without mentioning the purpose, and at a later stage in the conclusion, for instance, they mention the potential use to be decision making or landuse planning, etc., despite the fact that the purpose should be defined first, followed by the analysis. Hence, these researches do not target to fulfil any specific requirements of the potential end-users but conclude with possible general uses. Surprisingly, 20 of the research papers did not mention any purpose-related information. Both of these classes indicate that the map preparation is not really directed towards fulfilling any specific requirements but rather demonstrating a particular method of analysis. Out of the 100 papers considered, only 18 considered a specific purpose with more detail. Out of the 100 papers considered, only 18 considered a specific purpose with more detail. However, to what extent they fulfilled the requirements based on the defined purpose is a matter of further research. In this research, we have listed three examples of the specific purposes together with a remark on their mapping approach based on the review (*Table 3.4*).

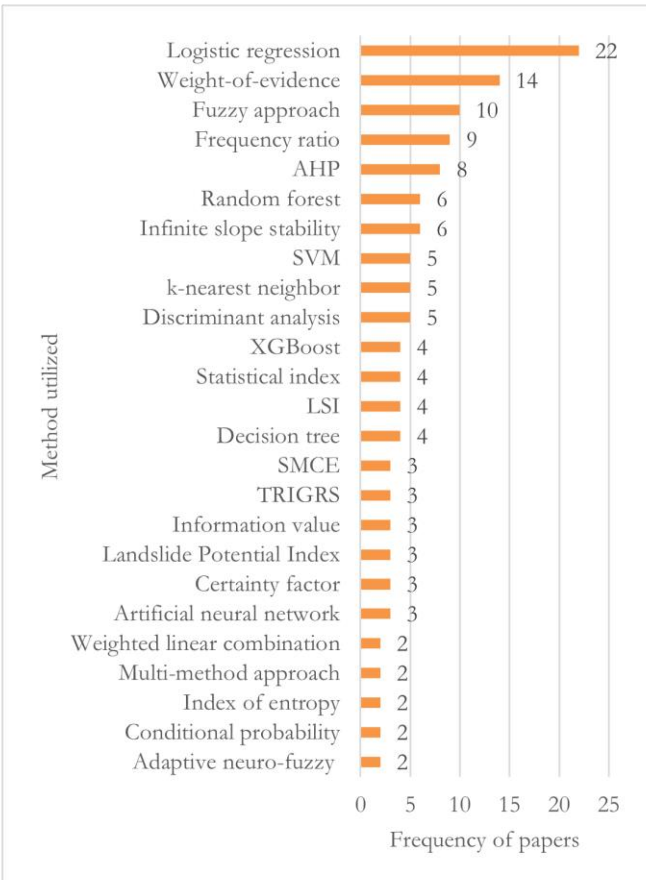

Figure 3.4: Frequency of methods utilized in the 100 selected papers

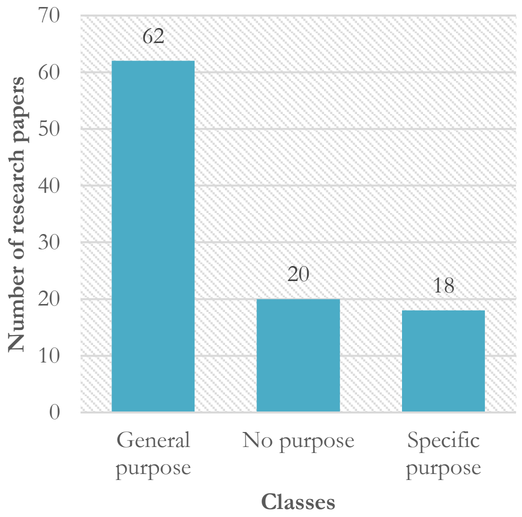

Figure 3.5: Literature classification by purpose detail

Figure 3.6: Most frequently used words for purpose description

To better understand this, we have also extracted purpose-related text and created a word frequency chart (*Figure 3.6*). Majorly, two types of words can be seen: 1) Application-based (e.g., planning, management, decision-making), and 2) End user-based (e.g., planners, engineers, decision-makers, authorities). In both cases, these words are very general, which again highlights the lack of detail in the purpose described. For example, in planning itself, there are various applications such as master-level planning, risk-informed spatial plans, and road network planning, and each individual application requires the identification of specific requirements as well as specific end-users (e.g., Senior town planner, town planning department, etc.). At the same time, we should identify these applications with more precision beforehand and then formulate the data collection methods, the scale of analysis and methods, and the way of presenting the outcome.

N	Author	Specific purpose	A remark on mapping approach
1	(Bostjancic et al., 2021)	Reduce the investigation area for large-scale analysis, and direct resources and detailed research in highly susceptible areas	The area was mapped at a scale of 1:100,000 The objective was attainable with standard mapping, so we did not observe any significant modifications to the strategy. However, the author was very clear about the map's purpose and the limitations on its usability, as well as how it can be used.
2	(Ozdemir, 2009)	Assessment of landslide damage potential in the near vicinity of a major landslide	The evaluation was conducted with an emphasis on urban areas at a scale of 1:25,000 using the conditional probability method. They indicated potential damage zones based on standard susceptibility mapping, but mapping runout zones would have been more appropriate for this purpose.
3	(Hussain et al., 2022)	Assist highways in ensuring safe and smooth driving.	A standard mapping technique employing three machine learning algorithms was used, with only the highway removed from the entire area. Although the map is still useful, it has been designed to generate greater value.

Table 3.4: A remark on mapping approach of Specific purpose researches

Table 3.4 presents three examples of the specific purposes together with a remark on their mapping approach. The table shows that even defining a specific purpose is insufficient. For example, if specific purpose 2 was to "*Assess the landslide potential damage in the vicinity of a major landslide*", the researcher investigated the entire area on a scale of 1:25000 using the Conditional Probability method. From the standpoint of susceptibility mapping, it does indicate areas with higher chances of failure; however, not the areas with higher damage potential, which could have been achieved by modeling runout zones alongside the probability of failure; thus, it does not fulfill the stated purpose but instead produces a general-purpose map. The author did not mention the way map can be used.

In contrast, Bostjancic et al. (2021) explicitly described the user's method of application and the map's limitations. This presents a user-centric approach to mapping landslide susceptibility. We can conclude that indetification of the specific purpose is crucial, but it is even more crucial to approach the evaluation in a way that achieves that purpose. In cases where it is not possible due to a lack of data availability, data quality, etc., the researcher should indicate the limitations and uncertainties of the map.

3.4.3. Interview with map producers

The map producers of the GSI map, the KU&MTU map, and the NCESS map were interviewed in order to better understand the map's purpose and potential applications of the landslide susceptibility maps generated by them.

1) **Producers of GSI map:**

   As described in Chapter 2, the map was produced under the National Landslide Susceptibility Mapping (NLSM) programme. They mentioned that the map can be used for any possible use, and it was specifically made for the state governments. They discussed the map requirements with the state government. The interpretation of the map classes in terms of expected losses or landslides are unknown and this type of analysis has not been carried out. Mostly, these classes are interpreted in relative terms, e.g., high class would expected more landslides than medium class.

2) **Producers of KU&MTU map:**

   Map producers indicated that local governments are intended to used this map. However, they did not discuss the map requirements with end-user. The idea was to provide an updated map to help the local government, since NCESS map was in vector format and generated some years ago and it was relevant to develop a new raster based map with recent datasets. The interpretation of the map classes in terms of expected losses or landslides are unknown, since this type of analysis was not carried out.

3) **Producers of NCESS map:**

   The map was required by the state for macro-level risk-informed spatial planning and it was supposed to be used by the district administration for anticipatory actions. The map requirements were discussed with state government. Similar to other two maps, the expected losses or landslides in unknown for different classes.

These interviews are further discussed in the chapter summary.

3.4.4. Interview with map users

The goal of interviewing map users was to better understand their needs for the specific purposes for which they require these maps. Therefore, Five end-users were interviewed, who have been using NCESS map and were shown KU&MTU and GSI maps for their responses so that they could compare the outcomes to their intended use.

1) **Senior town planner:**

   The Senior Town Planner was primarily responsible for planning activities such as critical road network planning and risk-informed master planning. Critical roads connect critical infrastructures such as hospitals and fire departments. These roads are the most needed in the event of a hazard event, so they must be weatherproof and able to withstand the emergency. They require information on roads that will be affected on an annual, decade, or bi-decade basis. Because construction of critical road infrastructure requires extensive planning, financing, and labor and the susceptibility information must be highly accurate. Inaccuracy is a serious issue they are currently dealing with, because large-scale town planning, for example, requires highly accurate information to design and propose infrastructure, as well as the frequency of occurrence of a hazard event. They also stated that having three landslide susceptibility classes is sufficient, as having more would complicate planning. However, during the interview, we noticed that the planner's interpretation of the landslide susceptibility classes was unclear and asked me to explain. Habitable areas are the planners' primary concern since they are mostly involved with city planning and require more accurate information throughout the city. Master plans, for example, are legal documents that require at least a 1:5,000 scale map with high accuracy; but, available maps are of limited use. Planners need to know what and where the damage will occur, which is not provided in most susceptibility maps, and they are unaware of this limitation. They must be aware of the potential consequences of a landslide moving downhill in order to plan accordingly. They no longer use the map when they notice damage in low-hazard areas. They indicated that restriction of development activities is not the way forward; instead, incorporating preventive measures in areas prone to landslides can allow for some planning.

2) Environmental lawyer:

In the context of landslides, the environmental lawyer was mostly involved in cases involving a conflict of interest between the people and authorities (in this case, the KSDMA) regarding the use of an area (e.g., quarrying). Normally, the authorities are silent in these cases, so they go to court. The landslide susceptibility maps are used as a legal document or as evidence in court. The map can be used to impose restrictions on certain activities (for example, quarrying) in areas with medium and high vulnerability. Courts are unfamiliar with coordinate systems, as well as latitude and longitude. As a result, they approach the disaster management authority or the district collector, or other authorities to confirm the susceptibility of a particular area. Obejectively, interpretation of the map classes and the types of activities permitted must be clear. If it is low and denoted in "Green," it is understood to be "safe," and the court asks the authority why the activity is not permitted if the area is low or medium susceptible. Even lawyers are unaware of what activities are permitted and prohibited in a given class. The law only recognizes 'black' and 'white' interpretations; grey areas are difficult to deal with. This highlights the most difficult aspect of the map's usability on the ground, because people without a background in landslide sciences should not be expected to understand the meaning of landslide susceptibility classes.

There are several issues with implementation of the law: To begin, disaster management plans are required for District Disaster Management Authorities (DDMA) under the Disaster Management Act of 2005 and must be submitted to KSDMA. However, many DDMAs have not submitted such a plan, and no legal action can be taken against them due to inconsistencies in the law's implementation. Second, officers pretend to be ignorant of facts. When asked about providing clearance in a medium or high hazard zone, they say they didn't realize it was medium or high hazard. Sometimes village officers disregard the fact that such a map is available for use and required by law. Third, the implementation of such maps obstructs a wide range of developmental activities, particularly business; as a result, politicians are unwilling to impose such maps because it would jeopardize their political careers.

3) Disaster management plan implementor:

The implementor of the disaster management plan was in charge of preparedness, mitigation, and response activities. They require information on 'safe' locations for relocation planning, so highly reliable information is required to ensure people's safety. They need information on highly populated areas in high-risk areas so that they can train people to survive in an emergency. One of the critical pieces of information required for an effective response is early warning. As a result, map accuracy is extremely important.

4) Quarry Owner:

Quarry owners run businesses for extracting building stone to meet the state's demand for building materials. After 2002, even looking for building materials required an environmental clearance. Building stone is a scarce resource in the state, and prices for the material have risen exponentially in recent years. When they want to quarry in areas where building stone materials, such as granite, are available but have been designated as a high hazard zone. When investigated the area on the field, they discovered highly compact hard rock with little to no potential for landslides This causes problems in their business, especially given the scarcity of the material in Kerala. They propose that the hazard zonations should be reevaluated and a new classification provided, particularly based on field investigations. They understand that people's safety must be ensured, but developmental activities should not be hampered by such decisions, or at least some scope of activities should be left open. For micro-level resource planning, they require highly accurate maps based on field investigations conducted by a local research body.

5) Disaster manager:

The disaster manager is the primary user of the landslide susceptibility maps and has a statutory position in the management. Due to privacy concerns, additional information is not provided. The disaster manager stated that the NCESS map was created to provide macro-level zonation for the state of Kerala for land use restrictive zoning and risk-informed spatial planning. The NCESS map was created in 2010 and has been legally used since 2016. Despite its low resolution, it adequately serves the purpose and allows them to use it as a state statutory map. Due to a conflict of interest, the disaster manager was even sued, but was able to prove its legality in court. This provides a real-world example of the map's usability and emphasizes the importance of its accuracy.

The newly created GSI map will replace the NCESS map for administrative purposes. However, the disaster manager raises concerns about the practical application of the GSI map for a variety of reasons. Despite the fact that the GSI map was recently prepared with higher resolution and possibly better accuracy than the NCESS map, ground application of the map necessitates a different approach. The mapping unit of the GSI map is 30 x 30 m grid, with three classes - Low, Medium, and High. None of the areas are excluded from the susceptibility mapping, which is frequently misinterpreted on the ground. For example, if an area is mapped as "low hazard," it will be difficult for people to build houses or shops. Since people with conflict of interest can use this map to obstruct development activities for personal vendetta and use it to challenge in the court. Since the court may interpret "low hazard" as "low but still hazardous area." If such a map is made legal, it could have serious consequences for the population.

This demonstrates that even a higher quality maps in terms of spatial resolution and accuracy can be of less use if user requirements are not considered. The manager requires the landslide susceptibility maps for land use restrictive zoning and risk-informed spatial planning.

Table 3.5 presents the summary of map end-users' responses for the NCESS map. The table describes the specific purposes of landslide susceptibility maps, the information needed to fulfil those purposes, and the operational challenges associated with their use.

End-user	No	Specific purpose	Information required	Serve the Purpose?	Operational problem (s)
Senior town planner	1	Road network planning	Potential landslide damage areas	No	Runout info required, large-scale maps required
	2	Critical road connectivity plan	Frequency and location of the landslides	No	Accurate information is not available
	3	Risk-informed masterplan	Multi-hazard Risk information	No	1:5000 scale map required, Risk information required
Environmental lawyer	4	Managing a case on conflict of interest for the use of land	Whether a piece of land is susceptible or not	Somewhat Yes	Courts do not understand geo-coordinates or degree of susceptibility, no strict law, political influence, playing ignorance of the fact

	5	The case against activity restriction	Degree of susceptibility and associated allowed activities	Yes	Generally, lawyers are not aware of non-(permissible) activities
Disaster management plan implementor	6	Planning relocation	Whom to relocate and where to?	Somewhat yes	1:5000 map is required, runout info required
	7	Preparedness, mitigation, and response	Which districts to give what directions	Yes	Mismatch within the Susceptibility classes
	8	Capacity building	Whom to train	Somewhat yes	-
	9	Early warning	Susceptible classes with landslide rainfall thresholds	No	Lack of Automatic Weather Stations (Need 256 but only nine are available)
Quarry owner	10	Identification of potential quarry areas	Is quarrying allowed in this land parcel?	No	The accuracy and resolution of the map are not sufficient
	11	Challenging authorities for susceptibility maps	Not allowed; why?	Yes	Ground reality does not match the map information
Disaster manager	12	Landuse restrictive zoning	Susceptible land uses	Yes	Map uncertainty may hamper the development process
	13	Risk-informed regional disaster management planning	Overall regional susceptibility status	Yes	-
	14	Cadastral or real estate level planning	Local Landslide prone areas	Somewhat yes	1:5000 scale required; does not have desired information; people understand cadastral information
	15	Emergency management operations	Risk information	No	Irrespective of susceptibility class, anticipatory actions are taken

Table 3.5: Responses of end-user for NCESS map

It is important to note that specific purposes (1, 2, 3, 6, 10, 14) that necessitate large-scale analysis are not being fulfilled because their application requires more detailed susceptibility information. Other purposes (1, 3, 9, 15) are not being fulfilled due to the type of information required to fulfill those purposes. For example, a risk-informed master plan requires multi-hazard risk information to develop a comprehensive plan; therefore, even a high-quality landslide susceptibility map, in terms of spatial resolution and predictive ability, cannot serve the purpose, given that it requires vulnerability and exposure information of the same quality, which is often not available.

3.5. Chapter Summary

A better understanding gained from map producers and end-users will enable landslide scientists to prepare maps that are more valuable to the user community, and the published literature will shift focus from the map producers to create more user-oriented landslide susceptibility maps which will gain more acceptance in the decision-making and planning. When we compare the nature of information required by the end-user to that provided by map producers, we see a significant difference in terms of detailing, type, and amount of information required. This emphasizes the critical importance of a collaborative map-making process that is more user-oriented rather than map producers working in silos.

Now referring back to the research questions of sub-objective 1, we answer as follows:

1. *What are the proposed purposes of landslide susceptibility maps indicated by map producers, and to what extent do they serve these purposes?*

   The literature review revealed that the majority of studies proposed a generic purpose for the maps, typically concluding, "*This map can be utilised for land use planning and decision making.*" The proposed purposes are extremely broad and do not aim to meet the specific needs of the end-users. Other literature indicated specific purposes such as "damage potential asssement in the near vicinity of a major landslide", but ended up conducting a standard landslide susceptibility mapping which do not provide runnout zones for potential damage but only initiation information. The findings of the literature review were confirmed by the interview with the map producers, who reported a similar approach to identifying end-users and the map's purpose. The literature does not provide a descriptive operational use of the map for the stated purpose or any other purpose. Typically, map producers do not discuss user requirements with end-users; consequently, the maps do not appear to serve their intended purpose. Producers of GSI and NCESS map indicated that they had discussed requirements with end-users, but did not describe user requirements explicitly during the interview. In the case of KU&MTU, such communication was absent. We indicate that the purpose of the map and the needs of the user are not in the focus of map producers; as a result, they do not consciously think about them and incorporate them into the mapping process. Consequently, it is crucial to emphasize the significance of defining specific purposes and taking end-user requirements into account.

2. *What information do end-users require from landslide susceptibility maps, and what are the operational problems in using landslide susceptibility maps in planning and decision making?*

   Specific purpose require specific information. Senior town planner required information on the potential damage areas and frequency of an event for critical infrastructure road network planning. Risk informed mast plan required information the multi-hazard risk information. Disaster manager required a map which can be used to impose land use restriction in the area, in which not all the areas should be mapped beause of their mis-interpretations and mis-use on the ground. As per interviews with map end-users, they have specific requirements that landslide susceptibility maps typically do not meet due to irrelevant information, map scale and resolution, and map inaccuracy.

   As noted in the interviews with map users, the landslide susceptibility maps have several operation problems. Firstly, scale of the maps is not sufficient for application requiring large scale information such as town planning or relocation planning. Secondly, most of the purposes require highly accurate information, therefore, even the slightest doubt on the accuracy of the map prevent the end-users from using them. Thirdly, interpretation of the map classes is not clear and people without background in landslides sciences do not understand the meaning of these classes. For example, courts do not understand geocoordinates or these classes but they require "*black & white*" interpretation of the classes for a fair judgement. Fourthly, most of these maps provide landslide initiation information, however, for example, road and infrastructure planning require runnout information. They require information for the damage areas and frequency of the event. Fifthly, uncertainty in the maps may cause distress in the authorities as well as people, for example, as observed for quarry owner, constant conflict between the KSDMA and quarry owner was observed. Even to an extent that it was charged with a law suite. Sixthly, low political will, soft implementation of law and playing ignorance of the fact to prevent themselves from implementing the maps on ground for their personal good is another issue.

4. LANDSLIDE INVENTORY GENERATION

The purpose of this chapter is to achieve sub-objective 2, which is to generate a landslide inventory for the study area that will be used to evaluate the three landslide susceptibility maps.

4.1. Purpose and background

4.1.1. Purpose of landslide inventory generation

The landslide inventory was required to assess the predictive capability of the three landslide susceptibility maps. Thus, it is critical to generate a robust landslide inventory, which is accurate and complete, so that errors and uncertainty in the landslide inventory do not hamper the evaluation process. We mapped landslide initiation points as well as landslide polygons in the study area from the year 2018 to 2021 so that the landslide point and area density can be considered in the evaluation.

4.1.2. Methods of landslide inventory generation

Landslide inventories have been identified as the critical landslide susceptibility and hazard assessment dataset. There are seven landslide mapping techniques (van Westen et al., 2008; Corominas et al., 2014), including (1) image interpretation, (2) field investigations, (3) archive studies, (4) dating methods for landslides and (5) monitoring networks (6) (semi) automated classification based on spectral characteristics, (7) (semi) automated classification based on elevation characteristics.

Image interpretation includes visual analysis of stereo aerial photos, high-resolution satellite imageries, LiDAR shaded relief maps and RADAR images. Although, mapping using stereo images can be time-consuming and requires an expert mapper of the technique. At the same time, aerial photographs, LiDAR, and RADAR images are often not available in a short time (Martha et al., 2010) or sometimes never. Traditionally, field investigations have been there before the availability of remote sensing datasets, although they advanced with better tools and techniques (e.g., mobile GPS and GIS, etc.). Archive studies make use of newspapers, interviews, road maintenance, etc. Dating methods are performed in laboratories with the help of dendrochronology, radiocarbon dating, etc. Monitoring networks such as Extensometer, EDM, GPS, total stations, etc., can provide continuous information such as movement velocity. (semi) automatic classification based on spectral characteristics includes object-oriented image analysis (Martha et al., 2010; Stumpf and Kerle, 2011). However, the spectral information can be combined with the elevation information in other (semi) automated methods, such as artificial neural networks (ANN), support vector machines, and other deep learning methods like Fully Convolutional networks (FCN) (Ghorbanzadeh et al., 2021).

Particularly, Fully Convolutional Network (FCN) methods may achieve high accuracy but require very high-resolution imagery, sufficient training datasets, and computation space to perform the detection. Besides that, selecting the appropriate architecture and fine-tuning parameters is crucial for FCN to outperform other methods (Ghorbanzadeh et al., 2021). The FCN describes the linkage of each pixel to a specific class label, such as landslides and non-landslides. Some of the authors have used this to accomplish pixel-by-pixel semantic segmentation in the venture of landslide detection (Liu et al., 2018; Lei et al., 2019; Peng et al., 2019; Shi et al., 2020; Soares et al., 2020; Meena et al., 2021). The essential properties of FCN are the end-to-end learning of the upsampling approach with the help of encoder-decoder structure and skip connections to fuse data from diverse depths in the network (Long et al., 2015).

FCN model variations such as U-Net and attention-U-Net have recently been found to be effective in detecting landslides as well as transferable across different regions (Ghorbanzadeh, 2021; Meena et al., 2022). However, these studies mapped comparatively large landslides by utilizing high-resolution spectral (5 m) and topographical information (5 m) having similar spatial resolution. In the study area, the landslides are small-size shallow landslides which are difficult to map. Therefore, we utilized another FCN model, i.e., Multi-scale attention U-Net, which is designed to detect small features in the images and was initially utilized in biomedical image segmentation research (Oktay et al., 2018; Abraham and Khan, 2018). The goal of employing Multi-scale attention U-Net was to automatically detect landslides that occurred in isolation and might go undetected when mapping using visual interpretation. However, the number of landslides is fairly limited in any case, but deep learning allows for the generation of a relatively complete landslide inventory.

4.1.3. Problems with landslide inventories

Many investigators have stressed enough the requirement of landslide inventory for the susceptibility and hazard assessment and how the completeness, in terms of spatial and temporal coverage, as well as the geographical and thematic accuracy of landslide inventory, influence the quality of the assessment (Galli et al., 2008; van Westen et al., 2006b, 2008; Jaiswal and van Westen, 2009; Guzzetti et al., 2012; Ghosh et al., 2012; Steger et al., 2016). Landslide inventories suffer from severe problems propagating into the landslide hazard assessment (Steger et al., 2016). However, Steger et al. (2016) artificially introduced positional errors in the inventory and revealed valuable insights for a statistical model (logistic generalized linear model). The positional errors subsequently distort the modeling results, although the interrelation between the inventory-based errors and subsequent models is complex. Furthermore, the error-propagation is not only limited to the positional inaccuracies of the inventories but also the spatial representation of landslides and the environment (causal factors), landslide magnitude, and the characteristics of the study area, the selected classification method, and an interplay of predictors within multiple variable models. Although, these errors can be adapted to the model by generalizing the input data, and selecting an intense generalizing classifier. However, adjusting the data to these errors is likely to produce a weak prediction.

van Westen et al. (2006b) indicated other major landslide inventory problems. They discuss that unlike other hazards like earthquakes or flooding, landslides occur in isolation, making detection a tedious job. While mapping landslides by visual interpretation, it is quite common to miss the slope failures that occurred in isolation, especially small in size. In addition, when mapping one by one, there may be different attributions to the same type of landslides. Usually, countries do not have a single agency performing landslide mapping. It introduces variations in landslide inventories based on the particular interest of the agency, e.g., the road department will only be concerned about landslide occurrences affecting roads, hence only mapping them. The list of problems with landslide inventories is quite long; nevertheless, the focus should be on the standardization of mapping methods with proper attribution designed for various purposes of landslide zoning like information, advisory, statutory, and design (Corominas et al., 2014).

4.2. Datasets and methodology

Figure 4.1 presents the procedure for compiling a landslide inventory in the study area. We created three data combinations from Planetscope images and ALOS palsar DEM and fed them into a deep learning model to detect landslides. Training, Testing, and Validation sets were created from the data. The DL model learns from the training

S. no	**Datasets**	**Format (resolution)**	**Remarks**
Spectral and topographic information			
1	Planetscope images (2018)	Raster (3 m)	Used for Spectral information (VNIR)
2	ALOS Palsar DEM	Raster (12.5 m)	Used for generating slope, profile curvature, planar curvature, and aspect
Landslide inventories			
3	NRSC	Polygon	Used as reference
4	GSI	Points	Used as reference
5	Lina hao et al	Points	Refined from NRSC and GSI inventory, main reference

More details of the datasets are provided in section Data acquisition

Table 4.1: Datasets used for landslide inventory generation

set, validates or calibrates on the validation set, and the Testing set is used to evaluate the model's accuracy in the final stage. The deep learning model was used to detect landslides in 2018, while Google Earth images were used to compile the inventory for 2019-2021. Since 2018 was a catastrophic year with a large number of landslides, it was worthwhile; however, in other years there were fewer landslides, so the following procedure was not as advantageous as visual interpretation from Google earth. *Table 4.1* presents the datasets utilised to generate the landslide inventory in the study area. Planetscope images were used for spectral information and generating NDVI, since it is considered as a promising indicator for landslide detection (Lu et al., 2019). In addition, topographic information is considered important, given that steep slopes are more prone to landslides than the flat areas. Apart from slope, other DEM derivatives such as aspect, profile curvature and planar curvature can play a role (Ohlmacher, 2007; Ghorbanzadeh et al., 2019), since these topographical information are considered proxy to weathering agents such as wind, sunlight and precipitation received (Pourghasemi et al., 2018).

Therefore, we utilized ALOS-Palsar DEM to generate slope, profile curvature, planar curvature, and aspect. Other critical datasets were landslide inventories generated by NRSC, GSI, and Lina Hao et al. (2020), which formed the basis for generating a training dataset for the detection model and later for comparison.

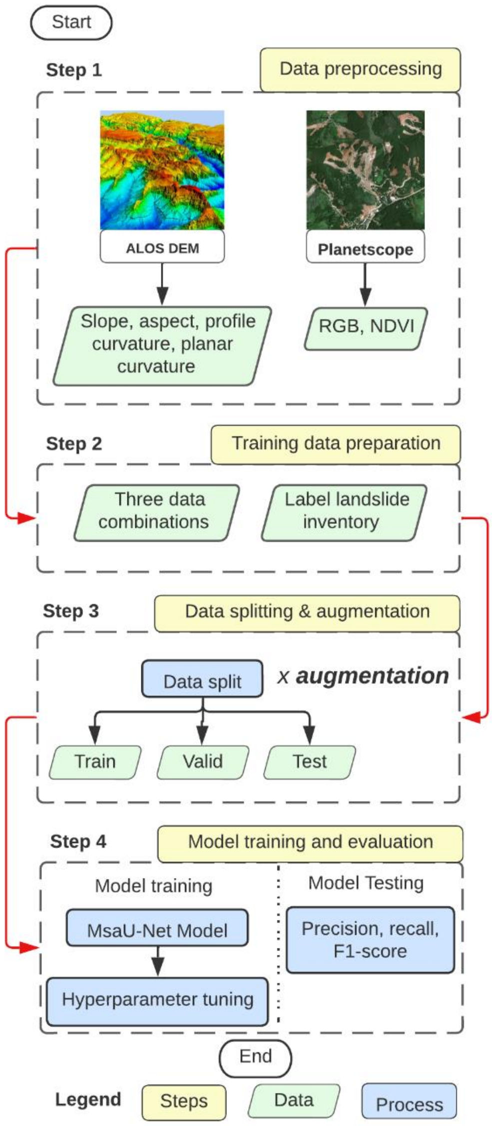

Figure 4.1: Landslide inventory generation methodology

4.2.1. Data preprocessing

The data was preprocessed using ArcGIS pro, and ERDAS IMAGINE software. PlanetScope images and ALOS DEM were separately mosaicked and visually inspected for any geometric and radiometric errors. The "Fill (Spatial Analyst)" tool in ArcGIS pro was used to fill the missing values in the ALOS DEM dataset. DEM was used to generate slope, aspect, profile curvature, and planar curvature after adjustments. Using the nearest neighbor resampling approach, these derivatives were resampled and aligned to match the resolution and extent of PlanetScope images. We acknowledge that we may have added some inconsistencies to the dataset through this process, but the topographical information is still indicative of the original data. PlanetScope images were used to create the Normalized Difference Vegetation Index (NDVI).

Even though we had access to three landslide inventories, we were unable to directly employ any of them for the study due to missing landslides and incorrect boundaries, which may not be useful. Details of the problems and their correction are given in the next section.

4.2.2. Training data preparation

Figure 4.2 presents a snapshot of GSI and NRSC inventory. Since NRSC inventory was generated for providing landslide event information by rapidly mapping them, it had issues in terms of missing landslides or shifted landslide boundaries. Another issue was that NRSC inventory was generated using IRS-LISS-IV(5.8m) images; therefore, polygons do not align with PlanetScope images, which is undesirable and problematic since it may introduce mixed-pixel information and deteriorate the

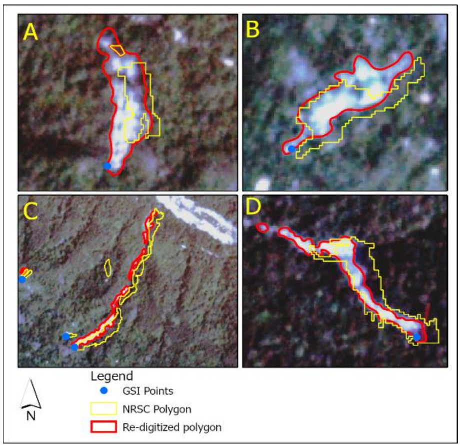

Figure 4.2: GSI & NRSC inventory, and re-

model's quality (Pattathal V. et al., 2022). Therefore, incorrect landslide polygons were re-digitized or shifted so that they align with PlanetScope images (*Figure 4.2*). The inventories by GSI and Lina hao were in point format, therefore, they cannot be utilized in model training since we require a polygon inventory; however, they were used as reference when creating training polygons using Google Earth Pro and PlanetScope images. The label polygons were rasterized and resampled to align with PlanetScope images. Spectral (VNIR and NDVI) and topographical information (DEM derivatives) were used to create three data combinations(Table 4.2):

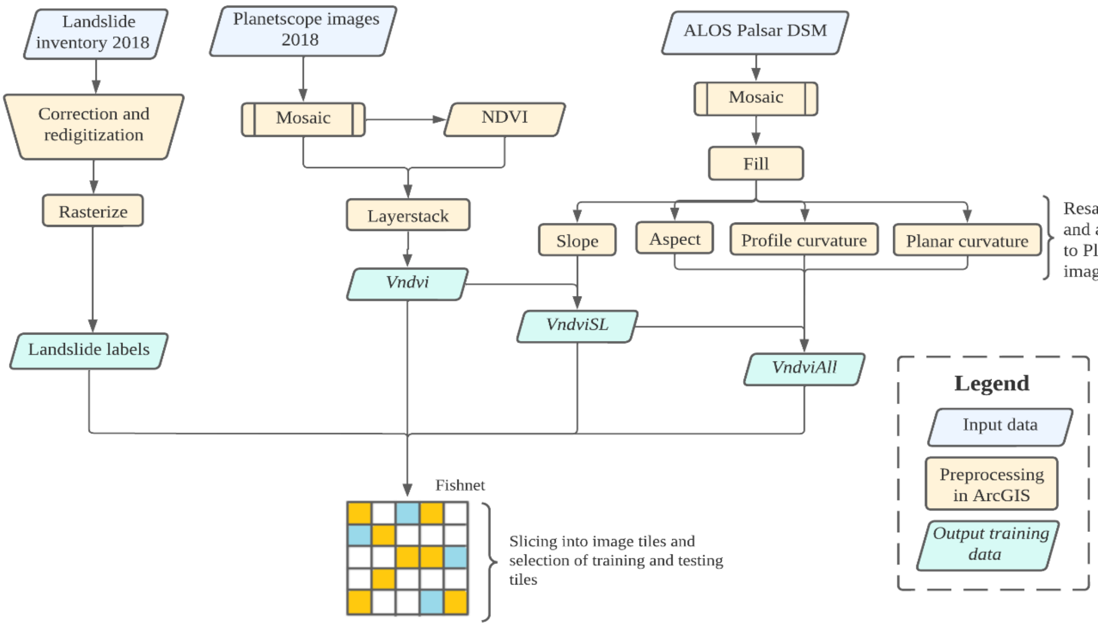

Figure 4.3: Data preparation workflow

Combination	**Rasters (nos.)**	**Layers**
Vndvi	5	Visible, near-infrared, NDVI
VndviSL	6	Vndvi, slope
VndviAll	9	VndviSL, aspect, profile curvature, planar curvature

Table 4.2: Training data combination

Topographic information was split into *Vndvi* with only slope (*VndviSL*) and with all other information (*VndviAll*) so that the influence of the type of additional information could be noted more explicitly. Since slope is a continuous first-order DEM derivative, whereas aspect is a categorical first-order and profile & planar curvature are second-order DEM derivatives. Hence, the type of information is different from than slope and kept separately in another combination.

After the preparation of each dataset, a single Fishnet was used to slice each data combination into uniform tiles of 640 x 640 pixels. These tiles were then patched into 64 × 64 pixel patches prior to the training, and any patch devoid of landslides was eliminated. Small and sparsely spaced landslides necessitated covering a big area to generate plenty of training samples. The whole procedure is displayed in *Figure 4.3*.

4.2.3. Data splitting, augmentation, and training strategy

All the data combination layers, *Vndvi*, *VndviSL,* and *VndviAll,* were sliced into 86 tiles for each combination with a size of 640 x 640 pixels. These tiles were further split into training (73 %), validation (11%), and test sets (16%), which were strategically distributed in the study area to avoid *Geo-spatial autocorrelation*[8]. Remotely sensed data naturally feature *spatial autocorrelation*, which is the foundation for any pixel-based classification algorithms; yet, ignoring the spatial

[8] *Geo-spatial autocorrelation* describes the degree to which one pixel resembles other neighboring pixels.

dependency between training, validation, and test sets might lead to overestimation of *generalisation capabilities*[9] (Karasiak et al., 2022). Therefore, we considered the visual variations between the tiles and complexity within the tiles in terms of mixed pixels, low contrast and presence of objects with a spectral signatures similar to landslides etc. This allows us to maximize the generalisation capability of the model and decrease the false predictions. *Table 4.3* shows the number of patches and split percentage for each split set.

Data distribution	*Number of tiles*	*Number of patches*	*Split (%)*
Training set	63	6300	73.1
Validation set	9	900	10.5
Testing set	14	1400	16.3
	Total	8600	

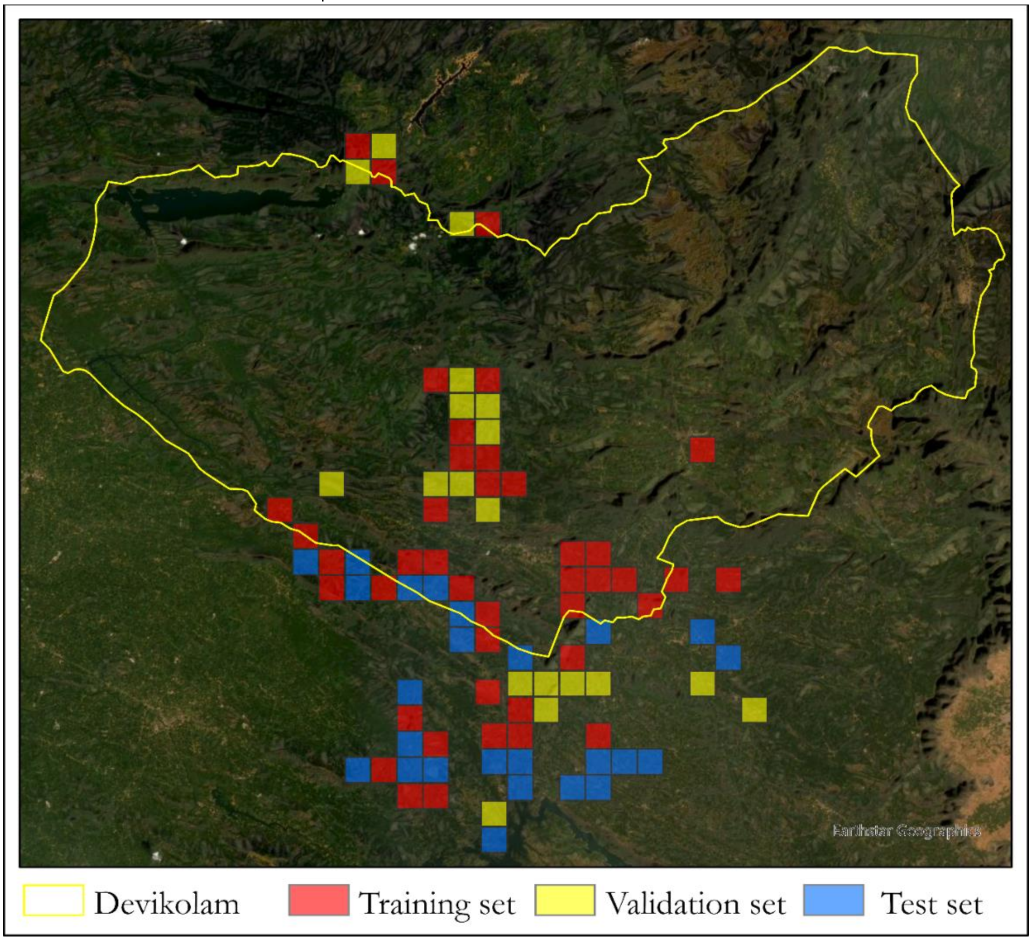

Figure 4.4: Distribution of training, validation and test datasets

Figure 4.4 presents the distribution of the training, validation, and testing tiles in the study area. It shows that we trained on the landslides outside the study area as well to capture more inferences of the landslides. Given that training datasets were low, we adopted two strategies: **1)** *Data augmentation*, and **2)** *Sample generation using a semi-trained model.*

Figure 4.5: Manual selection of predictions made by semi-trained model

[9] *Generalisation capability* is the model's ability to adapt properly to new, previously unseen data.

Data augmentation is a method of increasing the training datasets by introducing slight variations to the existing datasets. This prevents *model over-fitting* [10]and improves the model's *generalisation capability* (Shorten and Khoshgoftaar, 2019). Geometric transformations such as flipping, colour space, cropping, rotation, translation, noise injection, and colour space transformation are examples of data augmentation techniques (Shorten and Khoshgoftaar, 2019). Firstly, augmentation techniques, i.e., horizontal flip, vertical flip, rotation (45 deg), and shear along the x- and y-axis. Prior to augmentation, there were 8,600 patches, which increased to 60,200 patches after augmentation. The second strategy was *Sample generation using a semi-trained model*. A *semi-trained model* can be referred to as a model whose hyperparameters are not optimal to achieve the best results but still can predict very well. We used a semi-trained model to predict on an unseen *Vndvi* dataset and then manually selected the correct predictions by overlaying in Google Earth Pro (*Figure 4.5*).

4.3. Deep learning model setup

4.3.1. The rationale of model selection

U-Net, Attention U-Net, and Multi-scale attention U-Net have been applied effectively in biomedical image segmentation with promising outcomes(Ronneberger et al., 2015; Abraham and Khan, 2018; Oktay et al., 2018). Numerous authors have shown applications of U-Net (Ghorbanzadeh, 2021; Meena et al., 2022) and Attention U-Net (Nava et al., 2022) for landslide detection and demonstrated their efficacy in detecting landslides. Multi-scale attention U-Net (MsaU-Net) is utilized in biomedical image segmentation, which is specially designed for detecting small features with less training labels. Although, it has not been utilized in landslide detection yet. MsaU-Net model is the improved verison of U-Net and Attention U-Net, although, improvement in a model may not directly imply that it would be optimal for the problem under observation. It can also be difficult to choose a model based on the literature, given the complexity of the study area can be different. Therefore, we utilized U-Net, Attention U-Net and MsaU-Net for initial experimentation. Surprisingly, MsaU-Net outperformed the other two models, which was evaluated based on the F1-score (an evaluation metric) explained in section 4.3.2.3. Hence, we utilized MsaU-Net for further experimentations and is explained in detail below.

4.3.2. Multi-scale attention U-Net (MsaU-Net): Model architecture

The detection of landslides in the study area was carried out using the MsaU-Net (Abraham and Khan, 2018). Multi-scale attention U-Net is an improved version of Attention U-Net. More importantly, a novel *loss function*[11] named Focal

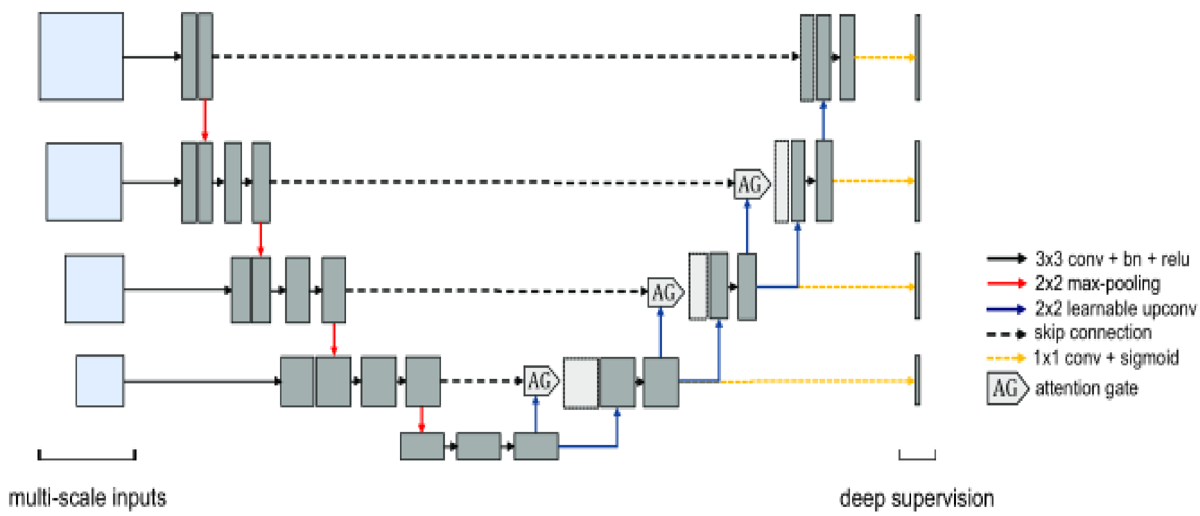

Figure 4.6: MsaU-Net architecture (Abraham and Khan, 2018)

[10] *Model over-fitting* is the model's tendency to exactly mimic the training dataset and memorizing the noise in the dataset. This decreases the model's ability to predict accurately on unseen datasets.
[11] *Loss function* calculate how far an estimated value deviates from its actual value.

Tversky Loss (FTL) was implemented together with MsaU-Net, which is specifically designed to detect small features and handle the data imbalance in the dataset, which is one of the challenges the landslide detection.

Figure 4.6 present the architecture of MsaU-Net, which consists of a contracting path (left) and an expanding path (right) with skip connections (dash lines) adjoining them to effectively extract the high-resolution spatial and contextual information to result in an efficient semantic segmentation result. These skip connections provide input to the Attention Gates(*Figure 4.7*), which extract relevant information from contracting and expanding paths and promote more semantically meaningful outputs. Multi-scale inputs (*Figure 4.6* - left) together with deep-supervision provides better intermediate feature representation that might be lost otherwise due to convolution.

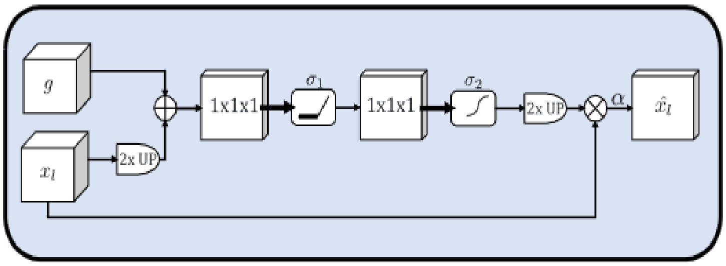

Figure 4.7: Additive Attention Gate (AG) adapted by Abraham and Khan (2018)

The results of the model predictions are in binary form, which differentiates between landslide pixels from the background pixels. The training of the network was performed on the Center of Expertise in Big Geodata Science (CRIB) computing platform of ITC-UT using python JupyterLab.

As proposed by Bottou (2010) and Mezaal et al. (2017), model optimisation was performed utilizing the Adam optimiser instead of the standard Stochastic Gradient Descent optimiser. The former is significantly quicker due to its adaptive learning capabilities and converges faster to decrease the loss, hence enhancing the overall precision. To optimize training speed and avoid overfitting the network model, learning rate and weight decay settings were used. This stage would provide heat maps with probability values classified as "landslides" and "non-landslides." The next section includes a list of hyper-parameters that were optimized and used in model training.

4.3.2.1. Hyper-parameter tuning and experimentations

Hyperparameter tuning is a crucial part of optimizing the results of a deep learning model. The tuning aims to find an optimal set of hyper-parameters and build a high-quality model that can generalize well on datasets with huge variations (Hovden, 2019). Hyper-parameters are the variables that determine the network architecture and how the network is trained. *Table 4.4* presents the list of hyperparameter combinations utilized to achieve the optimal model for final landslide detection.

Parameters (nos.)	Instances
Learning rates	1e-3, 1e-4, 1e-5
Batch Size	8, 16, 32
Number of filters	8, 16, 32
Gamma values (FTL)	0.80, 0.85, 0.90
Data combinations*	*Vndvi*, *VndviSL*, *VndviAll*

Not a hyperparameter

Table 4.4: Hyperparameter combinations

The descriptions of the hyperparameters, models, and data utilized are as follows (*Table **4.4***):

1. *Learning rate*: The learning rate is an optimization parameter that determines the step size of each iteration as the loss function approaches its minimum.
2. *Batch size:* The batch size refers to the number of training patches sent across the network in a single iteration.
3. *Filters:* Filters extract features by concatenating multiple kernels of size (x * y) and input channels (z). The dimensions of the filter would be (x * y * z).
4. *Gamma value:* A parameter to enforce the Focal Tversky Loss (FTL) function to handle data imbalance.

5. *Data combinations*: As described in section 4.2.2, the data combinations were generated by combining visible, near-infrared, NDVI, and DEM derivatives. The combinations mentioned in the table above experimented with.

Other significant parameters, such as the Number of *epochs* [12]*(100, 200, 250)* and *weight decay rate*[13] *(0.20, 0.3),* were experimentally determined on the fly based on the model's behaviour and without fixation. As proposed by Ghorbanzadeh et al. (2019), *patch sizes*[14] *64x64* and *128x128* were employed; however, it was discovered that the *64x64 patch size* yielded significantly better results due to the small average size of the landslides, so the remaining experiments were conducted with this patch size. The optimal combination of these various options was determined through testing. Nevertheless, testing each of these permutations may be impractical. Combinations that performed poorly in the preliminary stages were therefore eliminated.

4.3.2.2. Combination elimination criteria

To eliminate combinations that would take a long time and a lot of computing power, a performance-based elimination was used. Initially, it was found that Multi-scale attention U-Net outperformed Attention U-Net and U-Net in the majority of the hyperparameter combinations, which could be attributed to MsaU-Net's ability to detect smaller objects with less number of training samples and relatively efficient handling of the training data imbalance. Therefore, we continued the remaining experiments with MsaU-Net. Apart from that, a *patch size* of *128 x 128* gave comparatively low F1-scores than *64 x 64*; thus, we utilized this *patch size*.

4.3.2.3. Model evaluation metrics

For the results generated by different models, standard accuracy assessments such as Precision, Recall, and F1 score were utilized using base metrics such as *True Positives* (TP), *False Positives* (FP), and *False Negatives* (FN)(*Table **4.5***). When the model correctly predicts the positive class[15], this is referred to as a *True Positive*. A true negative, on the other hand, is referred to when the model correctly predicts the negative class[16]. A *False positive* is the incorrect prediction of the positive class by the model. A *False negative* is the incorrect prediction of the negative class by the model. Precision is the proportion of landslides correctly identified by the given method. The recall is the percentage of labelled landslides detected correctly by the method. The *F1-Score* is used to find the right balance of *Precision* and *Recall*.

Standard accuracy assessment metrics	
$\boldsymbol{Precision} = \frac{\boldsymbol{TP}}{\boldsymbol{TP} + \boldsymbol{FP}}$	$Recall = \frac{TP}{TP + FN}$
$\boldsymbol{F1} = 2 \times \frac{\boldsymbol{Precision} \times \boldsymbol{Recall}}{\boldsymbol{Precision} + \boldsymbol{Recall}}$	

Table 4.5: Model evaluation metrics

4.4. Results

All the initial experiments were conducted using *Vndvi* datasets, and optimized hyperparameter combinations were achieved. Top 5 hyperparameters were then utilized for training on *VndviSL* and *VndviAll* datasets to limit the number of experiments. Thus, we first present the results of hyperparameter tuning experiments using the *Vndvi* dataset, indicating the top five combinations, and then present the results of using those five combinations on the other two datasets to determine the impact of topographic information on model performance.

---

[12] *Epochs* are the number of full training passes through a training dataset.
[13] *Weight decay rate* is a hyperparameter that prevents the weights of a model from becoming too large by causing them to exponentially decrease to zero.
[14] *Patch size* is the input size of the image fed into the network.
[15] The *positive class* is the feature class under consideration (or feature of interest)
[16] The *negative class* is everything else except feature of our interest

4.4.1. Overall results of the different hyperparameters combinations for the *Vndvi* dataset

Table 4.6 depicts a green to red spectrum of model performances in terms of *F1-score* against all the hyperparameters. A number of *Filters* and *Learning rate* are shown in rows, and the *Batch size* and *Gamma values* (FTL) are shown in columns. Green cells have the highest F1-scores, red cells have the lowest, and values in between are represented by a combination of the two colours. F1-scores in bold font indicate the best score of the group of combinations contained in that area with a thick black border. Overall, the best model was able to attain an F1 score of 0.7851, which is an average performance. It can be observed that *Learning rate* of 1e-3 with a *Batch size* of 8 produced the best results; on the other hand, batch size of 32 with a learning rate of 1e-5 produced the worst results. A medium *Learning rate* of 1e-4 with a *Batch size* of 32 produced average *F1-scores*. Sample results with Precision and Recall scores can be found in **Annexure 3**.

Learning rate		Batch size 8			Batch size 16			Batch size 32		
		g{0.8}	g{0.85}	g{0.9}	g{0.8}	g{0.85}	g{0.9}	g{0.8}	g{0.85}	g{0.9}
1e-5										
Number of filters	8	0.6851	0.6507	0.6661	0.6787	0.6005	0.6047	0.5788	0.5586	0.6042
	16	0.7230	0.7187	0.7174	0.7094	0.7091	0.6977	0.6564	0.6768	0.6540
	32	0.7401	**0.7545**	0.7471	0.7491	**0.7526**	0.7449	0.7156	0.7334	**0.7426**
1e-4										
Number of filters	8	0.7614	0.7661	0.7715	0.7396	0.7378	0.7174	0.7483	0.7328	0.7315
	16	**0.7736**	0.7606	0.7640	0.7660	**0.7712**	0.7622	0.7377	0.7392	**0.7545**
	32	0.7720	0.7712	0.7683	0.7669	0.7615	0.7605	0.7401	0.7471	0.7491
1e-3										
Number of filters	8	0.7631	0.7711	0.7731	0.7642	0.7646	0.7662	0.7702	0.7658	0.7667
	16	0.7766	0.7807	**0.7836**	0.7728	0.7707	0.7757	0.7642	0.7817	**0.7838**
	32	0.7760	0.7730	0.7622	**0.7851**	0.7769	0.7766	0.7734	0.7782	0.7622

Table 4.6: F1-score for each hyperparameter combination

4.4.2. Influence of batch size and learning rate combinations on F1-score

Figure 4.8 presents the *F1-scores* for *Batch size* and *Learning rate* combinations when *Gamma value* and *Filters* are kept constant at 0.85 and 16, respectively. It can be observed that lower learning rates in combination with higher batch

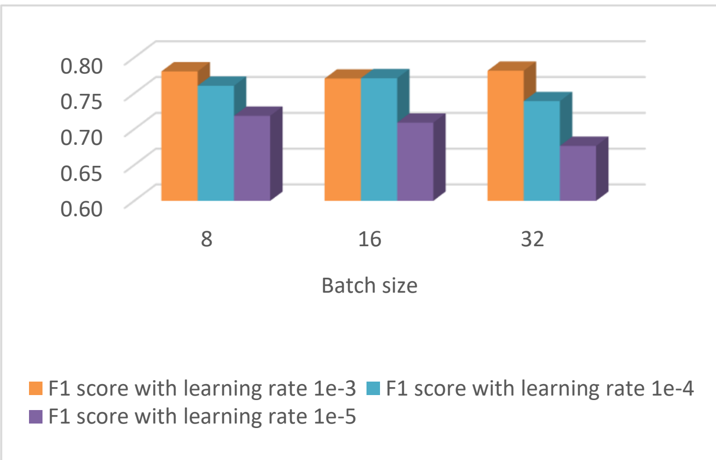

Figure 4.8: Influence of batch size and learning rate on F1-score

size produced low *F1-scores*. However, a learning rate of 1e-3 gave better results irrespective of the batch size used. The best results were achieved by using a learning rate of 1e-3 and a batch size of 8.

4.4.3. Influence of filters and learning rate combinations on F1-score

Figure 4.9 presents the *F1-scores* for *Filters* and *Learning rate* combinations when *Gamma value* and *Batch size* are kept constant at 0.8 and 16, respectively. Similar to previous results, a learning rate of 1e-3 produced the best results irrespective of number filters utilised. The best results were achieved with higher number of filters, which logical since filters are the number of features learned by the model; higher number of features learned imply that model will be able to learn comparatively better than 8 and 16 filters. Simlar observations were made by Zebin et al. (2019).

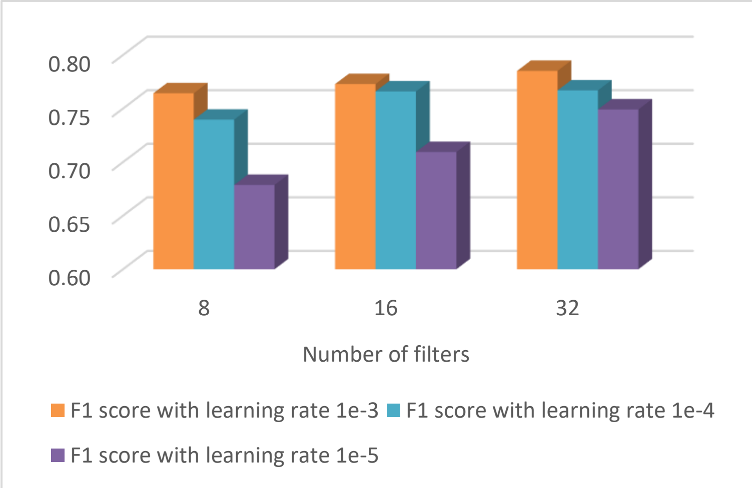

Figure 4.9: Influence of filters and learning rates on F1-scores

4.4.4. Influence of gamma value and learning rate combinations on F1-score

Figure 4.10 presents the *F1-scores* for *Gamma value* and *Learning rate* combinations when *Batch size* and *Filters* are kept constant at 8 and 32, respectively. The gamma value compels the FTL to focus on the less dominating class, which in this case is landslides. It can be seen that increasing Gamma values yielded decreasing F1-scores, which may signal that a gamma value of 0.8 was more efficient in dealing with imbalance in the dataset than 0.85 and 0.9. However, the F1-score is the greatest at 0.85 gamma for learning rates of 1e-5.

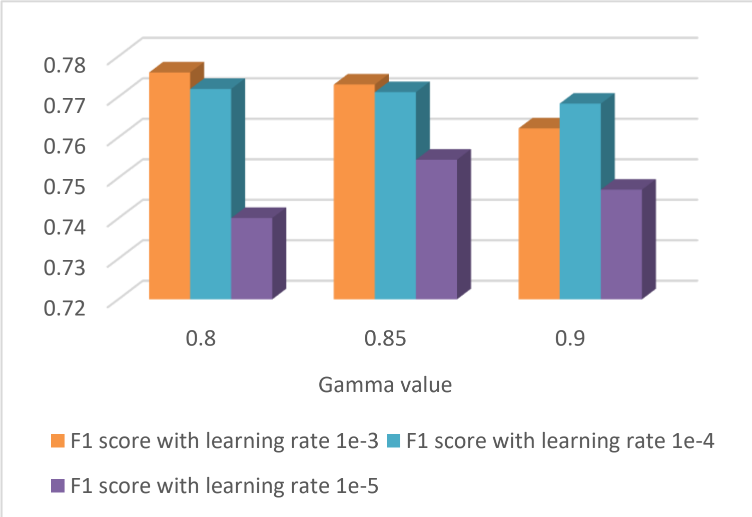

Figure 4.10: Influence of gamma values and learning rates on F1-scores

4.4.5. Best parameter combinations: Comparison for different datasets

Table 4.7 presents the top 5 hyperparameter combinations which yielded the best F1-scores when trained with the *Vndvi* dataset. These combinations were further utilized for training the model on *VndviSL* and *VndviAll* datasets; resulting F1 scores are presented in the table. The table shows that a learning rate of 1e-3 generated the best outcomes for various combinations of F1-scores. Although the difference between the top five hyperparameters is not considerable, using any other combinations could be less efficient. Statistically, the best performance was achieved utilising the *Vndvi* dataset only, followed by *VndviAll* and *VndviSL*. Our hypothesis that additional topographic information will improve accuracy; proved to be incorrect. However, when we predicted utilizing the model trained with *VndviAll*, it decreased the number of false positives, but landslide boundaries were not crisp.

Combination rank	Learning Rate	Batch Size	Filters	Gamma	*F1 -score*		
					Vndvi	*VndviSL*	*VndviAll*
1	1e-3	16	32	0.8	**0.7851**	0.7157	**0.7613**
2	1e-3	32	16	0.9	0.7838	**0.7429**	0.7587

3	1e-3	8	16	0.9	0.7836	0.7370	0.7461
4	1e-3	32	16	0.85	0.7817	0.7259	0.7432
5	1e-3	8	16	0.85	0.7807	0.7113	0.7385

Table 4.7: Results of best parameter combination using Vndvi, and then applied to VndviSL and VndviAll

Possibly, the poor performance could be attributed to the following reasons:

1) **The disparity in spatial resolution between PlanetScope and ALOS DEM:**
The spatial resolution of ALOS DEM is four times the PlanetScope images; therefore, the information is not comparable spatially. Moreover, the information utilized as topographic information is second-order DEM derivatives meaning that the derivative pixel is calculated using 8 neighbouring pixels. Thus, generalises the information to some extent. At the same time, the landslides are significantly smaller, which may not be represented by the DEM in use.

2) **Small patch size:**
We observed that a patch size of 64 × 64 gave relatively better outcomes because the model is better able to learn local characteristics when the patch size is smaller, as opposed to contextual information when the patch size is larger (Kervrann and Boulanger, 2008). Thus, a change in patch size (smaller or larger) would result in the loss of either spectral or topographic information regarding a landslide in terms of local information.

4.4.6. Final landslide detection in Devikolam

We utilised the best hyperparameters combination as indicated in the previous section, i.e., *Learning rate* of 1e-3, *Batch size* of 16, 32 *Filters*, and a *Gamma value* of 0.8 to train the model for final predictions on *Vndvi* dataset to landslides for the entire Devikolam taluk. Since predicting on the entire image may produce boundary artefacts due to patch level predictions, a sliding window method with a stride of 24 was employed to generate overlap images. The predictions in overlapping regions are averaged to produce a final prediction for the entire image. The purpose of post-classification was to eliminate false positives and merge polygons that belonged to the same landslide. *Table 4.8* displays the final prediction scores for the test *Vndvi* dataset. The landslide polygons are indicated in red polygons; white boxes indicate false positives. We will discuss the most common false positives in the study area in the discussion section.

Metrics	Scores	Scores (%)
Accuracy	0.9511	95.11
Precision	0.7810	78.10
Recall	0.7922	79.22
F1-Score	0.7851	78.51

Table 4.8: Final prediction results for the test Vndvi dataset

4.4.7. Finalisation of landslide inventory

Referring back to our purpose of generating a robust landslide inventory for evaluation of the three susceptibility maps, we wanted to reduce the percentage of error as much as possible. Therefore, a thorough post-classification cleanup was performed in Google Earth Pro software by utilising high-resolution satellite information with a possibility of 3D visualisation aiding in interpretation (Hao et al., 2020). Landslides missed due to the relatively small size of the landslide were digitised, and landslides from 2019-2021 were completely mapped on Google Earth Pro. Once a polygon inventory was finalised, it was utilised to generate a point inventory by automatically extracting the initiation point using ALOS DEM (*Figure 4.11*).

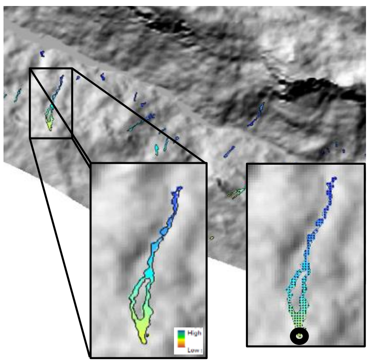

Figure 4.11: Extracting initiation point using ALOS DEM

Finally, we generated an inventory of 864 landslides in point and polygon format, with a total landslide area of 1.70 km², indicating an average landslide size of around 2000 m². *Figure 4.12* present the final landslide inventory map and *Table 4.9* distribution of landslides in each year and final method used to map them.

Years	Number of landslide mapped	Method
2018	788	Deep learning + Visual interpretation
2019	6	Visual interpretation of high resolution Google earth images
2020	47	
2021	23	
	864	

Table 4.9: Number of landslide mapped in each year

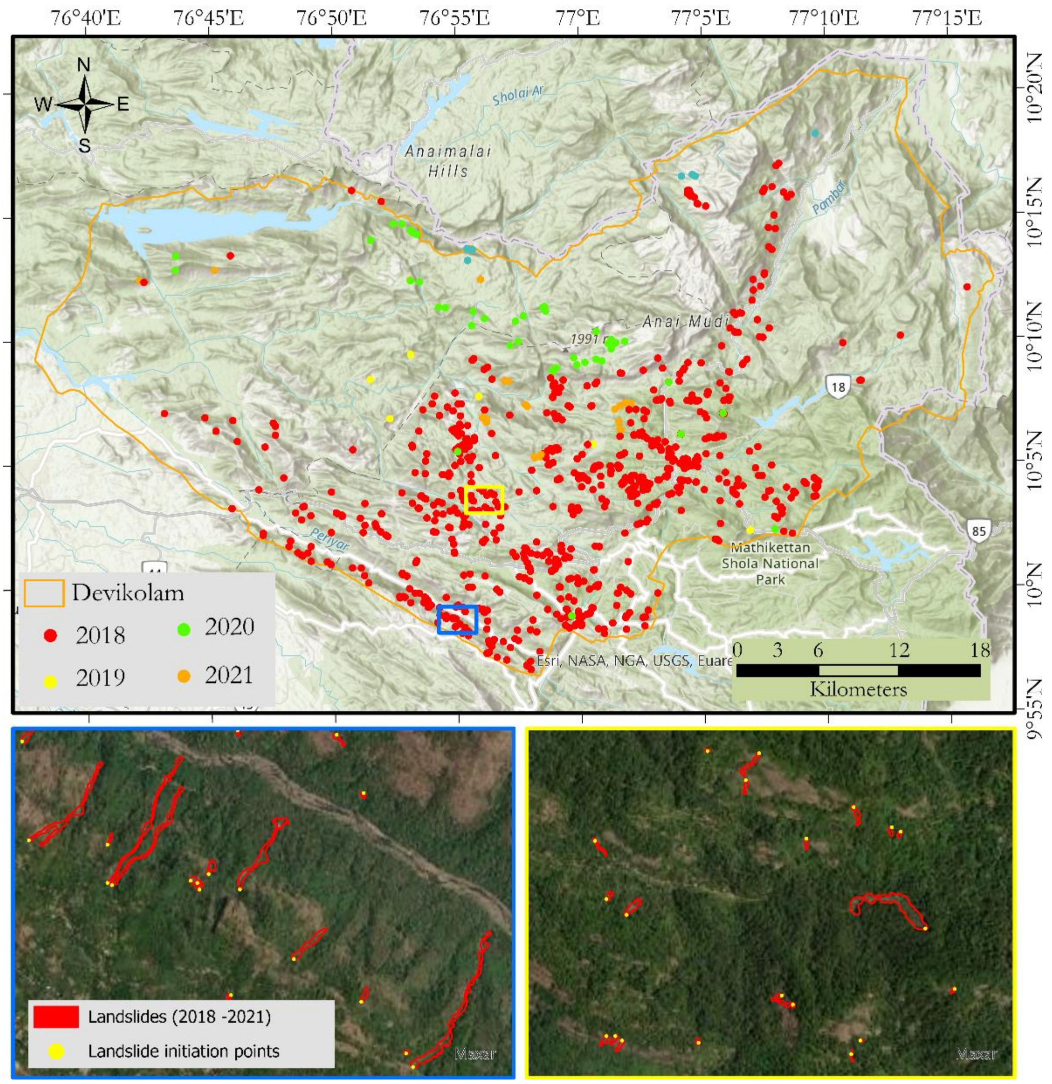

Figure 4.12: Final landslide inventory map (2018 – 2021)

4.5. Discussion

A wide range of model performances against different sets of hyper-parameter combinations indicates the significance of its optimisation. It was realised that the learning rate and batch size greatly influenced the model performance. Since Gamma values enforce the Focal Tversky Loss to focus on the less dominant feature class, it indirectly handles the problem of data imbalance and reduces the training loss effectively. Different combinations of Gamma values for FTL indicate that higher gamma values do not always indicate better handling of data imbalance because it depends on the degree of data imbalance in your dataset and how effective enforcement would be. The number of filters demonstrates that a greater number of filters always aids the model in learning more characteristics of the datasets, resulting in superior results. However, a large number of filters requires more processing power and time, so there is a trade-off. Experiments also indicate that a smaller number of batch sizes is preferable because the model has less information to learn from at one time and, as a result, does not precisely replicate the entire dataset, resulting in greater generalisation. Aside from hyper-parameters, the analysis indicates that incomparable spatial resolution between spectral and topographical information may not aid the model in learning the topographic information; however, we observed that it reduced false positives caused by riverine sand and built-up in low-lying areas but at the expense of arbitrary landslide boundary on steep slopes. We highlighted that having a small patch size can aid the model in learning spectral features but leaves out the possibility of learning topographic information due to its coarser spatial resolution. The comparison between *VndviSL* and *VndviAll*, indicates that utilising other DEM derivatives than just slope helps the model to learn more topographic characteristics.

In the final predictions, a large number of false positives were observed, although the majority of landslides were accurately detected. Given the similar spectral and spatial characteristics of landslides to other features such as urban areas, riverine sand, unpaved roads, and barren land, landslide detection is a difficult classification problem. *Figure 4.13* is a comparison of spectral profiles from Devikolam, which shows that the spectral signatures of landslide initiation and built-up area are similar, whereas an unpaved road closely aligns with a landslide toe or a small revegetated landslide. In addition, the presence of overhanging trees on the landslide scar prevents the detection of landslides using optical datasets, even when visual interpretation is employed. Even within a single landslide, a great deal of spectral variation can be observed (e.g., the difference in spectral signature between the landslide's initiation, body, and toe), resulting in partial landslide detection or arbitrary boundaries. Moreover, revegetation on landslides prevents landslide detection, particularly in our study area with a tropical wet climate with intense rainfall and high temperature, thereby promoting rapid regrowth of vegetation (Schuster and Highland, 2007).

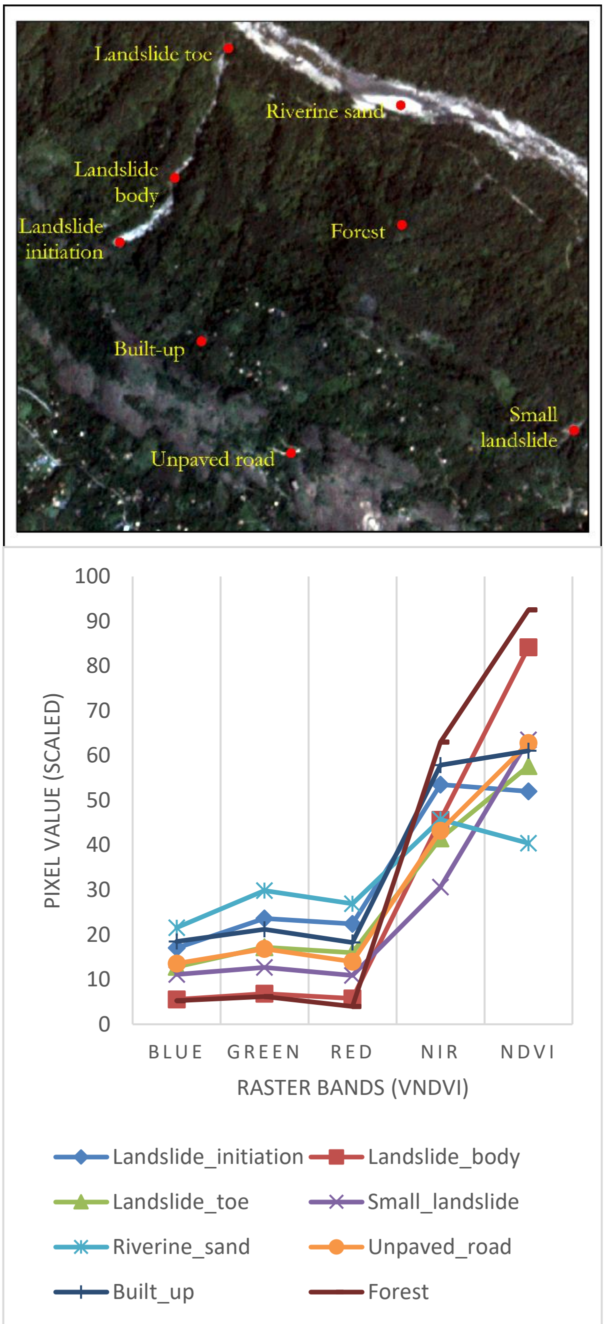

Figure 4.13: Comparing spectral profile of landslides and similar features

Th number of false positives can be reduced by employing DEM derivatives created from similar spatial resolution, as also proposed by Ghorbanzadeh et al. (2019); however, in our case, it was incomparable. Although, problems like revegetation and overarching trees will still be difficult to handle. We discuss more the possible solutions to handle the detection complexity in the recommendation section in chapter 7.

4.6. Chapter Summary

The chapter starts by indicating the purpose of the generation of landslide inventory and providing a background of the inventory generation methods and associated problems. Suggestions from the literature review and understanding of the complexity of having small landslides in the study area, we first experimented with three models and finalised MsaU-Net due to its ability to detect small features with deep supervision and multi-scale input approach together with a customised Focal Tversky Loss for handling data imbalance. We described different datasets and their preparation, training strategy and experimentations. Later, we explained different sets of hyperparameters utilised and their influence on the model performance and overall performance spectrum was presented. Once all the experiments were carried out, we provided top-performing hyper-parameters combinations for *Vndvi* dataset, which were later used to train on the *VndviSL* and *VndviAll*. The performance of the same was compared, and finally, *Vndvi* dataset with the best parameter combination was utilised to predict landslides in the study area. Those predictions were post-processed and more landslides were added in the cleanup process. Lastly, we finalised the inventory in point and polygon format with a total of 864 landslides.

5. PREDICTIVE CAPABILITY EVALUATION

This chapter aims to accomplish the third sub-objective of evaluating the predictive capabilities of landslide susceptibility maps. This is done by comparing the three landslide susceptibility maps with the point and polygon landslide inventories generated from the satellite data and deep learning model presented in the previous chapter. This chapter includes the description of the datasets and their preparation, and presents the evaluation strategy, results, discussion and the chapter summary.

5.1. Datasets and their preparation

Mainly two datasets were utilized in the evaluation process: 1) Landslide susceptibility maps, and 2) Landslide inventories. Landslide susceptibility maps and their map generation process have been described in section 2.3.1. Before the evaluation, these maps were processed in three steps:

1. All the maps were co-projected and clipped to the study area,
2. Since the GSI and KU&MTU maps were in raster format, the NCESS map (Polygon) was also rasterized with the same pixel size as the GSI map (50 m), which had the largest pixel size of the three maps.
3. We observed that NCESS and KU&MTU maps had some unclassified areas; consequently, they cannot be used directly for comparison or evaluation. It would have been even more difficult if the maps had differing numbers of classes. Fortunately, each map had three landslide susceptibility classes. Unclassified areas of the NCESS map had the same meaning as low-class areas on the other two maps, whereas unclassified areas on the KU&MTU map were due to the exclusion of water bodies and areas with gradual slopes after the map was created. All of these regions were categorized as low on the other two maps, so we considered the unclassified regions as low. *Table 5.1* displays the original map classes presented by the producer and the final map classes used for our evaluation. Preparation of the landslide inventory was already described in the previous chapter and is now used in the evaluation process.

Original map classes			Classes finally used as
GSI	KU&MTU	NCESS	
-	Unclassified	Unclassified	Low susceptibility
Low	Low	Low	Low susceptibility
Moderate	Medium	Medium	Medium susceptibility
High	High	High	High susceptibility

Table 5.1: Reconsidered landslide susceptibility map classes

5.2. Evaluation metrics and rationale

Based on the literature, we will describe the commonly used evaluation metrics and the rationale for chosen evaluation metrics here.

The review by Reichenbach et al. (2018) indicates that success/prediction rate curve (PRC) is the most commonly utilized metric, followed by landslide density or frequency (Baeza and Corominas, 2001), receiver operating characteristics (ROC), and other evaluations based on standard confusion matrices. To visualize the performance of a statistically-based quantitative susceptibility model, the receiver operating characteristics (ROC) curves are well-established (Beguería, 2006a; Frattini et al., 2010). They show the proportion of true positives (TP - landslide) correctly predicted against the proportion of true negatives (TN – Non-landslide) incorrectly predicted for all the range of landslide susceptibility values. For a higher proportion of true positives and a lower proportion of true negatives, the curve tends to move towards the top left corner of the ROC diagram. The area under the ROC (AUROC) is calculated to determine the overall accuracy of the map.

Having continuous quantitative susceptibility values is a major requirement for generating a ROC or PRC curve. Once a map had been created and used in planning and decision making, it was classified into three discrete classes: low, medium, and high and serves as the foundation for policies and decisions. Hence, evaluation should also be conducted on the classified map since continuous quantitative values did not play a role in decision-making and planning. Also, the classification of the map is part of the the map-making process, and the classified map is considered the final product on which decisions are made. Therefore, we could not utilise ROC and PRC curves to evaluate the maps, which made the evaluation process more challenging.

We evaluated three classified maps (GSI, KU&MTU, and NCESS) and one unclassified map (KU&MTU), with a special focus on the classified maps. To assess the classified maps, metrics such as landslide density and relative landslide density index (R-index) can be utilised since they do not require continuous quantitative values and can indicate the consistency of landslide distribution for various susceptibility classes (Baeza and Corominas, 2001). Therefore, we mainly utilize density-based indices together with correlation analysis of FoS values (KU&MTU map) with landslide point occurrences, which can give us insight into the classification and predicted FoS values of the map. But, these density-based metrics require evaluation units (same as mapping units), which can be used to calculate densities. All these maps are either pixel-based (ranging from 30m to 50m) or large polygon-based zonations, which cannot be utilized for the calculation of density and are also not geomorphologically meaningful. Therefore, we had to choose suitable evaluation units which could be utilised for density calculations. The rationale for the evaluation units and their generation are described in the next section.

5.3. Evaluation units, rationale and strategy

In this section, we first describe the evaluation units and rationale of the chosen units, followed by the evaluation unit generation workflow and finally, the evaluation strategy explaining three different scenarios.

5.3.1. Evaluation units and rationale

A mapping unit is chosen when generating a landslide susceptibility map. Similarly, evaluation is also performed based on these units, which are referred to here as 'Evaluation units'. Idealistically, it is the smallest meaningful spatial unit in the analysis because each unit is assigned a unique susceptibility value having a unique set of terrain conditions (Beguería and Lorente, 2002). It should closely reflect the topography pertaining to landslide triggering conditions and similar terrain characteristics. *Table 5.2* presents the advantages and disadvantages of different evaluation units. The slope of a terrain is considered to be the most influential factor in landslide triggering, but it is not taken into account in the grid or administrative units, making them less relevant from an evaluation standpoint. Geomorphic units require

Evaluation units	Advantages	Disadvantages
Grid	Easy to process in GIS software, Equal area of evaluation unit, easy to generate, high objectivity	Do not represent similar landslide triggering condition, not related to geology or geomorphology
Administrative	Useful for decision-making and planning, readily available	Usually large size, not related to terrain conditions, assessment may not be reliable
Slope	Good representation of similar terrain conditions, assessment could be reliable	Difficult to generate, shallow slope toes with low landslide triggering potential clustered with steep slope
Unique Condition*	Better representation of similar landslide triggering slope units + angles	Difficult to generate, may introduce many smaller units
Geomorphic	Better representation of terrain features	Manual interpretation required, division of units is subjective

Generated by intersection of slope units and generalized slope classes

Table 5.2: Evaluation units - advantages and disadvantages

expert-level interpretation skills and can be time-consuming; however, they provide more reasonable terrain division.

Slope units can be generated automatically and used to represent generic terrain features, but they can be incorrect if the method is not optimized.

However, in comparison to geomorphic units, these units can be generated in less time for large regions. The fact that slope units define a single slope as a unit composed of a number of slope angles pertaining to differing landslide triggering potential is a major issue. For example, a single slope unit may contain steeper slope angles (e.g., 40 degrees), where landslides initiate, and gentle slopes of valley areas (e.g., 15 degrees), where landslide material accumulates with no potential for initiation. If we aggregate different causal factor values (e.g. mean or standard deviation of planar curvature) in those units, we may introduce significant discrepancies. Therefore, we need to consider different slope angles within slope units, which can be achieved by generating Unique Condition Units (UCUs). Depending on the purpose, unique conditions can be generated in a variety of ways, such as by intersecting slope and administrative units to create a unique set of units that provide favourable landslide-triggering conditions and can be utilized in decision-making due to administrative boundaries. For the purpose of evaluation in this research, we considered unique condition units generated by intersecting slope units and generalized slope classes (<15, 15-35, >35 degrees), which relates to the landslide potential.

5.3.2. Generation of the Unique Condition Units (UCUs)

Since the objective of UCUs was to create evaluation units that can represent slope angles within slope units, the following steps were taken generate them- **Step 1:** Slope unit generation, **Step 2:** Slope class map generation (generalized), **Step 3:** Intersection of slope units with slope class maps and omission of sliver polygons and arbitrary UCUs.

The ALOS Palsar DEM with 12.5 m resolution, downloaded from Alaska Satellite Facility (ASF) was utilized to generate slope units and slope classes as well. Before utilizing the DEM, it was preprocessed with ArcHydrology (fill operation), and NoData values were interpolated using the nearest neighbourhood operation and compared with the SRTM DEM to ensure that it did not contain any significant errors that could compromise the accuracy of our results.

5.3.2.1. Slope unit generation

The slope units (SUs) were generated in GRASS GIS software using the *r.slopeunits* software algorithm developed by Alvioli et al. (2016). To accomplish this, the algorithm uses *r.watershed* module in GRASS GIS, which utilizes DEM to represent terrain morphology by adopting an advanced flow accumulation (FA) area analysis. FA information is used to single out streams and divides, which are the main elements of SU delineation (Carrara, 1988).

The r.slopeunits software requires a DEM and user-defined parameters to delineate the slope units presented in *Table 5.3*. SU1 and SU2 indicate the parameter combinations used to generate two sets of Slope Units: SU1 and SU2. The algorithm utilizes an iterative strategy given by Carrara (1988), which first delineates a small number of large areas (e.g., half basins) and then iteratively decreases the area sizes with respect to streams and divides.

No.	Parameter (s)	Abbrevia.	SU1	SU2
1	Flow accumulation area threshold	thresh	800,000	500,000
2	Minimum area size of SU (square meters)	areamin	40,000	20,000
3	The minimum circular variance of terrain aspect within a slope unit	cvmin	0.4	0.3
4	Reduction factor	rf	10	10
5	A threshold value for the cleaning procedures	cleansize	20,000	10,000

Table 5.3: Parameters values combinations (SU1 & SU2)

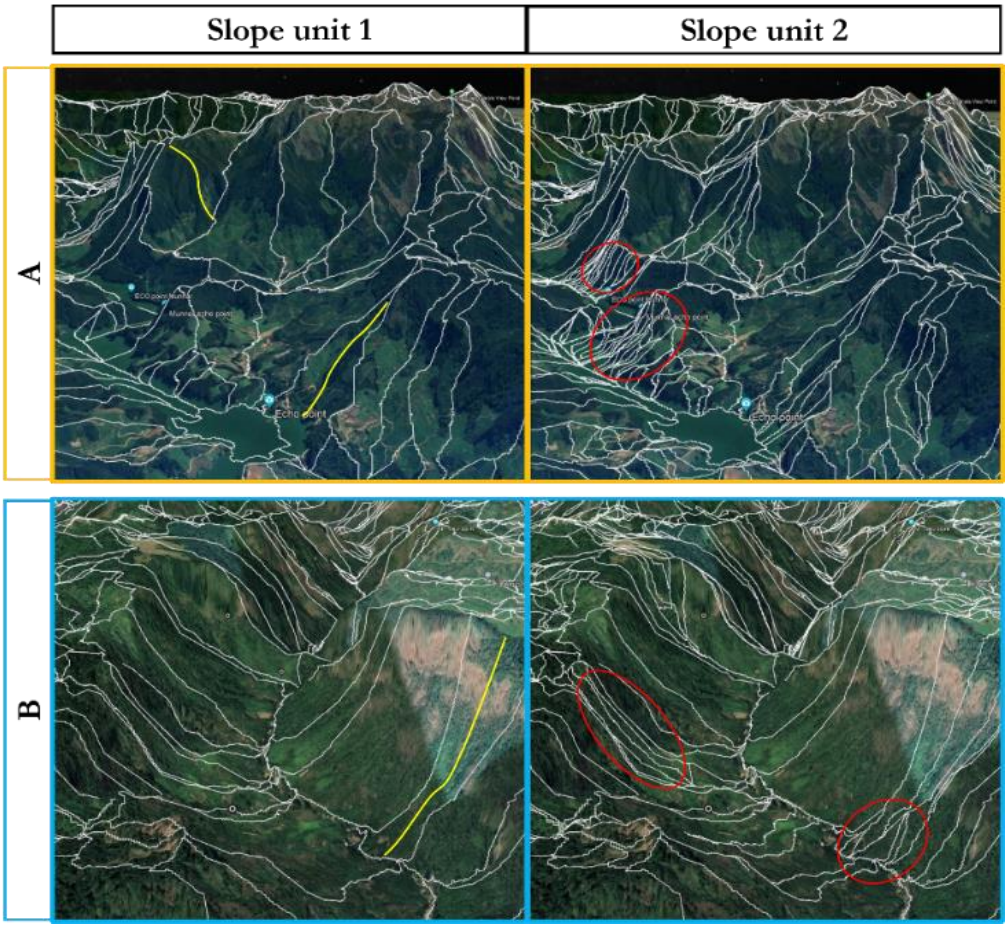

Figure 5.1: Slope units resulting from SU1 and SU2 parameter sets (Example A and B in rows)

In the iterative process, the Flow accumulation area (FA) threshold and reduction factor (rf) regulate the numerical convergence but have no explicit geomorphological meaning. Whereas the minimum area (areamin) and minimum circular variance (cvmin) define the size and regulate the aspect of the SUs. Ideally, experimenting with these parameter combinations is necessary to achieve the optimized slope unit divisions. Unfortunately, the optimization process costs huge computation power and time to run multiple combinations of parameter values, which is a limitation of this approach. Therefore, based on experiments done by Alvioli et al. (2016), we heuristically utilized two set of parameters values to generate SU1 and SU2 (*Table 5.3*). The output of the algorithm is in shapefile vector format, therefore it can be manipulated easily.

SU1 and SU2 were overlaid and compared in Google Earth Pro, which provides high-resolution topographic information. A total of 5300 polygons for SU1 and 11801 polygons for SU2 were generated. As shown in *Figure 5.1*, SU2 exhibited comparatively excessive partitioning of the terrain (red circles) because the parameters circular variance and the minimum area size of SU2 was comparatively lower than SU1 (see *Table 5.3*), which generated arbitrary partitions of the terrain. On the other hand, SU1 was missing some critical terrain divisions (yellow lines), which were manually added; however, these were few in comparison to SU2. As a result, SU1 was chosen for further investigation.

5.3.2.2. Slope class map generation

The next step was to intersect slope units with a slope class map, thus requiring vectorized polygons of classified raster slope angle maps. Therefore, we first calculated slope angles using ALOS DEM (12.5) and classified them into three classes: *Less than 15 degrees*, *15 – 35 degrees*, and *More than 35 degrees*. The classification was based on the distribution of landslides in different slope classes. The largest number of landslides were observed on slopes ranging from 15 to 35 degrees (*Figure 5.3*). The idea was to separate slopes with a higher potential for landslides from slopes with a lower potential for landslides. We observed that 64 percent of all landslides (of a total of 864) occurred in slopes between 15 and 35 degrees, 22 percent in slopes greater than 35 degrees, and only 15 percent in slopes less than 15 degrees.

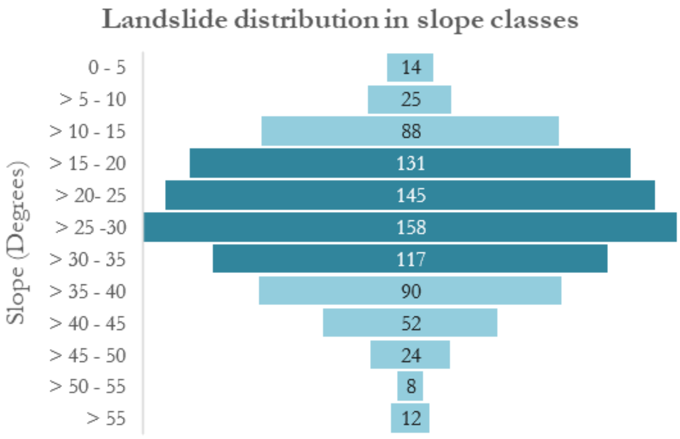

Figure 5.3: Landslide (2018) distribution in slope classes

After the classification of the slope map, a *'salt-and-pepper'* effect[17] was observed in the raster map due to pixel-based threshold-dependent classification. Since the final slope map had to be vectorized, this effect could have generated a large number of small polygons, resulting in a large number of UCUs. Consequently, it was necessary to generalize the classified slope map by minimizing the number of isolated slope class pixels that were mixed with other major classes. We utilized an iterative majority filtering technique implemented in QGIS 3.10, which reduces the number of isolated pixels with each iteration while preserving the majority classes locally. With a total of four iterations with a 5 x 5 majority filter was used. During experimentation, we observed that a 3 x 3 filter required more iterations but still left many isolated pixels, whereas a 7 x 7 filter overgeneralized the raster map in just two iterations, so we chose a 5 x 5 filter. During the filtering process, we lost a significant amount of slope information, which may not be ideal in many situations. However, since the goal of this filtering was to generate a generalized map that can indicate the major slope classes, this technique was deemed acceptable. *Figure 5.2* shows the classified slope map, a visual representation of the majority filter utilized, and

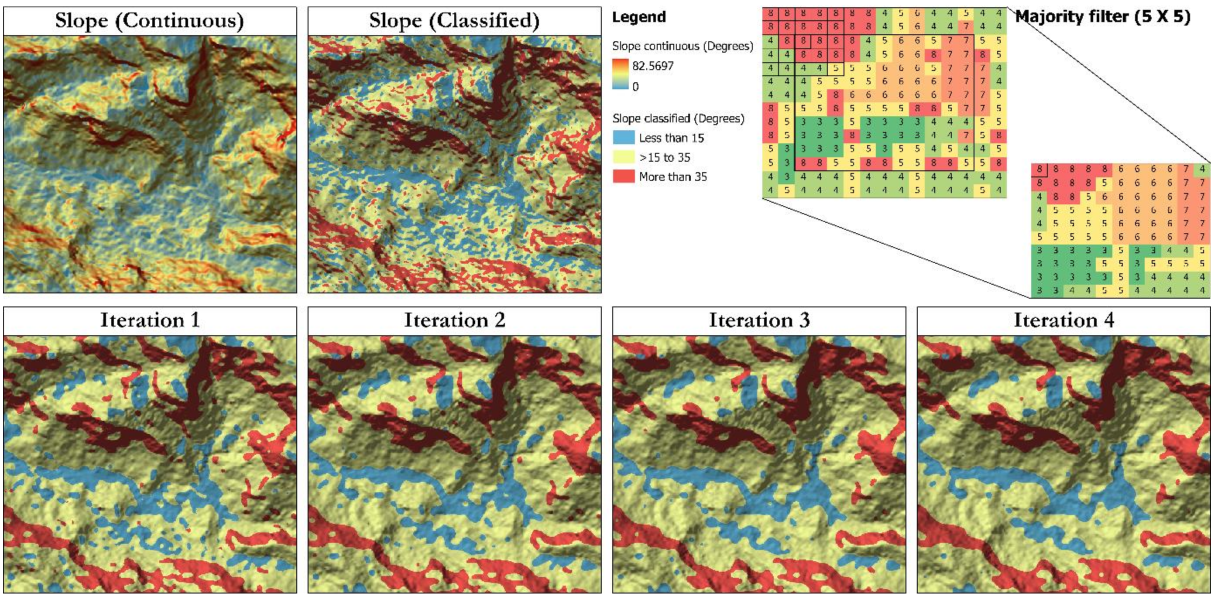

Figure 5.2: Slope map (top left), Slope classified map (top center), Majority filter (top right), Filtering iterations (below)

snapshot of results of each iteration in the bottom part of the figure. It can be observed that the first iteration removed the majority of the isolated pixels from the classified slope map (shown on the top); subsequent iterations smoothed the remaining isolated pixels (shown below). Finally, the generalized slope map was vectorized after the fourth iteration and used for intersection with slope units generated in the previous section.

[17] '*Salt-and-pepper*' effect or raster speckling is a result of significant local spatial heterogeneity between adjacent pixels.

5.3.2.3. The intersection of slope units with slope class maps

The slope unit vector polygons and slope class map were intersected using the overlay operation in the ArcGIS pro software. During the intersection of these two layers, many sliver polygons[18] and arbitrary polygons were generated, and some of these polygons were also generated during the slope unit generation process, which was one of the major challenges of this process. Manually altering or removing these many polygons can be time-consuming and infeasible, so automatic removal was required. These sliver polygons all had one thing in common: they were either very small or narrow-shaped or a combination of the two. These characteristics can easily be captured in order to distinguish them from other polygons by computing the polygon area size and shape attributes. This, however, was insufficient because these polygons needed to be merged with their respective neighbouring polygons in order to form the best possible polygon boundary based on the two polygons.

To achieve the above-mentioned, we performed the following process: firstly, we calculated two parameters of the polygons: 1) Polygon area (m^2), and 2) Polygon circularity. Polygon circularity is given by the equation: **Circularity = 4π × Area/Perimeter²**. The circularity ratio will be 1 for a circle and less than 1 for non-circular shapes. Hence, narrow polygons will have even lower circularity as compared to wide polygons. The following criteria were utilised to select the unfit polygons based on experimentations (in ArcMap SQL expression with a where clause): a) Polygons with Area < 60,000 m^2 AND Circularity < 0.25, b) Area < 20,000 m^2, and C) Circularity < 0.15. These criteria were chosen based on the visual analysis of the polygons by iteratively selecting the polygons in an experimentative manner. After selecting all of the polygons, another visual check was performed to ensure that no critical polygons boundaries were being removed. The selected polygons were merged with adjacent polygons in ArcMap using the "Eliminate selected polygons" tool, which merges the selected polygons with adjacent polygons that share the longest border. *Figure 5.4* shows area (in red) and circularity (in yellow) values labelled for each polygon; polygons selected based on the criteria (Part A) and merged polygons resulting from elimination based on the criteria (Part B). *Figure 5.5* depicts an example of the area and circularity of various polygons selected using the defined criteria. It can be observed that unfit polygons have combinations of low circularity and large area or high circularity and low area. Therefore, these polygons can easily be distinguished and eliminated. As shown in the figures, vectorized boundaries from raster images have undesirable texture (zig-zag boundaries) due to heterogeneity in the pixels, which is unappealing

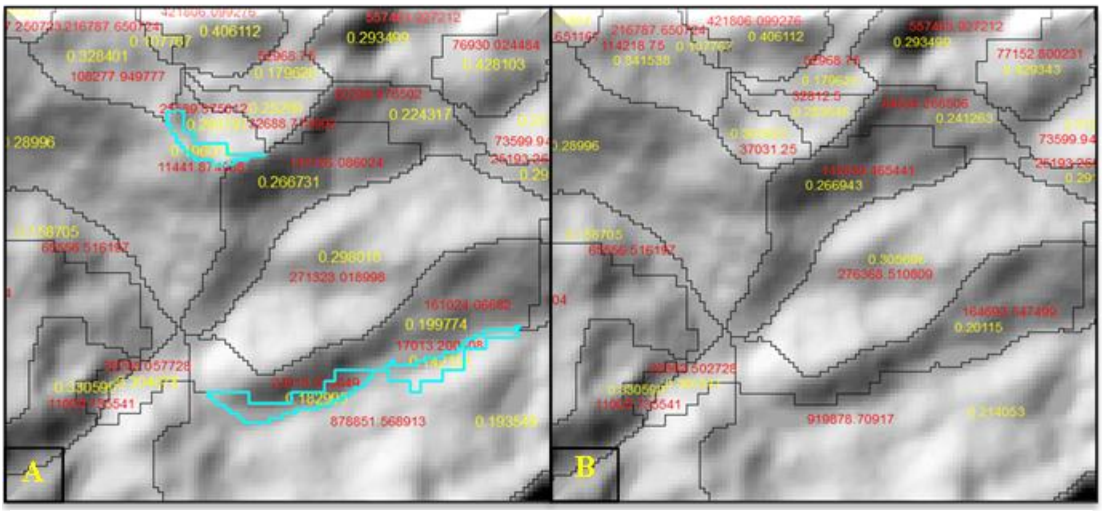

Figure 5.4: A - Selected polygons based on the area (red) and circularity (yellow), B - Selected polygons merged with polygons sharing the longest boundary

[18] Sliver polygons are small or thin polygon features that appear along the polygon edges or borders following an overlay of two or more vector shapefiles.

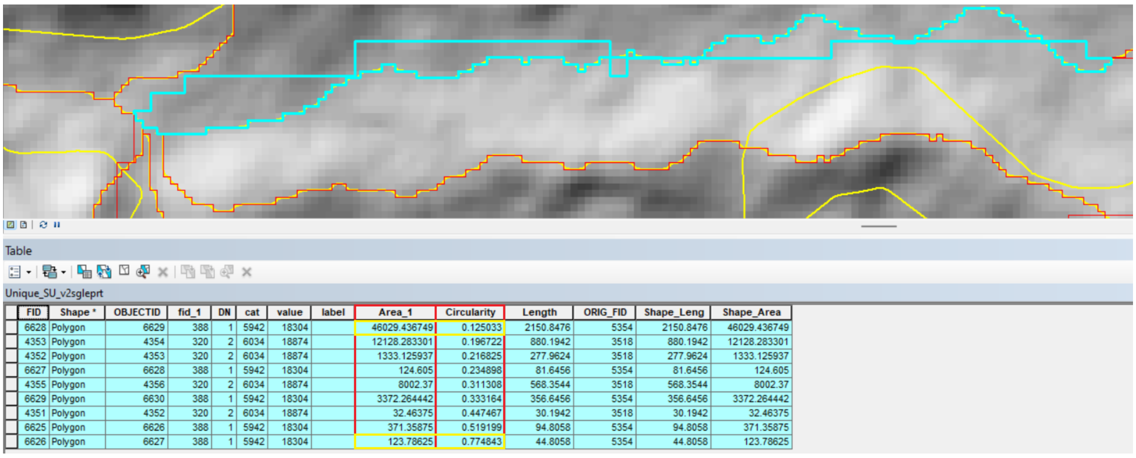

FID	Shape *	OBJECTID	fid_1	DN	cat	value	label	Area_1	Circularity	Length	ORIG_FID	Shape_Leng	Shape_Area
6628	Polygon	6629	388	1	5942	18304		46029.436749	0.125033	2150.8476	5354	2150.8476	46029.436749
4353	Polygon	4354	320	2	6034	18874		12128.283301	0.196722	880.1942	3518	880.1942	12128.283301
4352	Polygon	4353	320	2	6034	18874		1333.125937	0.216825	277.9624	3518	277.9624	1333.125937
6627	Polygon	6628	388	1	5942	18304		124.605	0.234898	81.6456	5354	81.6456	124.605
4355	Polygon	4356	320	2	6034	18874		8002.37	0.311308	568.3544	3518	568.3544	8002.37
6629	Polygon	6630	388	1	5942	18304		3372.264442	0.333164	356.6456	5354	356.6456	3372.264442
4351	Polygon	4352	320	2	6034	18874		32.46375	0.447467	30.1942	3518	30.1942	32.46375
6625	Polygon	6626	388	1	5942	18304		371.35875	0.519199	94.8058	5354	94.8058	371.35875
6626	Polygon	6627	388	1	5942	18304		123.78625	0.774843	44.8058	5354	44.8058	123.78625

Figure 5.5: Example of selected polygons based on their selection attributes

aesthetically and makes vector processing time-consuming. We smoothed the polygon boundaries as part of the cleaning procedure, with a smoothing tolerance of 5 meters given the resolution of the ALOS DEM (12.5 m) on which the slope units and slope class map are based. As the final unique condition units, 11661 vector polygons were generated. We propose that these unique conditions units can be used not only as evaluation units but also as mapping units for landslide susceptibility mapping. *Figure 5.6* presents the finalized UCUs, which present slope units interesected with slope classes. It can be seen that slope units having gentle slopes (slope <15^0) have been separated from moderately steep (slope 15^0 -35^0) and steep (slope >35^0) slopes. This highlights the issue with slope units, as they do not deal with different slope angles, making them less efficient, given that moderately steeper slopes have more potential than gentle slopes.

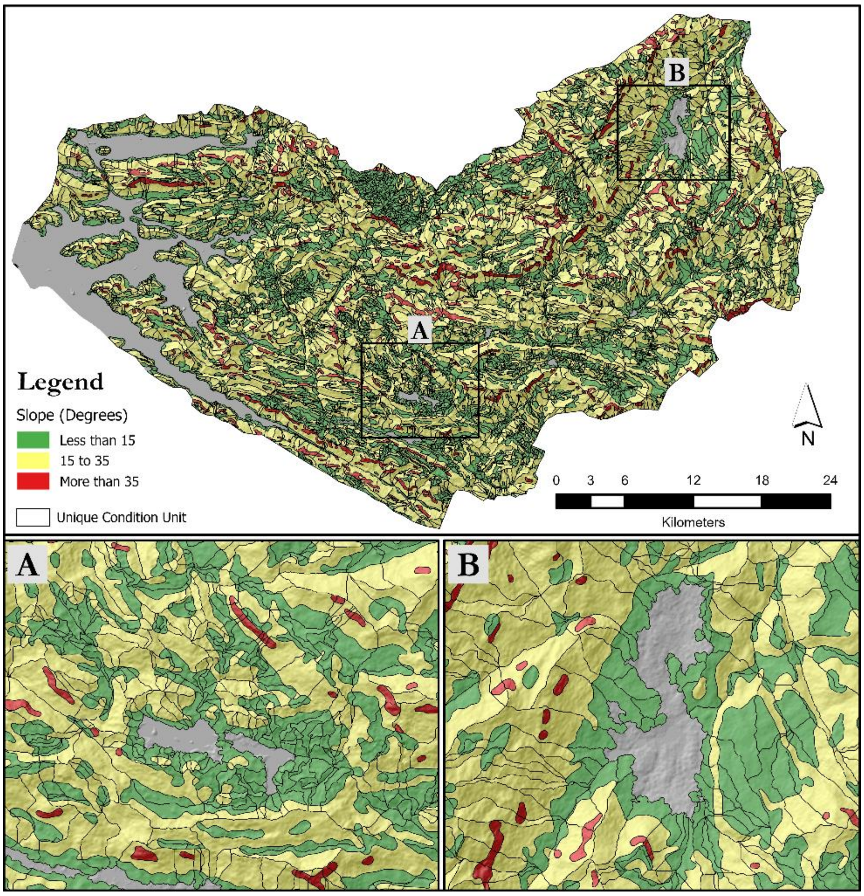

Figure 5.6: Finalized Unique Condition Units (UCUs)

5.3.3. Evaluation strategy – Three evaluation scenarios

Our evaluation strategy consisted of three evaluation scenarios, 1) Overall evaluation, 2) Evaluation based on Unique Condition Units (UCUs), and 3) Comparative evaluation.

5.3.3.1. Scenario 1: Overall evaluation

Figure 5.7 depicts the workflow of scenario 1, in which the landslide susceptibility classes of the maps were considered as evaluation units. These evaluation units or susceptibility classes of each map were intersected with the landslide initiation points and polygons. The number or areas of landslides falling into each unit was aggregated. These numbers were simply used to calculate two metrics: 1) Landslide density and 2) Relative landslide density index (R-index) (Baeza and Corominas, 2001).

$$\textit{Landslide density} = \frac{\text{number or area of landslides in Class a } (n_i)}{\textit{total area of Class a } (\mathrm{N}_i)}$$

$$\textit{Relative landslide density} = \frac{\left(\frac{n_i}{\mathrm{N}_i}\right)}{\sum\left(\frac{n_i}{\mathrm{N}_i}\right)} \times 100$$

Where, n_i is the percentage of landslide number or area observed within a susceptibility class and N_i is the percentage of area for the landslide susceptibility class.

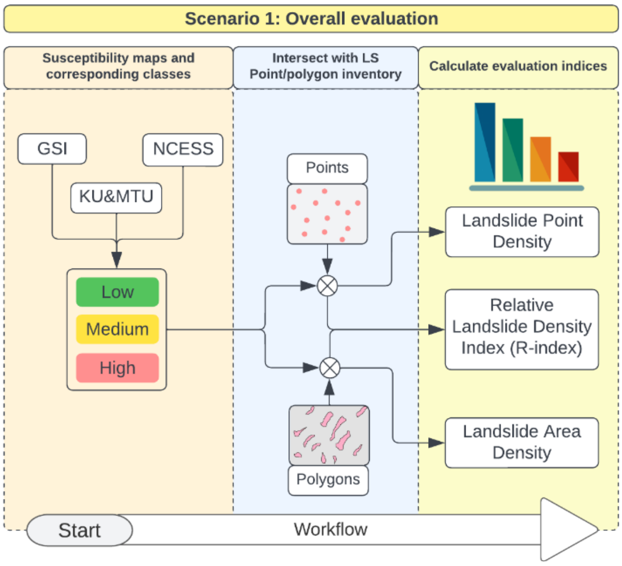

Figure 5.7: Scenario 1- Overall evaluation

5.3.3.2. Scenario 2: Evaluation based on Unique Condition Units (UCUs)

Figure 5.8 present the workflow of scenario 2, in which the evaluation was performed in comparatively smaller units, i.e., Unique Condition Units (UCUs), with the following three steps- **Step 1:** calculation of landslide density in each UCU, **Step 2:** aggregation of susceptibility classes and in each UCU, **Step 3:** a violin plot and correlation analysis using point and area densities. In **Step 1**, the landslide point and area densities were calculated for each UCU. In **Step 2**, for the classified maps, a majority vote was taken for landslide susceptibility classes (low, medium, and high) for each map (GSI, KU&MTU, and NCESS) in all UCUs. For the unclassified map of KU&MTU, a minimum a factor of safety (FoS) was taken for each UCU, as it represents the highest unstability within that UCU. Other aggregations, such as mean and median, cannot be used because they do not accurately reflect the stability of the region and can be misleading. In **Step**

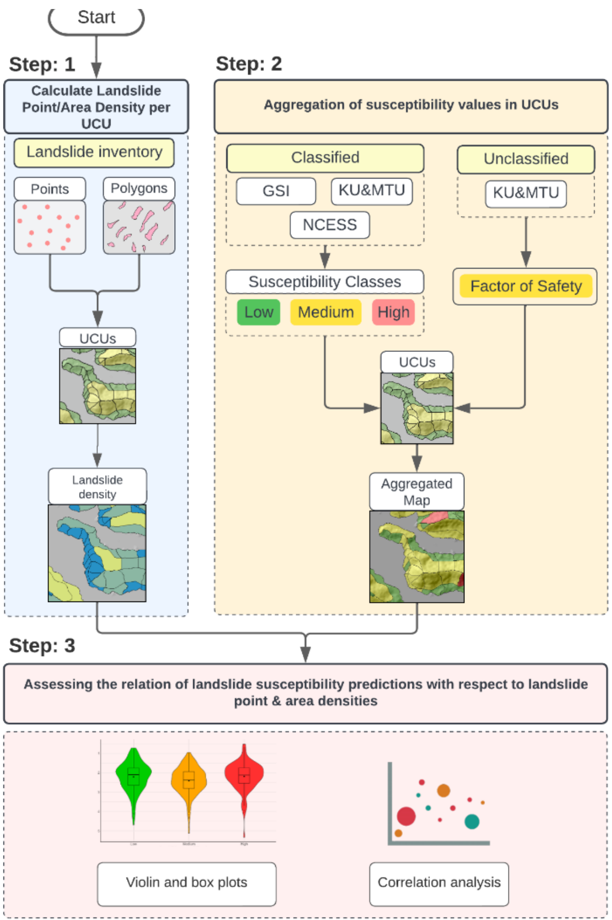

Figure 5.8: Scenario 2 - Evaluation based on unique condition units (UCUs)

3, we did violin plot and correlation analysis in R using the datasets generated above.

5.3.3.3. Scenario 3: Comparative evaluation of the landslide susceptibility maps

For the comparative evaluation, we compared maps with various map combinations and compared two maps with similar features. *Figure 5.9* shows the workflow of comparative evaluation of the landslide susceptibility maps. The following steps were taken: **1)** Rasterization and resampling of all the maps, **2)** Combine all the maps by sampling pixel values for each map, **3)** correlation and covariance analysis together with contingency bar plots for prediction pixel comparison.

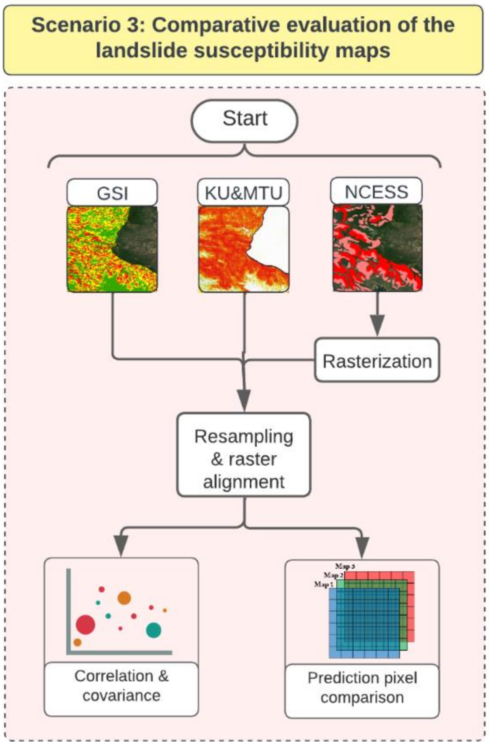

Figure 5.9: Scenario3 - Comparative evaluation of landslide susceptibility maps

Since all maps are generated for the same region, susceptibility must be represented similarly throughout the region. This enables us to evaluate the degree of agreement and discord between the three maps. For the comparison, each map was converted to the same datum and projection (WGS 84 & UTM 43N), data format (raster), and spatial resolution (50 m) using the ArcMap nearest neighbourhood operation. We recognize that some information may have been lost during this process, but the overall map values are representative of the actual values, especially when using the nearest neighbourhood resampling method.

Once all the maps were prepared, the susceptibility classes were given values from “1 to 3” for “Low to High” classes. These values were utilised for correlation and covariance analysis in ArcMap software. These maps were further utilised to generate contingency bar plots for overall comparison as well as comparison of two maps with similar features.

5.4. Results and discussion

5.4.1. Scenario 1: Overall evaluation

Firstly, we present an overview of landslide distribution together with the percentage of area under different classes. Secondly, we compare the landslide point and area densities. Thirdly, we present the relative landslide density (R-index).

Figure 5.10 compares the class area percentage with the percentage of landslides falling in those classes. NCESS map shows a concerning trend since around 60% of the landslides are falling in the “Low” class accounting for 65 % of the total map, while this class might have been considered “safe” in decision-making for the past ten years. In contrast, GSI and KU&MTU maps present relatively reasonable landslide distribution. Yet, 32% of the landslides are falling in the “Low” class of KU&MTU, which is still a considerable number. Almost half of the landslides on the GSI map are classified as "Medium," accounting for nearly 40 percent of the map. Already, the interpretation of classes of landslide susceptibility classes is unclear because it is unknown what can be anticipated in each class in terms of the number of landslides or expected

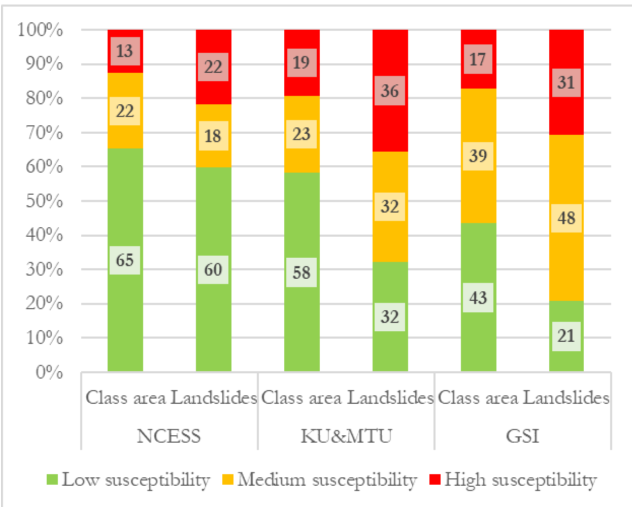

Figure 5.10: Distribution landslide (%) by susceptibility class area (%)

losses. The combination of ambiguous interpretation and such predictions will make decision-making difficult because if 50 percent of landslides are classified as "Medium," what kinds of activities can be permitted based on such a general forecast? Comparatively, KU&MTU map provides a better distribution of landslides, however, cannot be directly employed in decision-making given that 32% of the landslides still fall in "Low" class. Idealistically, a map having almost 10% of landslides in "Low", 25% of landslides in "Medium", and the remaining 65% of the landslides in "High", could be more useful for planning decision-making. However, making such a good prediction is expected, but the absence of high-quality datasets, i.e., high-resolution DEM, and a complete landslide inventory, makes it a difficult task (van Westen et al., 2006b). Yet, maps tending to predict such a landslide distribution should always be preferred.

Figure 5.11 depicts the absolute area and density of points on maps of landslide susceptibility. All the maps depict increasing landslide densities in proportions that vary. The increasing trend of densities suggests that these maps present consistent susceptibility levels overall but unacceptable densities of the area and point density. For instance, the "Low" class of the NCESS map displays a landslide point density of 0.45, which corresponds to one landslide every 2 km². In contrast, the KU&MTU and GSI maps have a point density of 0.70 and 0.60 for the "Medium" class, respectively, indicating that there will be nearly two landslides every 3 km² according to both maps, which is quite unexpected for a "Medium" class. Comparable observations can be made regarding area densities as well. Therefore, these maps cannot even be used for regional-scale planning (1:30,000), and we strongly advise against using them for large-scale planning (1:10,000).

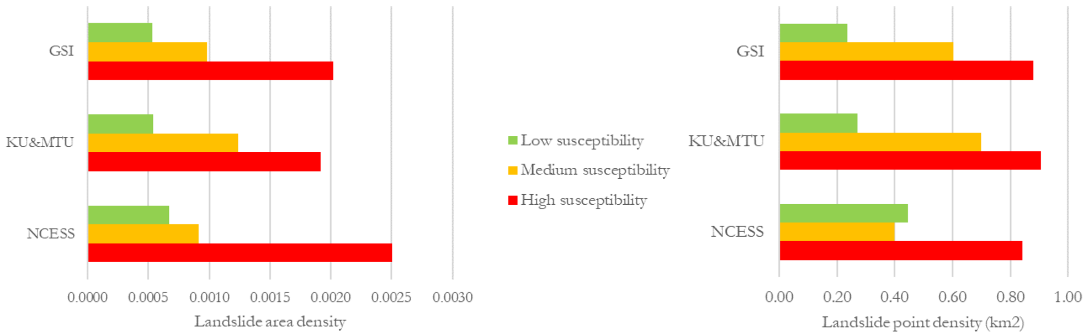

Figure 5.11: Landslide area and point densities

Figure 5.12 present the results of the relative landslide density index (R-index). A detailed calculation table for landslide area and point density, and R-index can be found in **Annexure 4**. The R-index for landslide points and area follows an increasing trend for all the maps from low to high susceptibility class, which is considered ideal for any map (Baeza and Corominas, 2001); since the index represents the ratio between the density of landslides in a given susceptibility class and the overall density of landslides. This metric allows us to compare the point and area distribution of landslides across different maps, but it cannot be used to present the likelihood of an element-at-risk being hit by a landslide. A larger ratio indicates higher susceptibility relative to the region's overall susceptibility. Notably, R-index values for both points and areas are remarkably similar for GSI and KU&MTU maps with an average difference of 4% per class, indicating consistent susceptibility levels and a general agreement between these maps and the distribution of landslides across different classes. However, it can also be observed that the "Medium" class of GSI &MTU exhibit almost 30-35%

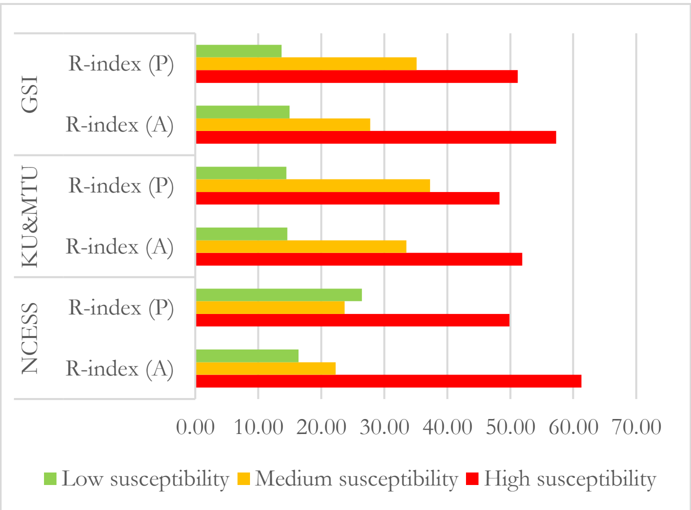

Figure 5.12: Relative landslide density Index for landslide points (P) and area (A)

susceptibility to the overall susceptibility of the maps for both point and area densities. Similarly, the "high" class exhibit almost 50% susceptibility to the overall susceptibility of almost all the maps.

It can be concluded that the overall distribution of landslides within susceptibility classes demonstrates a positive correlation; however, the distribution levels may not be acceptable for a particular purpose. Therefore, we propose that the map classifications be revised or reevaluated so that the majority of landslides can be predicted as in "High" class. KU&MTU and GSI maps provide generic predictions, particularly for the "Medium" class; consequently, classification or the analysis itself must be reconsidered. The NCESS map has been used as it is, mainly for land-use planning and restrictive zoning for the past ten years. The analysis present that this map should no longer be utilised for administrative purposes. This also begs the question of how long a map can be used for landslide prediction after its creation. The discrepancies can be attributed to the limitations of the map, such as coarse resolution datasets, generalized classes of factor maps, limited GIS software availability, and large grid size (250 m).

5.4.2. Scenario 2: Evaluation based on UCUs

Figure 5.13 depicts violin and box plots of landslide area and point densities calculated in UCUs for the susceptibility classes of all maps. Area density and point densities for the maps are presented in rows, in the order GSI, KU&MTU, and NCESS. Violin plots illustrate the probability distribution function (PDF) for landslide densities within each class, allowing us to highlight the most frequently observed densities in a particular class or its distribution as a whole. Given the small landslide sizes (total landslide area 1.70 km^2) and the low landslide density (864 landslides in 1200 km^2), the plots are presented on a logarithmic scale. Additionally, small differences in landslide densities are significant given the size and quantity of landslides. The boxplot inside the violin plot shows an average (black point), the median (centerline), 25^{th} and 75^{th} quartile (upper and lower blackline) and minimum and maximum (ends of the vertical black line) of the data series. Wider sections of the violin plot indicate a higher probability that a susceptibility class will have the given density, whereas narrower sections indicate a lower probability. Thus, violin plots are suitable for illustrating the PDF for landslides alongside quartiles of the datasets. Ideally, the landslide area or point density of landslides should increase from low to high class, and there should be little to no overlap between the landslide densities between the susceptibility classes. A clear distinction should be observed within the map.

Figure 5.13 displays violin and box plots for landslide densities across all maps. First, the plots reveal no statistically significant differences between the maps' distributions of landslide area and point densities. Greater density overlap indicates that there is no discernible difference in susceptibility between classes. *Figure 5.13 – A* depicts the plots for the GSI map, which demonstrates comparable area densities for the "Low" and "High" classes and relatively lower area densities for the "Medium" class. This confirms the findings of our previous evaluation, in which we identified issues with the "Medium" class. Close examination of the KU&MTU map reveals an increase in median landslide area density from low to high class, indicating a positive correlation (*Figure 5.13 - C*). The "High" class of the map has a wider, denser violin plot section. At the same time, it is concerning to observe a significant number of maps with high area densities in the "Low" classes. *Figure 5.13 – E* depicts a normal distribution of area densities in the "High" class, whereas a greater concentration of higher area densities is visible in the "Medium" class of the map. *Figure 5.13* – B, D, and F illustrate a highly variable distribution of landslide point densities across all classes without any discernible trend. For the GSI and NCESS maps, a decreasing trend is observed, but point densities are completely dispersed, whereas the KU&MTU map reveals no correlation between point densities and susceptibility classes.

The calculation of landslide area densities is complicated by the fact that even the smallest portion of the landslide that falls in each unit contributes to the density calculation of that UCU. In any case, area densities are always preferred over point densities because point densities do not account for the size of the landslides and do not indicate the likelihood that an object will be struck by a landslide. Obviously, a susceptibility map does not indicate the magnitude of a landslide, but it should indicate the likelihood of a landslide striking a single location. Landslide (initiation) point locations that fall within a specific UCU contribute to its point density calculations, even if the entire landslide (other than the initiation) falls within a different UCU, introducing inaccuracies. In addition to the inability of the maps to distinguish between high and low landslide densities based on susceptibility classes, the aforementioned issues may also explain why landslide point densities exhibit no discernible trend.

In conclusion, comparing all the three maps based on the distribution of area densities for the susceptibility classes, KU&MTU map presents a relatively better relationship or consistent susceptibility levels. The medium class of the GSI map show inconsistencies in scenario-1 and 2 as well. Nonetheless, none of the classes shows a significant expected relationship between landslide densities and susceptibility classes. Ideally, it is expected that "High" class will have relatively higher landslide densities, followed by "Medium" and "Low" classes. As "Low" class is interpreted as "safe", it should have little to no landslide density. However, there are no standard criteria for expected landslide densities for landslide susceptibility maps.

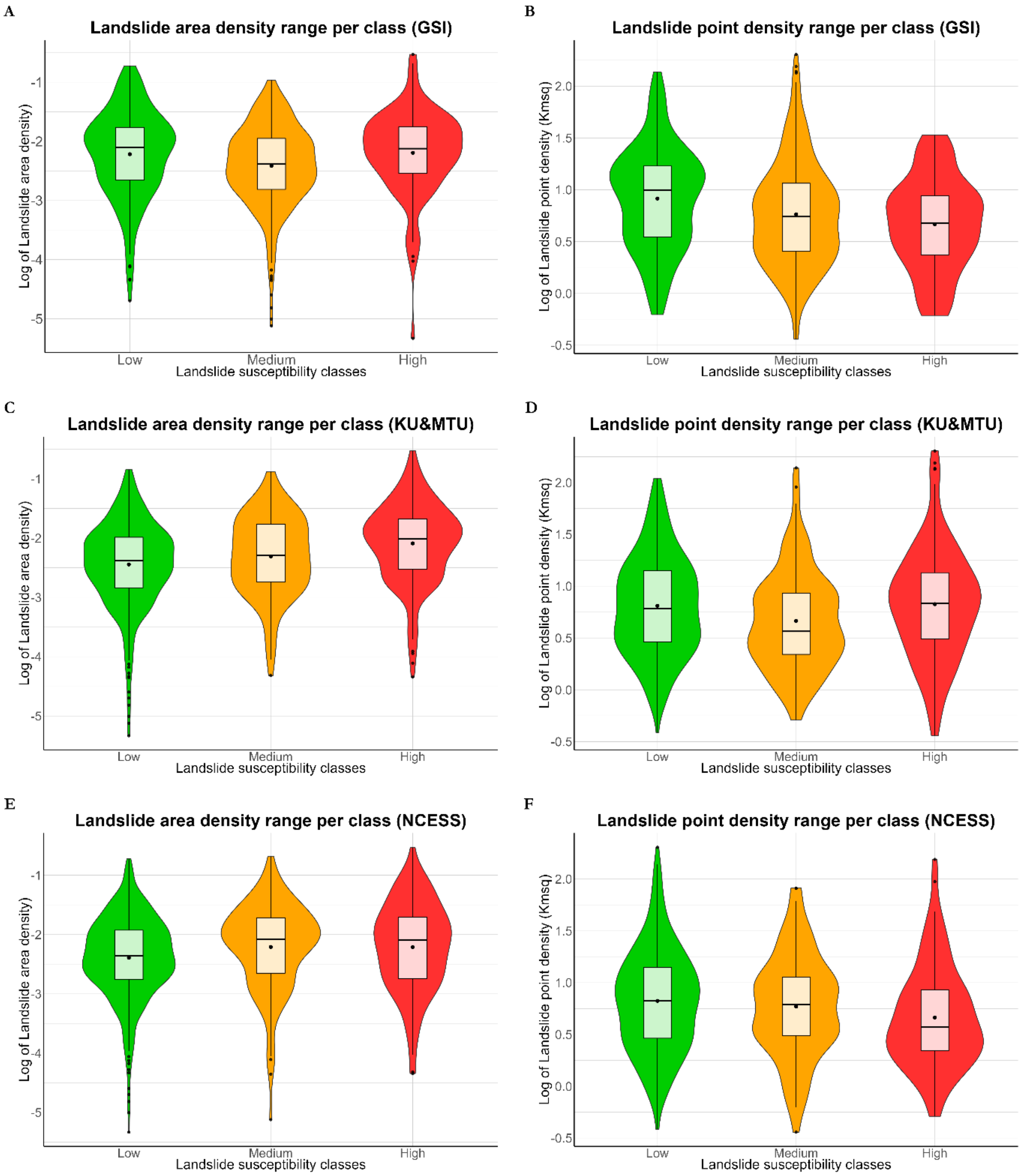

Figure 5.13: Violin plots for all the maps for landslide point and area densities

5.4.3. Scenario 3: Comparative evaluation of the landslide susceptibility maps

In the first section, we compare maps pixel-by-pixel and analyze their spatial correlation and covariance. We compare GSI and KU&MTU maps in greater detail in the second section due to their similarity in terms of mapping units and generation year.

5.4.3.1. Overall comparison

Figure 5.14 depicts a pixel-by-pixel comparison, indicating a comparison of all maps, as well as three other map combinations. As expected, there is a low agreement between all classes when comparing all of the maps simultaneously. For all maps, "Low" class agreement is greater than that of "Medium" and "High" classes, which have a negligible agreement. This suggests that all three maps predict the same region with varying susceptibility levels and that at least one of the three predictions made by the maps is inaccurate at each pixel. If we make a one-to-one comparison of the maps, the map combinations involving NCESS map present a lower agreement, whereas, GSI-KU&MTU map combinations present the highest agreement in all classes. Apart from their ability to predict similarly, it could also be beause of their pixel-based mapping unit which were generated in recent years, whereas NCESS map was a polygon-based map and was generated in the year 2010, when advanced GIS tools were not available and relatively low quality datasets were available. It should be noted that because we are examining the maps on a pixel-by-pixel basis, even the most random agreement between the three maps is being considered. Possibly, if we compare them on a coarser scale, the disparities will be even greater. If these three maps are presented to a decision maker, it would be extremely difficult to choose one.

The covariance matrix and correlation matrix for the GSI, KU&MTU, and NCESS maps are shown in *Table 5.4*. The covariance matrix contains variance (in bold) and covariance values. The variance is a statistical measure that shows the amount of variation within in a map, whereas covariance is a measure that expresses the variation of pixel values in two raster maps. It represents the maps' joint variation to the common mean of pixel values. Correlation matrix gives the correlation coefficients between the each combination of two maps.

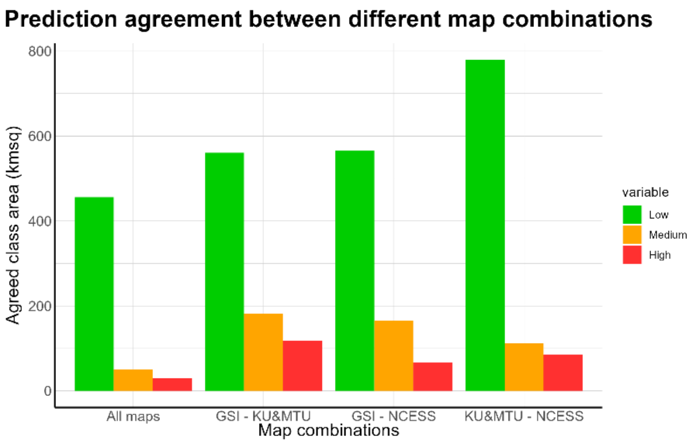

Figure 5.14: Prediction agreement between the three susceptibility

Covariance matrix			
Map	GSI	KU&MTU	NCESS
GSI	**0.28**		
KU&MTU	0.10	**0.33**	
NCESS	0.05	0.08	**0.27**

Correlation matrix			
Map	GSI	KU&MTU	NCESS
GSI	1.00		
KU&MTU	0.32	1.00	
NCESS	0.19	0.28	1.00

Table 5.4: Covariance and correlation matrix for the three maps

The correlation matrix reveals that all map combinations are positively correlated, with the strongest correlation being between GSI and KU&MTU (0.32), followed by KU&MTU and NCESS (0.28), and finally GSI and NCESS (0.30). (0.19). Which validates the conclusion from the pixel-by-pixel comparison that GSI and KU&MTU have the highest degree of agreement. However, the consensus remains extremely low. A correlation of 0.28 between KU&MTU and NCESS is the result of greater "Low" class aggreement. Similarly, we observe that covariance exhibits a similar trend; however, covariance values are interpreted according to the unit used to calculate them. Here, the amount of co-occurring change for the class values of the two maps is displayed. The covariance is the amount of change in class value. KU&MTU - GSI had the highest covariance of 0.10, followed by KU&MTU – NCESS (0.08), and GSI -NCESS (0.05). Which reconfirms the previous findings of the evaluation.

5.4.3.2. Comparing GSI and KU&MTU maps

Predictions may differ from one map to the next, but identifying the areas where they differ the most, can highlight the areas for improvement. *Figure 5.15* presents a prediction variation map based on UCUs and contingency bar plot showing the change of one class to another. The figure presents three types of prediction variations: **1)** Identical predictions, **2)** significantly different predictions, and **3)** predictions with some variations.

Identical predictions are those with exact same prediction in both the maps e.g., "*Low*" to "*Low*". Signifiantly different predictions are those with class rank difference of atleast two classes e.g., "*Low*" to "*High*", "*High*" to "*Low*", and these are the most concerning predictions. Lastly, predictions with some variations are those having a class rank difference of one, e.g., Low to Medium, High to Medium. In the end, we located areas on the map where significant differences were observed.

Figure 5.15 shows that the majority of the areas have been predicted identically, particularly for the "Low" class with 32% of total area, while only 7% and 11% are agreed for the "Medium" and "High" classes, respectively. Almost 10% of the area has a significant difference in predictions, and at a location, either map is inaccurate. Nearly forty percent of the map displays variations, which is also a disagreement but on a lesser scale. Nonetheless, sufficient to confuse the decision makers. This raises the question of whether a specific class of landslide susceptibility (e.g., high) indicates the same thing on two different maps. If not, then how much difference is there in their susceptibility levels and how can it be quantified beyond its relative interpretations? This raises the previously posed question of what these classes mean in terms of the expected number of landslides or losses.

Type	Class variation	Class area (%)
Identical predictions	Low_to_Low	31.81
	Medium_to_Medium	10.33
	High_to_High	6.70
Significant difference	Low_to_High	5.50
	High_to_Low	4.48
Some variations	Low_to_Medium	6.17
	Medium_to_High	6.92
	High_to_Medium	6.00
	Medium_to_Low	22.10
	Total	100.00

Table 5.5: Percentage of prediction variations from KU&MTU to GSI

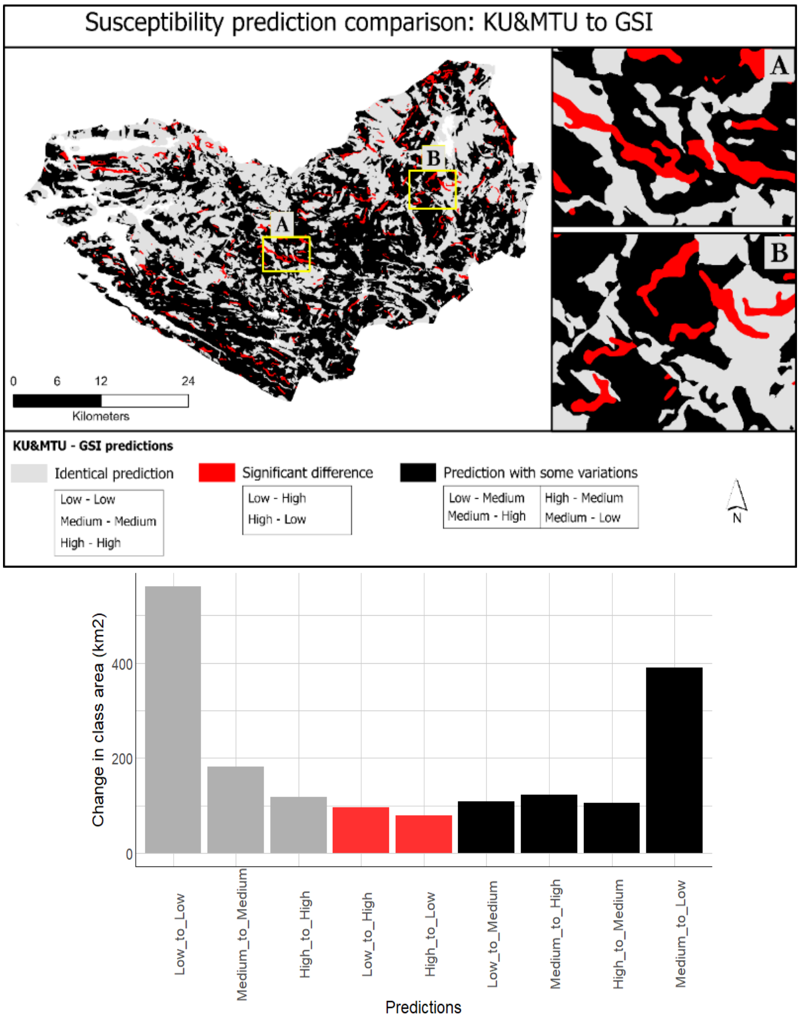

Figure 5.15: Susceptibility prediction comparison: KU&MTU to GSI map

5.5. Chapter Summary

We mentioned that evaluation should be conducted on the classified map, as decisions are dependent on the classification. Nonetheless, this does not preclude the evaluation of continuous maps whenever they are available. Especially when evaluating classified maps posteriorly, it can be difficult to establish a correlation between them and actual landslide occurrences because the scope of quantitative assessment decreases exponentially and qualitatively establishing a correlation is challenging due to the discrete classes. Another difficulty is the evaluation unit used in the evaluation procedure, which is analogous to the mapping unit used in map generation. We propose that the Unique Condition Units (UCUs) generated by crossing slope units and generalized slope classes be used, given the varying susceptibility within slope units with varying slope angles. However, the slope units themselves must be optimized by experimenting with various algorithm parameters. Simultaneously, evaluation metrics are already scarce, but they become even scarcer when evaluating classified susceptibility maps. For instance, we could not utilize the area under the receiver operating characteristics due to the absence of continuous susceptibility values in classified maps, which prevented their application.

We evaluated the maps in three distinct scenarios; Scenario-1 revealed that the maps present overall consistent susceptibility levels, but those levels may not be acceptable to the decision-makers. Scenario-2 indicated that the consistency could not be observed for individually defined units or did not present a strong relationship. This implies that evaluations should be conducted in various units (susceptibility classes, districts, UCUs) to present the degree to which the map provides reasonable accuracy at different scales. For example, GSI and KU&MTU maps can be used to allocate funding based on their overall consistent susceptibility levels after reconsidering classification. However, they cannot be used for urban planning at the UCU scale because they do not demonstrate a strong relationship between landslide densities and susceptibility levels in the UCUs. Area densities demonstrated a stronger relationship between susceptibility and densities than point densities, as area densities consider the number of failed pixels in a given unit, whereas point densities consider each occurrence as a single number, regardless of the number of failed pixels in that unit. Scenario-3 presented that higher agreement can be achieved for areas classified as “Low”, whereas there are significant differences for “Medium” and “High” classes. It also implies that at a location, at least one map prediction is inaccurate. This scenario highlighted the problem of varying interpretation of susceptibility classes and unclear interpretation in terms of expected landslide numbers of losses.

In three of the scenarios, we discovered that none of the maps had reasonable accuracies. We demonstrated that the NCESS map is no longer useful for its intended purpose and should not be used in practice. The KU&MTU map provided slightly better predictions for Scenarios-1 and 2, but not enough to make a decision. We identified issues with the GSI map's medium susceptibility class due to landslide density overlap with other classes and prediction overlap with other maps, and thus the classification can be revised. Furthermore, bodies of water may be excluded, and a new classification system must be implemented.

6. LANDUSE/COVER CHANGE AND PREDICTIVE CAPABILITY

This chapter addresses sub-objective 4 which attempts to answer "*If landuse/cover changes can thwart the predictive ability of the landslide susceptibility map?*". Which means that an area predicted to be low-susceptible or medium susceptible experienced a large number of landslides due to significant landuse/cover changes that altered the region's susceptibility between the creation of the map and the occurrence of landslides. Given the landcover changes, any decisions made regarding land use planning and restrictive zoning based on these maps may be unjustifiable. Therefore, assessing the possible landuse/cover changes after map creation and landslide occurrences would be relevant. A fieldwork investigation was conducted in February-March 2022 to observe the influence of LULC changes on the landslide occurrences in the study area.

First, we provide a background on literature that attempts to establish a relationship between landuse/cover change and landslide occurrences. Second, we describe the fieldwork investigation, which will be referred to in several sections, together with supporting literature to highlight the challenges in establishing such a relationship. Thirdly, we present a case study highlighting the importance of landuse/cover changes. Finally, we present the discussion section and summary of the chapter.

6.1. Landuse/cover change and landslides occurrences: A review

Anthropogentically induced land use, and land cover (LULC) changes such as unregulated building and road construction (Karsli et al., 2008; McAdoo et al., 2018; Hürlimann et al., 2022), forest logging (Jakob, 2000), hill cutting (Rahman et al., 2017), mining (Fathi Salmi et al., 2017), and other unsustainable land-use practices are known to contribute to slope instability (Glade, 2003a; Reichenbach et al., 2014). Therefore, LULC changes should not be overlooked in the landslide risk reduction strategies, specifically in the context of adapting sustainable natural hazard risk management (Promper et al., 2015). These human-induced LULC changes can have hydrological and mechanical effects on the slope. For example, vegetation significantly alters soil hydrology by increasing rainfall interception, infiltration, evapotranspiration, and soil mechanics through soil reinforcement and slope loading (Beguería, 2006b). Hence, vegetation removal will reduce the terrain's stability in most cases (sometimes not, e.g., slope loading by timber may increase the probability of failure)(Beguería, 2006b).

Numerous researchers associate landslide occurrences with LULC changes. An evidence-based study of historical landscape dynamics in New Zealand (Glade, 2003a) investigated geomorphic evolution resulting from anthropogenic LULC changes. Some studies assessed the effect of LULC changes on the landscape of the Pyrenees and found that vegetation recovery could reduce the frequency of shallow landslides (Beguería, 2006b; Shu et al., 2019). Similarly, Schmaltz et al. (2017) confirmed the findings by utilizing multi-temporal landslide inventories based on remote sensing data in Austria. Persichillo et al. (2017) and Gariano et al. (2018) focused on the effect of agricultural activities and land management on triggering regional landslides in Italy by utilizing heuristic and multivariate approaches, respectively. Other studies utilised process-based stability models to assess the impacts of modelled future LULC changes on the Spatio-temporal probability of landslides (Reichenbach et al., 2014). Despite utilising varying methods, all the studies indicated that LULC changes could influence the propensity of hillslopes to landslides. When addressing the issues of slope failures, it is crucial to obtain dynamic information on land use and land cover in a timely and precise manner.

6.2. Field investigation for LULC changes and landslides

Thirty-seven landslide locations were visited in the Munnar region of Devikolam taluk to investigate the influence of LULC changes on landslide occurrences. *Figure 6.1* presents the distribution of landslides visited during the fieldwork, indicated with observed LULC on the ground. *Table 6.1* presents number of landslides with observed LULC on the ground and their predictions by the three landslide susceptibility maps.

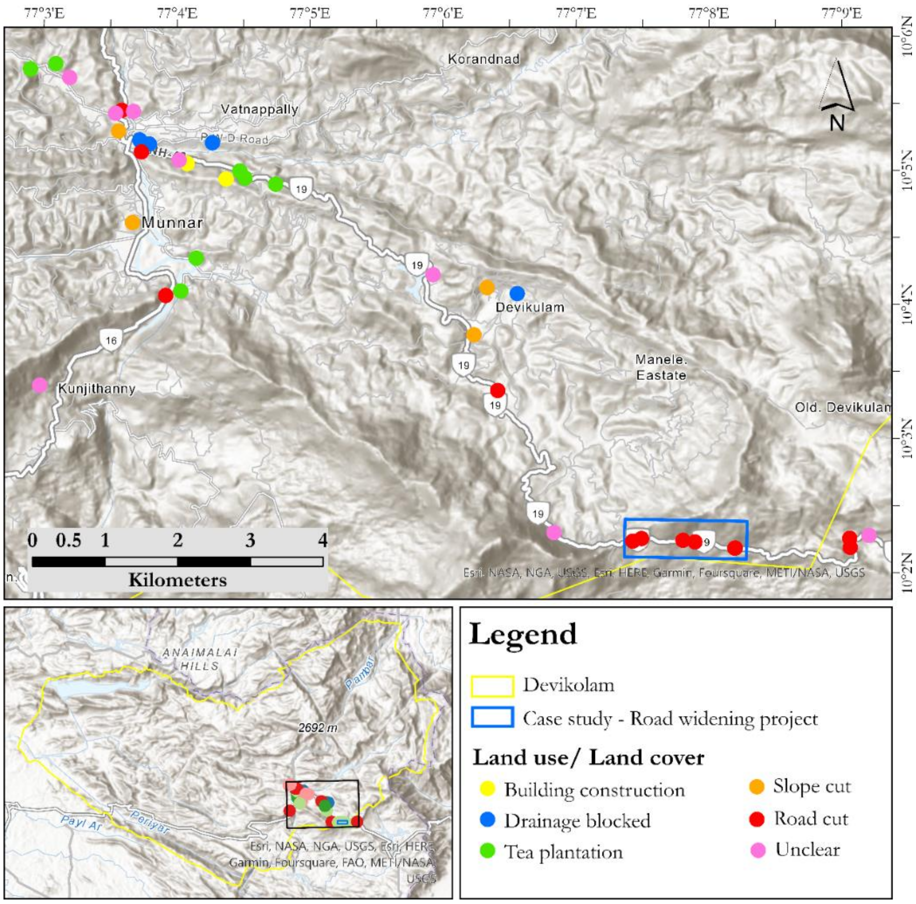

Figure 6.1: Location and LULC of the landslides visited during the fieldwork

The table shows that most (12) of the landslides were caused due to road cuts made along the roads, whereas a number of landslides (8) were either occurred naturally or had unclear LULC change. Because it not possible to determine the LULC change of the landslide even by field observations. It is also possible that LULC change that occurred at the location was washed away by the landslide itself. For example, a landslide at Munnar Arts College was caused due unregulated construction on an old landslide (2005) during the heavy downpour of 2018 monsoon. The landslide swiped away the newly constructed buildings downhill leaving no evidence of LULC change that it caused it. The location was also specifically marked potentially unstable by Sajinkumar et al. (2017), just a year before the occurrence, and the areas was marked high susceptible by all the three maps, however, no attention was paid to any of the available information. Which highlights that landslide susceptibility maps or any other literature are not considered before the construction of buildings in the region.

Landslide nos.	**Land use/ land cover**	**GSI**			**KU&MTU**			**NCESS**		
		Low	Medium	High	Low	Medium	High	Low	Medium	High
2	Building construction		1	1	1	1				2
4	Drainage blocked		3	1	2	1	1	4		
12	Road cut	4	3	**5**	**5**	1	**6**	**8**		4
4	Slope cut	3		1	3	1		4		
7	Tea plantation		**6**	1	3	2	2	4		3
8	Unclear	**5**	1	2	**5**	2	1	**6**	1	1
37	Total	12	14	11	19	8	10	**26**	1	10

Table 6.1: LULC of the landslides and their predictions by the maps

None of the maps predicted highest number of these landslides in the high susceptibility classes. Surprisingly, 26 of the landslides are falling in the "Low" class of the NCESS map, and only 10 in "High".

It would be intuitive to conclude that the landslides were caused due LULC change in the region after the creation of the map, however, question can be raised on whether these maps could capture this detail level of LULC changes to predict them. Since all of these maps used LULC maps at scale of 1:50,000 with general class details. Given that they are difficult to determine even on the field. Whether it would be fair to evaluate these small scale maps based on the LULC changes which are so localized and spatially confined to a few meters of range.

Figure 6.2 shows a rotational landslide on NH-85 Munnar to Bodimettu highway. The space was required for toll plaza construction, so transport authorities cut the slope, which resulted in slope failure; however, this slope consisted of highly weather wet material.

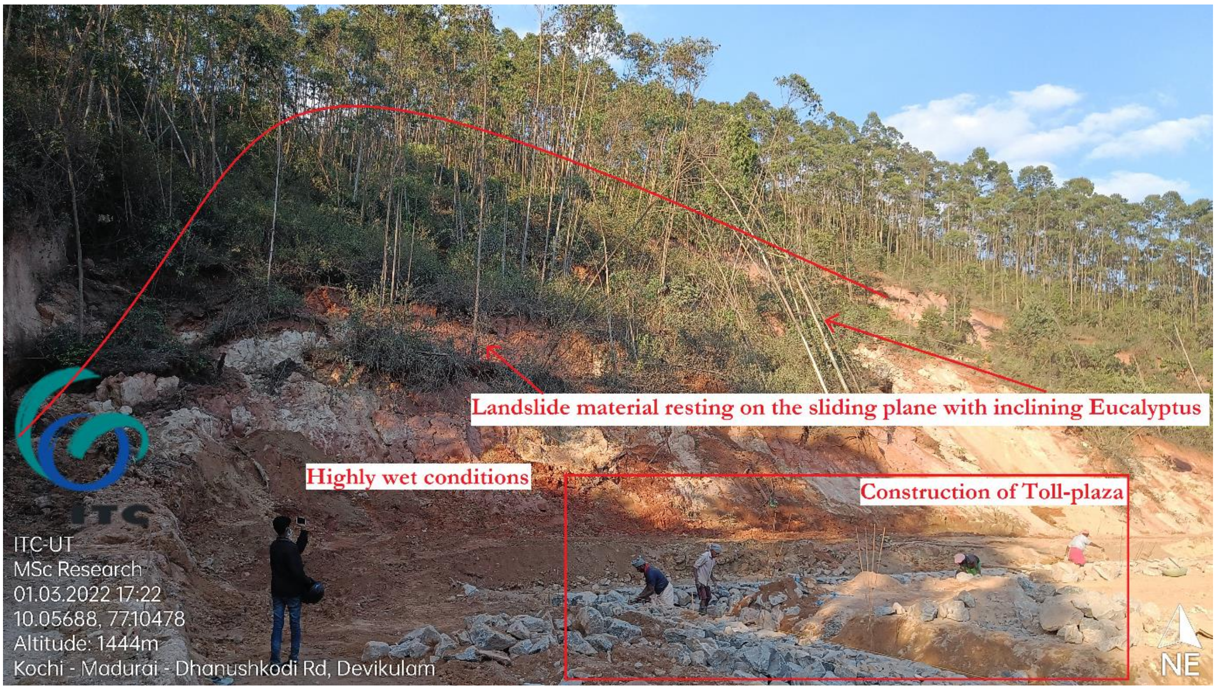

Figure 6.2: A shallow rotational landslide with a construction activity on the landslide toe

6.3. Challenges in establishing a relation between landuse changes and landslide occurrences

The purpose of establishing a relationship between LULC changes and landslide occurrences is to identify the changes that actually modify the susceptibility of a region so that these LULC changes can be incorporated into landuse/cover planning and restrictive zoning, and sustainable land practices. LULC changes can increase or decrease the susceptibility of a mountainous region (Beguería, 2006b; Chen et al., 2019), or some LULC changes may not change the susceptibility at all. However, there are challenges in establishing those relationships, which can be described in two major challenges: 1) Limited Spatio-temporal resolution of the satellite images and LULC maps, and 2) Possible time delay between landuse change and landslide occurrences.

6.3.1. Limited Spatio-temporal resolution of the satellite images and LULC maps

Satellite remote sensing methods are the most common source of LULC information. The key step for acquiring LULC information is image classification (Shrestha et al., 2019). Uniformity in spatial and spectral satellite information is critical for generating comparable LULC information and reducing false changes in the LULC change analysis (Deng et al., 2009; Verburg et al., 2011). *Table 6.2* presents the satellite information used by different authors to establish a relationship of LULC changes and landslide occurrences.

Sr. No.	Author	Years of analysis	LULC maps/images	Spatial resolution/Scale	Study area

1	Glade (2003b)	Multiple years	Historical datasets (written docs, drawings and photos)	Unknown	New Zealand
2	Beguería, (2006b)	1957	B&W Aerial photos	1:32,000	Spain
		1977		1:18,000	
		2002	Colour orthophoto	1 m	
3	Karsli et al. (2008)	1973	Aerial images	1:23,000	Turkey
		2002	Aerial images	1:16,000	
4	Reichenbach et al. (2014)	1954	B&W Aerial photos	1200 dot/in. scan resolution	Italy
		2009	QuickBird	2.4 m, later pan-sharpened with 1 m	
5	Persichillo et al. (2017)	1954	Aerial photos	0.5 m	Italy
		1980	Photo interpretation (TEM1 flight)	1:50,000	
		2000	Photo interpretation (IT2000 flight)	1 m	
		2007	Colour and infrared orthophotos (IT2007)	50 cm	
		2012	**Photo interpretation (AGEA)**	Unknown	
6	Gariano et al. (2018)	1956	**"Land Use Map" by CNR**	1:200,000	Italy
		2000	**CORINE Land Cover**	1:100,000	
7	Chen et al. (2019)	1992	Landsat TM	30 m	China
		2002, 2013	SuperView-1	2 m	
8	Senanayake et al. (2020)	2000	Landsat 7	30 m	Sri Lanka
		2010	Landsat 5		
		2019	Landsat 8		
9	Liu et al. (2021)	1980, 2000, 2018	**LULC maps derived from photo-interpretation of aerial photos and local field data**	Unknown	China
10	Hao et al. (2022)	2010, 2018	Google Earth images	0.30 m -15 m	India

Table 6.2: Geoinformation datasets utilized by different authors to establish a relationship between LULC changes and landslide occurrences

The table displays two types of datasets: raw images for LULC generation and pre-made LULCs (highlighted in bold). All of these studies have considered large time ranges (58 to 8 years) and have varying spatial resolutions, utilizing data from multiple sources due to the obvious data scarcity, which has the potential to cause several issues. First, multi-source LULC maps have different class criteria in terms of class numbers, classification levels (I, II, III, IV) (Anderson, 1976) or different class names for the same class (for example, Gariano et al. (2018)). Sometimes, the LULC classes of a multi-source dataset consist of classes within a distinct class (Hao et al., 2020). In order to detect changes, it is necessary to combine and aggregate these heterogeneous datasets, which may introduce errors such as spatial aggregation, classification, and thematic aggregation errors (Petit and Lambin, 2002; Falcucci et al., 2007). Due to the varying spatial resolution of the images, the details of the derived LULC maps do not match (e.g., Persichillo et al. (2017), Beguería, (2006b)), leading to the detection of false LULC changes. Thirdly, even if the spatial and spectral information is consistent (for example, Senanayake et al. (2020) used the Landsat series), if the resolution is insufficient to generate LULC maps with the desired level of detail, generic outcomes will result. Lastly, high spatial and spectral resolution images are often not freely available and cost significant amounts; therefore, it is not utilized.

Although, when a shorter period is considered for the analysis, 3D Google earth images (0.30 m – 15 m), Sentinel-2A (10 m), and PlanetScopes images (3 m) can be a good alternative in terms of spatial and spectral details, but may not be ideal for long term LULC analysis. Given the benefits, Hao et al. (2022) made a reasonable selection of datasets (Google Earth images) in light of the aforementioned issues. Although, a problem with Google Earth images is that they cannot be used for automatic classification since they can only be used for free on Google Earth Pro software.

In this case, Sentinel-2A and PlanetScope images, which have been available since 2016 and 2017, respectively, can be used; nevertheless, the automatic classification does not provide the desired accuracy and detail (Srivastava et al., 2012) due to the terrain's complexity and the required detailed land use legend, and it has proven extremely challenging to distinguish between natural land use types (for example, forest from the cultivated area)(Hao et al., 2020).

6.3.2. The possible time delay between landuse change and landslide occurrences

Another barrier is the time lag between a landuse change and the occurrence of a landslide. Because this time span can be very long or very short, depending on the prevailing geological conditions, rate of weathering and type or intensity of the landuse change that occurred. Cutting a slope, for example, can make a slope mechanically less stable; similarly, forest logging would alter the soil hydrology of the terrain and would most likely take longer to dismantle than the previous. As a result, landuse changes that have an immediate effect on the terrain would necessitate high temporal LULC information. Landuse changes with a delayed effect, on the other hand, can only be captured over a longer time span. *Figure 6.3* depicts a delayed landuse change effect observed during the field investigation at the Poopada hotel in the Munnar region of the study area. A slope cut was made at this location in the year 1984, and no

Figure 6.3: Poopada hotel landslide as a result of slope cut made in 1984. Left- 3D Google Earth images (2012, 2017, and 2018), Right- Google Earth image (top) and a field photo in the inset

other landuse change was observed during the years 2012 and 2017 (*Figure 6.3*-left), and the landslide occurred in the year 2018, 44 years later. Fortunately, no casualties were recorded in the event; however, it could have demolished the hotel building, possibly resulting in hundreds of deaths.

It can be argued further on the slope's before and after stability conditions when the slope cut was made. Nonetheless, it demonstrates that such delayed effects of landuse changes are difficult to capture. As stated in *Table 6.2*, the authors used varying time spans of LULC changes, and we indicate a possibility of missing out on information on the immediate effects of LULC changes when considering longer time spans (e.g. Gariano et al. (2018)) and for delayed effects when considering shorter time spans (e.g. Hao et al., 2020). It would be of utmost importance to compile a classified inventory of LULC changes in relation to geology based on the potential effective time at which they can trigger a landslide. For instance, immediate effects (2-4 years), road cuts in disintegrated rock sections, delayed effects (5-10 years), or extremely delayed effects (greater than 10 years) (10-20 years).

6.4. Assessment rationale of LULC changes in the study area

As stated at the start of this chapter, the initial goal of the study was to compare the landslide susceptibility map performance with LULC changes. Ideally, LULC change information was required at a detail that it can observe the slope cuts of 2-5 m length which caused the biggest landslides in the study area, which is not possible in Sentinel-2A or PlanetScope image, especially using automatic methods for a large area with complex terrain, as mentioned in section 6.3.1. Yet, targetting for larger LULC changes, we attempted to map LULC for the years 2017 and 2018 using Sentinel-2A images since this was the only year between the creation of the maps and landslide occurrences and availability of the Sentinel-2A data. In short, the mapping was performed using a semi-automatic classification plugin in Qgis using Spectral Angle Mapper (SAM) method, but the classification results were not promising even for those changes which were observed in the field investigation and actually caused landslides.. Therefore, it was not worth moving forward with it. Instead, we decided to select a case study of a road widening project as an example, where we compared the susceptibility of the region to LULC changes and resulting landslides in the next section.

6.5. Road widening project: A case of continuous landuse change

A road widening project by the ministry of road transport and the highway was carried out during the years 2017-2022 under the project "*Rehabilitation and upgradation of NH-85 (Old NH 49)*" with an investment of approx. Five hundred thousand USD (380.70 crore Indian rupees)(Press Information Bureau, 2020).

Over the course of five years, enormous slope cuts were made to increase the width of the road from an average of 2.5 to 5 meters to an upgraded double lane with an average width of 8 to 15 meters. *Figure 6.4* depicts photographs of the NH-85 taken in the field that depict massive landslides and prevailing unstable conditions as a result of slope cuts made in previous years. As an immediate consequence of the LULC change, these slope cuts triggered a rockslide because the area is predominantly composed of highly disintegrated rock with very steep topography. As a result, the immediate collapse of the overhanging rocks was caused by the removal of the slope's underlying support as a result of the cut (Varnes, 1978).

Figure 6.4: Field photos of (A) massive rockslide on NH-85 after the slope cuts made in year 2020, (B) Uncovered disintegrated rock segments, (C) Higly uncosolidated rock debris resting on a solid rock with a drainage opening

Figure 6.5 (left) compares the landslide susceptibility map for the region with landslides occurring between 2018 and 2021. The figure's right side depicts slope cuts (SC) and landslides that occurred during this time frame, along with the month and year of occurrence. These observations were made on Google Earth Pro using the history viewer tool, and the final map was made in ArcGIS Pro 3D because slope cuts and landslides were more visible in 3D. It can be observed that landslides that occurred in 2020 and 2021 occurred at the same location where slope cuts were made in 2018 and 2020. The largest landslide shown in 2021 in *Figure 6.5* corresponds to the field photograph depicted in *Figure 6.4* (A), which was the fourth largest landslide in the entire study area but was triggered by a relatively minor

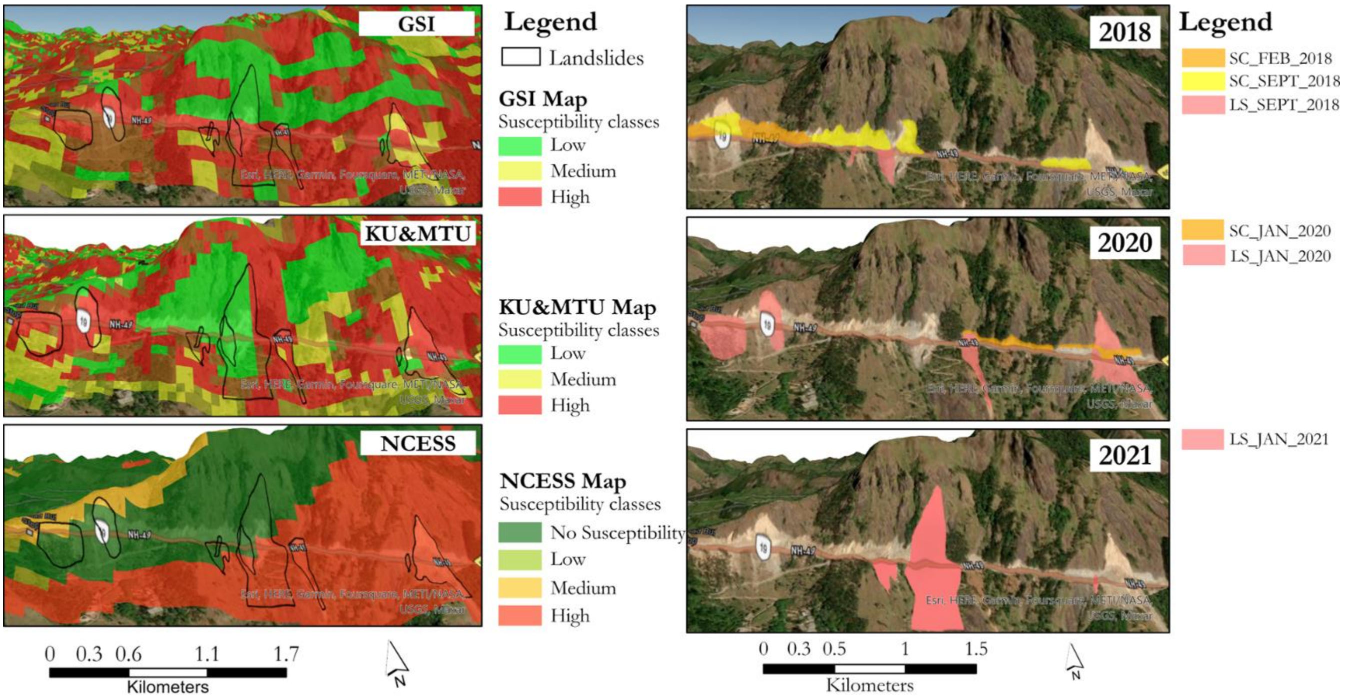

Figure 6.5: Left- Landslide susceptibility map prediction at the case study location, Right- Slope cut (SC) and landslide (LS) triggering maps for multiple years (All maps shown in 3D since slope cuts were not easily observable in 2D maps)

slope change. However, all susceptibility maps predict a low susceptibility class. Before this project began in 2017, Google Earth imagery revealed that the slope conditions were quite stable, as neither a LULC change nor a landslide could be observed. Nevertheless, other landslides belong to the high susceptibility classes, implying that the areas were susceptible, but slope cuts triggered the landslides. Anyway, we cannot conclude that LULC changes can or cannot thwart the predictive ability of the landslide susceptibility map based on this case study, but it is an intuitive example.

6.6. Chapter Summary

The chapter aimed at answering the question,

RQ 4 (a) *"How can landcover changes be mapped specifically influencing the landslide occurrences?*

In the study area, small-sized shallow landslides were observed, which are sparsely distributed. Given the limited spatio-temporal resolution of the datasets and possibility of missing information in the analysis, specifically mapping LULC changes influencing landslide occurrences is a challenging task. Therefore, we propose utilisation of high-resolution images and conduct field investigations wherever possible. We propose that preparing LULC change inventory with possible effective time to trigger landslides can aid the landslide susceptibility mapping, or rather hazard mapping.

RQ 4 (b) *Is it possible to establish a relation between the landcover changes and landslide occurrences? Can this relation influence the predictive performance of the lanslide susceptibility maps?*

We found that establishing a relationship between LULC changes and landslide occurrences itself is a challenging task due to possible time delay between the LULC changes and landslides. It also raises the question of how to assess the accuracy of such a relation, because establishing a statistical relation is not enough, given that landcover changes can indirectly influence the susceptibility of region(Chen et al., 2019). Futhermore, establishing a relation between map's predictive performance with LULC changes is another layer of difficulty.

7. LIMITATIONS, RECOMMENDATIONS AND FINAL CONCLUSIONS

In this chapter, we describe the limitations encountered and potential solutions to counteract the limitations, followed by recommendations based on the study's findings, and ending with the conclusion.

7.1. Limitations and suggestions

This section presents the study's limitations, followed by a potential solution to each limitation.

7.1.1. Landslide inventory generation

Accurate landslide invetory is anyway necessary but especially when testing the accuracy of the landslide susceptibility maps. Otherwise, it hampers the evaluation process and outcomes are of limited use. Basically, *"the proof of the pudding is in the eating",* in this context, it means that you really know if a map performs well if the landslides occur where you predicted them. To ensure high accuracy of the inventory map we utilised deep learning coupled with visual interpretation of high resolution satellite images from Google earth pro.

Lack of training labels has always been a problem for detection methods based on deep learning Since model performance is optimal when a massive dataset is available. However, we attempted to increase the number of training labels through *data augmentation* and *sample generation using a semi-trained model* (not fully optimized). However, data augmentation does not introduce variation in the spectral distribution of the dataset but instead replicates it and presents it to the model differently. Yet, it helps the model to some extent. In addition, the number of landslides was already relatively low, so there was very little room to expand the training sample. However, this was primarily a *needle in a haystack*[19] issue (Lotter et al., 2017; d'Ascoli et al., 2019).

At a later stage of our research, we discovered that our approach of "*sample generation using a semi-trained model*" is actually known as the "*active deep learning*" method in computer sciences (Gal et al., 2017) but implemented in a more extensive and statistically supported manner. The model training begins with a small number of samples, on which the model makes predictions on previously unseen datasets, which are verified by an Oracle (often a human expert). This procedure is repeated, with the training labels increasing over time. These models frequently result in significant reductions in the number of training labels needed to train a deep learning model (and, therefore, cost and time). It also actively maximizes the variation in the dataset's spectral distribution so that the model can generalize well to previously unseen datasets. As a result, we suggest this approach for dealing with the issue of data imbalance as well as low training labels. Consequently, it will also improve the average performance achieved in our research with a best F1 score of 78.51.

Another issue was the spectral mixing of landslides with similar classes, such as urbanized areas and riverine sand. We propose treating landslide detection not as a *binary classification problem*[20]but as a *multi-class classification problem*[21]. It is possible to generate training labels for urban and riverine areas independently. If available, we can use DEM with the same spatial resolution. However, we indicate that utilizing DEM can aid in reducing false positives such as riverine sand, but it will confuse the model to some extent because there are different slope angles within the same landslide polygon, and similar slope angles can be found in built-up areas and barren land with similar spectral signatures; therefore, the use of the DEM is less effective at distinguishing from surrounding areas.

---

[19] In the context of deep learning, *needle in a haystack* is a metaphor for the issue of data imbalance between feature classes, especially when features have similar spectral and spatial characteristics and very few samples are available overall.

[20] *Binary classification problem* involves distinguishing between two classes.

[21] *Multi-class classification problem* involves distinguishing between more than two classes.

7.1.2. Evaluation of landslide susceptibility maps

One significant limitation of the study was that only classified landslide susceptibility maps were available, preventing us from quantitatively evaluating these maps. This problem limited us to only density-based evaluation metrics from an already limited number of evaluation metrics. The continuous map of KU&MTU could not be used for the AUROC metric because the factor of safety (FoS) values are not probability values and must be treated as such. Factor of safety values below 1 indicate unstable pixels, and changing this arbitrarily as done in the AUROC method wouldn't make sense. Continuous statistically-based maps should be used for evaluation using metrics such as AUROC, success, and prediction rate curves when available. At the same time, classified maps play a role in decision-making and are considered a final product; therefore, it is equally logical to evaluate them using the method we presented. As a result, we propose that continuous and discrete landslide susceptibility maps are concurrently assessed and their performance compared. This comparison of quantitative and qualitative evaluation of maps will provide a better understanding of the consistency in susceptibility levels of the classified maps, which will be used in decision-making and planning. AUROC values provide a more objective and quantitative picture of the performance, but map classification significantly affects the map's performance later (Anagnostopoulos et al., 2015). The comparison could also aid in optimizing the classification of susceptibility maps, which is a known issue with a lack of standardization.

Another issue was the optimization of slope units, which were later used to generate Unique Condition Units. Because parameter optimisation is required to generate an optimal set of slope units, it was not possible to generate the best possible dataset due to the high computational and time costs. Despite the manual corrections of the slope units, we acknowledge that this may have also impacted the evaluation process. We used automatic manipulation techniques such as generalisation of slope classes, omission of arbitrary polygons based on polygon area and circularity in the UCU generation process, which may have introduced some inconsistencies in the datasets. Unfortunately, due to the large number of evaluation units, not all errors could not be manually assessed. We propose that the parameters should be optimised for slope unit generation when possible, followed by a geomorphic plausibility check and accuracy assessment of slope unit segmentation using evaluation metrics proposed by Alvioli et al. (2016, 2020).

7.1.3. LULC changes and landslide occurrences

Limited spatio-temporal resolution and the lack of the required level of detail of LULC information prevented us from analysing the impact of LULC changes on the predictive ability of the landslide susceptibility maps. In the context of our study area, the occurrence of small-sized shallow landslides requires detailed localized information on LULC changes. In order to assess such a relation, we suggest that LULC change information should be collected at the landslide location level along with the time of LULC change. Given that high-resolution images of the past cannot always be collected, the spatial and temporal resolution of satellite images will pose a problem. Consequently, community-based surveying can supplement the historical LULC change information. Generation of LULC change inventories based on the best available resolution of past satellite images, in combination with information on landslides and community knowledge can be a path forward.

7.2. Recommendations

Suggestions to handle each limitation were given in the previous section; in this section, we recommend certain aspects to be considered in the future:

1. The map producers should describe in an accompanying document the specific purpose for generating the landslide susceptibility map and the end-user who will use it; should be consulted before generation the final map. The document should also describe the dataset collection, method selection, the scale of analysis, and clear description of the legend classes.
2. Map producers should communicate with end-users to understand their requirements, and when the map is produced; clear communication of the map legend and its practical meaning, how the map can and cannot be used to make decisions, as well as the map's associated uncertainties.

3. The map users should be aware of the uncertainties of the landslide susceptibility maps for the application they are using it for. So that the user can incorporate these uncertainties to design more robust plans for their application.
4. Detection of landslides using automatic methods must always be accompanied by manual assessment and interpretation using high-resolution imagery as a base map. This will prevent false positives from being overlooked in the final inventory of landslides.
5. The method presented in our study to generate Unique condition units (UCUs), can also be used to generate mapping units for landslide susceptibility maps, particularly when causal factors are aggregated (mean, mode, median). Because slope units have varying slope angles within each unit, their potential to trigger landslides varies. Other considerations may include generating UCUs using LULC or a geology class map using the same technique.
6. We evaluated the maps in three distinct scenarios, which revealed that a map might present overall consistent susceptibility levels, but the same may not be true for individually defined units or may not present a strong relationship. Therefore, evaluations should be conducted in various units (susceptibility classes, districts, UCUs) that also indicate the degree to which the map provides reasonable accuracy.
7. A comparative evaluation of maps can enable decision-makers to select one of the available maps. The decision-makers can compare and utilise the consensus information from the two best sources of information. However, this is only the case when multiple maps exist for the same region.
8. LULC change information cannot be retrieved from coarse satellite data; however, other documents available with urban planning departments and community knowledge can assist in the collection of LULC data to some extent.

7.3. Final conclusions

The main goal of the study was to evaluate the predictive power of landslide susceptibility maps posteriorly, despite the fact that only classified susceptibility maps were available. As stated previously, the sole purpose of the study was to assess the utility and reliability of the landslide susceptibility maps for risk management and land-use planning. Accurate information is necessary to develop economically viable mitigation options in countries with limited financial resources. The research attempted to develop a method to assess the predictive capability of classified landslide susceptibility maps by utilising landslide inventory generated within the study. We employed state-of-the-art deep learning models to generate a robust inventory which can be utilised to evaluate the accuracy of the maps.

The research sub-objectives were achieved by first (1) assessing the purpose and utility of the landslide susceptibility maps by reviewing 100 research papers and interviewing map producers and end-users, followed by (2) generating a landslide inventory in the Devikolam area by using MsaU-Net model with an F1- score of 78%, and (3) utilised this inventory to assess the three landslide susceptibility maps with Unique Condition UnitsUCUs for density based evaluation. Lastly, (4) we attempted to assess the relation of the predictive ability of the landslide susceptibility maps with the LULC changes but ended up highlighting the challenges of establishing such a relationship and providing an insight into the complexity of the issue. It presents a method to generate landslide inventory in a region with relatively small-sized landslides using freely available satellite and topographic datasets by means of state-of-the-art deep learning models with an extensive experimental framework. The research provides a framework to assess classified landslide susceptibility maps, which play a role in decision-making, together with a comparative evaluation method that decision-makers can use to select maps for their application. The research highlights the significance of LULC changes at the same time and the challenges faced in deriving relevant LULC information.

We performed a coupled assessment of the usability and reliability of the landslide susceptibility maps to provide a comprehensive understanding of their use by their intended end-users. . The research shows that there is an urgent need for more clarity on the purpose and utility of landslide susceptibility maps, in order to be utilised by the end-users effectively. Unfortunately, much effort is lost in producing maps that are not reliable and that are not considering the needs of the map users. Landslide susceptibility map producers should always revisit the study area after a number of years, and evaluate the reliability of the map, and make an updated version. This should be done on average each five-ten years, or each time after a major landslide-triggering event has occurred.

LIST OF REFERENCES

Abraham, N., Khan, N.M., 2018. A Novel Focal Tversky loss function with improved Attention U-Net for lesion segmentation. arXiv:1810.07842 [cs].

Achu, A., Joseph, S., Aju, C.D., Mathai, J., 2021. Preliminary analysis of a catastrophic landslide event on 6 August 2020 at Pettimudi, Kerala State, India. Landslides. https://doi.org/10.1007/s10346-020-01598-x

Aleotti, P., Chowdhury, R., 1999. Landslide hazard assessment: summary review and new perspectives. Bull Eng Geol Env 58, 21–44. https://doi.org/10.1007/s100640050066

Alvioli, M., Guzzetti, F., Marchesini, I., 2020. Parameter-free delineation of slope units and terrain subdivision of Italy. Geomorphology 358, 107124. https://doi.org/10.1016/j.geomorph.2020.107124

Alvioli, M., Marchesini, I., Reichenbach, P., Rossi, M., Ardizzone, F., Fiorucci, F., Guzzetti, F., 2016. Automatic delineation of geomorphological slope units with <tt>r.slopeunits v1.0</tt> and their optimization for landslide susceptibility modeling. Geoscientific Model Development 9, 3975–3991. https://doi.org/10.5194/gmd-9-3975-2016

Anagnostopoulos, G.G., Fatichi, S., Burlando, P., 2015. An advanced process-based distributed model for the investigation of rainfall-induced landslides: The effect of process representation and boundary conditions. Water Resources Research 51, 7501–7523.

Anderson, J.R., 1976. A land use and land cover classification system for use with remote sensor data. US Government Printing Office.

Baeza, C., Corominas, J., 2001. Assessment of shallow landslide susceptibility by means of multivariate statistical techniques. Earth Surface Processes and Landforms 26, 1251–1263. https://doi.org/10.1002/esp.263

Beguería, S., 2006a. Validation and Evaluation of Predictive Models in Hazard Assessment and Risk Management. Nat Hazards 37, 315–329. https://doi.org/10.1007/s11069-005-5182-6

Beguería, S., 2006b. Changes in land cover and shallow landslide activity: A case study in the Spanish Pyrenees. Geomorphology 74, 196–206. https://doi.org/10.1016/j.geomorph.2005.07.018

Beguería, S., Lorente, A., 2002. Landslide hazard mapping by multivariate statistics: comparison of methods and case study in the Spanish Pyrenees.

Bostjancic, I., Filipovic, M., Gulam, V., Pollak, D., 2021. Regional-Scale Landslide Susceptibility Mapping Using Limited LiDAR-Based Landslide Inventories for Sisak-Moslavina County, Croatia. Sustainability 13, 4543. https://doi.org/10.3390/su13084543

Bottou, L., 2010. Large-Scale Machine Learning with Stochastic Gradient Descent, in: Lechevallier, Y., Saporta, G. (Eds.), Proceedings of COMPSTAT'2010. Physica-Verlag HD, Heidelberg, pp. 177–186. https://doi.org/10.1007/978-3-7908-2604-3_16

Brabb, E.E., 1985. Innovative approaches to landslide hazard and risk mapping, in: International Landslide Symposium Proceedings, Toronto, Canada. pp. 17–22.

Carrara, A., 1988. Drainage and Divide Networks Derived from High-Fidelity Digital Terrain Models, in: Chung, C.F., Fabbri, A.G., Sinding-Larsen, R. (Eds.), Quantitative Analysis of Mineral and Energy Resources, NATO ASI Series. Springer Netherlands, Dordrecht, pp. 581–597. https://doi.org/10.1007/978-94-009-4029-1_34

Carrara, A., Guzzetti, F., Cardinali, M., Paola, R., 1999. Use of GIS Technology in the Prediction and Monitoring of Landslide Hazard. Natural Hazards 20, 117–135. https://doi.org/10.1023/A:1008097111310

Chacó, J., Irigaray, A.C., Ferná Ndez, A.T., Hamdouni, A.R.E., Irigaray, C., Hamdouni, Á.R.E., Hamdouni, R.E., Ferná Ndez, T., 2006. Engineering geology maps: landslides and geographical information systems. Bulletin of Engineering Geology and the Environment 65, 341–411. https://doi.org/10.1007/s10064-006-0064-z

Chen, L., Guo, Z., Yin, K., Shrestha, D.P., Jin, S., 2019. The influence of land use and land cover change on landslide susceptibility: a case study in Zhushan Town, Xuan'en County (Hubei, China). Natural Hazards and Earth System Sciences 19, 2207–2228. https://doi.org/10.5194/nhess-19-2207-2019

Chung, C.-J.F., Fabbri, A.G., 2003. Validation of Spatial Prediction Models for Landslide Hazard Mapping, Natural Hazards.

Corominas, J., van Westen, C., Frattini, P., Cascini, L., Malet, J.-P., Fotopoulou, S., Catani, F., Van Den Eeckhaut, M., Mavrouli, O., Agliardi, F., 2014. Recommendations for the quantitative analysis of landslide risk. Bulletin of engineering geology and the environment 73, 209–263.
d'Ascoli, S., Sagun, L., Biroli, G., Bruna, J., 2019. Finding the needle in the haystack with convolutions: on the benefits of architectural bias. Advances in Neural Information Processing Systems 32.
Deng, J.S., Wang, K., Hong, Y., Qi, J.G., 2009. Spatio-temporal dynamics and evolution of land use change and landscape pattern in response to rapid urbanization. Landscape and Urban Planning 92, 187–198. https://doi.org/10.1016/j.landurbplan.2009.05.001
Dilley, M., Chen, R.S., Deichmann, U., Lerner-Lam, A.L., Arnold, M., 2005. Natural Disaster Hotspots: A Global Risk Analysis. World Bank, Washington, DC. https://doi.org/10.1596/0-8213-5930-4
Escobar-Wolf, R., Sanders, J.D., Vishnu, C.L., Oommen, T., Sajinkumar, K.S., 2021. A GIS tool for infinite slope stability analysis (GIS-TISSA). Geoscience Frontiers 12, 756–768. https://doi.org/10.1016/j.gsf.2020.09.008
Falcucci, A., Maiorano, L., Boitani, L., 2007. Changes in land-use/land-cover patterns in Italy and their implications for biodiversity conservation. Landscape Ecol 22, 617–631. https://doi.org/10.1007/s10980-006-9056-4
Fathi Salmi, E., Nazem, M., Karakus, M., 2017. Numerical analysis of a large landslide induced by coal mining subsidence. Engineering Geology 217, 141–152. https://doi.org/10.1016/j.enggeo.2016.12.021
Fell, R., Corominas, J., Bonnard, C., Cascini, L., Leroi, E., Savage, W.Z., 2008. Guidelines for landslide susceptibility, hazard and risk zoning for land use planning. Engineering Geology 102, 85–98. https://doi.org/10.1016/j.enggeo.2008.03.022
Fleuchaus, P., Blum, P., Wilde, M., Terhorst, B., Butscher, C., 2021. Retrospective evaluation of landslide susceptibility maps and review of validation practice. Environ Earth Sci 80, 485. https://doi.org/10.1007/s12665-021-09770-9
Frattini, P., Crosta, G., Carrara, A., 2010. Techniques for evaluating the performance of landslide susceptibility models. Engineering Geology 111, 62–72. https://doi.org/10.1016/j.enggeo.2009.12.004
Gal, Y., Islam, R., Ghahramani, Z., 2017. Deep bayesian active learning with image data, in: International Conference on Machine Learning. PMLR, pp. 1183–1192.
Galli, M., Ardizzone, F., Cardinali, M., Guzzetti, F., Reichenbach, P., 2008. Comparing landslide inventory maps. Geomorphology, GIS technology and models for assessing landslide hazard and risk 94, 268–289. https://doi.org/10.1016/j.geomorph.2006.09.023
Gariano, S.L., Petrucci, O., Rianna, G., Santini, M., Guzzetti, F., 2018. Impacts of past and future land changes on landslides in southern Italy. Reg Environ Change 18, 437–449. https://doi.org/10.1007/s10113-017-1210-9
Ghorbanzadeh, O., 2021. A comprehensive transferability evaluation of U-Net and ResU-Net for landslide detection from Sentinel-2 data (case study areas from Taiwan, China, and Japan). Scientific Reports 20.
Ghorbanzadeh, O., Blaschke, T., Gholamnia, K., Meena, S.R., Tiede, D., Aryal, J., 2019. Evaluation of Different Machine Learning Methods and Deep-Learning Convolutional Neural Networks for Landslide Detection. Remote Sensing 11, 196. https://doi.org/10.3390/rs11020196
Ghorbanzadeh, O., Crivellari, A., Ghamisi, P., Shahabi, H., Blaschke, T., 2021. A comprehensive transferability evaluation of U-Net and ResU-Net for landslide detection from Sentinel-2 data (case study areas from Taiwan, China, and Japan). Scientific Reports 11, 1–20.
Ghosh, S., van Westen, C.J., Carranza, E.J.M., Jetten, V.G., 2012. Integrating spatial, temporal, and magnitude probabilities for medium-scale landslide risk analysis in Darjeeling Himalayas, India. Landslides 9, 371–384. https://doi.org/10.1007/s10346-011-0304-6
Glade, T., 2003a. Landslide occurrence as a response to land use change: a review of evidence from New Zealand. CATENA, Geomorphic Responses to Land Use Changes 51, 297–314. https://doi.org/10.1016/S0341-8162(02)00170-4
Glade, T., 2003b. Landslide occurrence as a response to land use change: a review of evidence from New Zealand. CATENA, Geomorphic Responses to Land Use Changes 51, 297–314. https://doi.org/10.1016/S0341-8162(02)00170-4

GSI, 2022. Landslide Hazard [WWW Document]. URL https://www.gsi.gov.in/webcenter/portal/OCBIS/pages_pageGeoInfo/pageLANDSLIDEHAZRD (accessed 8.21.22).
Guzzetti, F., Cardinali, M., Reichenbach, P., Carrara, A., 2000. Comparing Landslide Maps: A Case Study in the Upper Tiber River Basin, Central Italy. Environmental management 25.
Guzzetti, F., Carrara, A., Cardinali, M., Reichenbach, P., 1999. Landslide hazard evaluation: A review of current techniques and their application in a multi-scale study, Central Italy, in: Geomorphology. Elsevier, pp. 181–216. https://doi.org/10.1016/S0169-555X(99)00078-1
Guzzetti, F., Mondini, A.C., Cardinali, M., Fiorucci, F., Santangelo, M., Chang, K.-T., 2012. Landslide inventory maps: New tools for an old problem. Earth-Science Reviews 112, 42–66. https://doi.org/10.1016/j.earscirev.2012.02.001
Guzzetti, F., Reichenbach, P., Ardizzone, F., Cardinali, M., Galli, M., 2006. Estimating the quality of landslide susceptibility models. Geomorphology 81, 166–184. https://doi.org/10.1016/j.geomorph.2006.04.007
Guzzetti, F., Reichenbach, P., Cardinali, M., Galli, M., Ardizzone, F., 2005. Probabilistic landslide hazard assessment at the basin scale. Geomorphology 72, 272–299. https://doi.org/10.1016/j.geomorph.2005.06.002
Hammond, C., 1992. Level I stability analysis (LISA) documentation for version 2.0. US Department of Agriculture, Forest Service, Intermountain Research Station.
Hao, L., Rajaneesh A, van Westen, C., Sajinkumar K. S, Martha, T.R., Jaiswal, P., McAdoo, B.G., 2020. Constructing a complete landslide inventory dataset for the 2018 monsoon disaster in Kerala, India, for land use change analysis. Earth System Science Data 12, 2899–2918. https://doi.org/10.5194/essd-12-2899-2020
Hao, L., van Westen, C., Rajaneesh, A., Sajinkumar, K.S., Martha, T.R., Jaiswal, P., 2022. Evaluating the relation between land use changes and the 2018 landslide disaster in Kerala, India. CATENA 216, 106363. https://doi.org/10.1016/j.catena.2022.106363
Hearn, G.J., Hart, A.B., 2019. Landslide susceptibility mapping: a practitioner's view. Bulletin of Engineering Geology and the Environment 78, 5811–5826.
Hovden, I.T., 2019. Optimizing Artificial Neural Network Hyperparameters and Architecture 36.
Huabin, W., Gangjun, L., Weiya, X., Gonghui, W., 2005. GIS-based landslide hazard assessment: an overview. Progress in Physical Geography: Earth and Environment 29, 548–567. https://doi.org/10.1191/0309133305pp462ra
Hürlimann, M., Guo, Z., Puig-Polo, C., Medina, V., 2022. Impacts of future climate and land cover changes on landslide susceptibility: regional scale modelling in the Val d'Aran region (Pyrenees, Spain). Landslides 19, 99–118. https://doi.org/10.1007/s10346-021-01775-6
Hussain, M.A., Chen, Z., Kalsoom, I., Asghar, A., Shoaib, M., 2022. Landslide Susceptibility Mapping Using Machine Learning Algorithm: A Case Study Along Karakoram Highway (KKH), Pakistan. J. Indian Soc. Remote Sens. 50, 849–866. https://doi.org/10.1007/s12524-021-01451-1
Jaiswal, P., van Westen, C.J., 2009. Estimating temporal probability for landslide initiation along transportation routes based on rainfall thresholds. Geomorphology 112, 96–105. https://doi.org/10.1016/j.geomorph.2009.05.008
Jakob, M., 2000. The impacts of logging on landslide activity at Clayoquot Sound, British Columbia. CATENA 38, 279–300. https://doi.org/10.1016/S0341-8162(99)00078-8
Karasiak, N., Dejoux, J.-F., Monteil, C., Sheeren, D., 2022. Spatial dependence between training and test sets: another pitfall of classification accuracy assessment in remote sensing. Mach Learn 111, 2715–2740. https://doi.org/10.1007/s10994-021-05972-1
Karsli, F., Atasoy, M., Yalcin, A., Reis, S., Demir, O., Gokceoglu, C., 2008. Effects of land-use changes on landslides in a landslide-prone area (Ardesen, Rize, NE Turkey). Environ Monit Assess 156, 241. https://doi.org/10.1007/s10661-008-0481-5
Kervrann, C., Boulanger, J., 2008. Local Adaptivity to Variable Smoothness for Exemplar-Based Image Regularization and Representation. Int J Comput Vis 79, 45–69. https://doi.org/10.1007/s11263-007-0096-2
Kjekstad, O., Highland, L., 2009. Economic and Social Impacts of Landslides, in: Sassa, K., Canuti, P. (Eds.), Landslides – Disaster Risk Reduction. Springer, Berlin, Heidelberg, pp. 573–587. https://doi.org/10.1007/978-3-540-69970-5_30

KSDMA, 2016. Hazard Maps – Kerala State Disaster Management Authority. URL https://sdma.kerala.gov.in/hazard-maps/ (accessed 8.22.22).
Kuriakose, S.L., 2019. Rebuild a new Kerala - A disaster risk management perspective. IEEE 11–17.
Kuriakose, S.L., Sankar, G., Muraleedharan, C., 2009. History of landslide susceptibility and a chorology of landslide-prone areas in the Western Ghats of Kerala, India. Environmental geology 57, 1553–1568.
Lacasse, S., Nadim, F., Lacasse, S., Nadim, F., 2009. Landslide Risk Assessment and Mitigation Strategy, in: Sassa, K., Canuti, P. (Eds.), Landslides – Disaster Risk Reduction. Springer, Berlin, Heidelberg, pp. 31–61. https://doi.org/10.1007/978-3-540-69970-5_3
Lei, T., Zhang, Y., Lv, Z., Li, S., Liu, S., Nandi, A.K., 2019. Landslide inventory mapping from bitemporal images using deep convolutional neural networks. IEEE Geoscience and Remote Sensing Letters 16, 982–986.
Liu, J., Wu, Z., Zhang, H., 2021. Analysis of Changes in Landslide Susceptibility according to Land Use over 38 Years in Lixian County, China. Sustainability. https://doi.org/10.3390/su131910858
Liu, T., Abd-Elrahman, A., Morton, J., Wilhelm, V.L., 2018. Comparing fully convolutional networks, random forest, support vector machine, and patch-based deep convolutional neural networks for object-based wetland mapping using images from small unmanned aircraft system. GIScience & remote sensing 55, 243–264.
Long, J., Shelhamer, E., Darrell, T., 2015. Fully convolutional networks for semantic segmentation. pp. 3431–3440. https://doi.org/10.1109/CVPR.2015.7298965
Lotter, W., Sorensen, G., Cox, D., 2017. A multi-scale CNN and curriculum learning strategy for mammogram classification, in: Deep Learning in Medical Image Analysis and Multimodal Learning for Clinical Decision Support. Springer, pp. 169–177.
Lu, P., Qin, Y., Li, Z., Mondini, A.C., Casagli, N., 2019. Landslide mapping from multi-sensor data through improved change detection-based Markov random field. Remote Sensing of Environment 231, 111235. https://doi.org/10.1016/j.rse.2019.111235
Martha, T.R., Kerle, N., Jetten, V., van Westen, C.J., Kumar, K.V., 2010. Characterising spectral, spatial and morphometric properties of landslides for semi-automatic detection using object-oriented methods. Geomorphology 116, 24–36.
McAdoo, B.G., Quak, M., Gnyawali, K., Adhikari, B., Devkota, S., Rajbhandari, P., Sudmeier, K., 2018. Brief communication: Roads and landslides in Nepal: How development affects risk (preprint). Landslides and Debris Flows Hazards. https://doi.org/10.5194/nhess-2017-461
Meena, S.R., Ghorbanzadeh, O., van Westen, C.J., Nachappa, T.G., Blaschke, T., Singh, R.P., Sarkar, R., 2021. Rapid mapping of landslides in the western ghats (India) triggered by 2018 extreme monsoon rainfall using a deep learning approach. Landslides 18, 1937–1950.
Meena, S.R., Soares, L.P., Grohmann, C.H., van Westen, C., Bhuyan, K., Singh, R.P., Floris, M., Catani, F., 2022. Landslide detection in the Himalayas using machine learning algorithms and U-Net. Landslides 19, 1209–1229. https://doi.org/10.1007/s10346-022-01861-3
Mezaal, M.R., Pradhan, B., Sameen, M.I., Mohd Shafri, H.Z., Yusoff, Z.M., 2017. Optimized neural architecture for automatic landslide detection from high-resolution airborne laser scanning data. Applied Sciences 7, 730.
Nava, L., Bhuyan, K., Meena, S., Monserrat, O., Catani, F., 2022. Rapid Mapping of Landslides on SAR Data by Attention U-Net. Remote Sensing 14, 1449. https://doi.org/10.3390/rs14061449
NDRF, 2018. Kerala Floods - 2018 | NDRF - National Disaster Response Force [WWW Document]. URL https://ndrf.gov.in/operations/kerala-floods-2018 (accessed 8.21.22).
Ohlmacher, G.C., 2007. Plan curvature and landslide probability in regions dominated by earth flows and earth slides. ENGINEERING GEOLOGY. https://doi.org/10.1016/j.enggeo.2007.01.005
Oktay, O., Schlemper, J., Folgoc, L.L., Lee, M., Heinrich, M., Misawa, K., Mori, K., McDonagh, S., Hammerla, N.Y., Kainz, B., Glocker, B., Rueckert, D., 2018. Attention U-Net: Learning Where to Look for the Pancreas. arXiv:1804.03999 [cs].
Oxford dictionary, n.d. reliability noun - Definition, pictures, pronunciation and usage notes | Oxford Advanced Learner's Dictionary at OxfordLearnersDictionaries.com [WWW Document]. URL https://www.oxfordlearnersdictionaries.com/definition/english/reliability (accessed 5.24.22).

Ozdemir, A., 2009. Landslide susceptibility mapping of vicinity of Yaka Landslide (Gelendost, Turkey) using conditional probability approach in GIS. Environ. Geol. 57, 1675–1686. https://doi.org/10.1007/s00254-008-1449-z

Pattathal V., A., Sahoo, M.M., Porwal, A., Karnieli, A., 2022. Deep-learning-based latent space encoding for spectral unmixing of geological materials. ISPRS Journal of Photogrammetry and Remote Sensing 183, 307–320. https://doi.org/10.1016/j.isprsjprs.2021.11.008

Peng, D., Zhang, Y., Guan, H., 2019. End-to-end change detection for high resolution satellite images using improved UNet++. Remote Sensing 11, 1382.

Persichillo, M.G., Bordoni, M., Meisina, C., 2017. The role of land use changes in the distribution of shallow landslides. Science of The Total Environment 574, 924–937. https://doi.org/10.1016/j.scitotenv.2016.09.125

Petit, C.C., Lambin, E.F., 2002. Impact of data integration technique on historical land-use/land-cover change: Comparing historical maps with remote sensing data in the Belgian Ardennes. Landscape Ecology 17, 117–132. https://doi.org/10.1023/A:1016599627798

Petschko, H., Brenning, A., Bell, R., Goetz, J., Glade, T., 2014. Assessing the quality of landslide susceptibility maps – case study Lower Austria. Natural Hazards and Earth System Sciences 14, 95–118. https://doi.org/10.5194/nhess-14-95-2014

Pourghasemi, H.R., Gayen, A., Park, S., Lee, C.-W., Lee, S., 2018. Assessment of Landslide-Prone Areas and Their Zonation Using Logistic Regression, LogitBoost, and NaïveBayes Machine-Learning Algorithms. Sustainability 10, 3697. https://doi.org/10.3390/su10103697

Premlet, 2019. Landslides in Kerala 2018. IEEE.

Press Information Bureau, 2020. Development of National Highways in Kerala [WWW Document]. Development of National Highways in Kerala. URL https://pib.gov.in/pib.gov.in/Pressreleaseshare.aspx?PRID=1663983 (accessed 8.15.22).

Promper, C., Gassner, Ch., Glade, T., 2015. Spatiotemporal patterns of landslide exposure – a step within future landslide risk analysis on a regional scale applied in Waidhofen/Ybbs Austria. International Journal of Disaster Risk Reduction 12, 25–33. https://doi.org/10.1016/j.ijdrr.2014.11.003

Rahman, Md.S., Ahmed, B., Di, L., 2017. Landslide initiation and runout susceptibility modeling in the context of hill cutting and rapid urbanization: a combined approach of weights of evidence and spatial multi-criteria. J. Mt. Sci. 14, 1919–1937. https://doi.org/10.1007/s11629-016-4220-z

Reichenbach, P., Mondini, A.C., Rossi, M., 2014. The influence of land use change on landslide susceptibility zonation: the Briga catchment test site (Messina, Italy). Environmental management 54, 1372–1384.

Reichenbach, P., Rossi, M., Malamud, B.D., Mihir, M., Guzzetti, F., 2018. A review of statistically-based landslide susceptibility models. Earth-Science Reviews 180, 60–91.

Remondo, J., González, A., Díaz de Terán, J.R., Cendrero, A., Fabbri, A., Chung, C.J.F., 2003. Validation of landslide susceptibility maps; examples and applications from a case study in northern Spain. Natural Hazards 30, 437–449. https://doi.org/10.1023/B:NHAZ.0000007201.80743.fc

Ronneberger, O., Fischer, P., Brox, T., 2015. U-Net: Convolutional Networks for Biomedical Image Segmentation. arXiv:1505.04597 [cs].

Sajinkumar, K., Oommen, T., 2017. Landslide atlas of Kerala. J Geol Soc India 90, 635–635. https://doi.org/10.1007/s12594-017-0797-2

Sajinkumar, K.S., Anbazhagan, S., Pradeepkumar, A.P., Rani, V.R., 2011. Weathering and landslide occurrences in parts of Western Ghats, Kerala. J Geol Soc India 78, 249. https://doi.org/10.1007/s12594-011-0089-1

Sajinkumar, K.S., Asokakumar, M.R., Sajeev, R., Venkatraman, N.V., 2017. A potential headward retreat landslide site at Munnar, Kerala. J Geol Soc India 89, 183–191. https://doi.org/10.1007/s12594-017-0582-2

Samia, J., Bregt, A., Ardizzone, F., Guzzetti, F., Wallinga, J., Temme, A.J.A.M., Rossi, M., Stuiver, H.J., 2018. Implementing landslide path dependency in landslide susceptibility modelling. Landslides. https://doi.org/10.1007/s10346-018-1024-y

Sanders, J., 2017. Developing a GIS tool for infinite slope stability analysis (GIS-TISSA) (Master of Science in Geology). Michigan Technological University, Houghton, Michigan. https://doi.org/10.37099/mtu.dc.etdr/461

Schmaltz, E.M., Steger, S., Glade, T., 2017. The influence of forest cover on landslide occurrence explored with spatio-temporal information. Geomorphology 290, 250–264. https://doi.org/10.1016/j.geomorph.2017.04.024
Schuster, R.L., Highland, L.M., 2007. Overview of the Effects of Mass Wasting on the Natural Environment. Environmental and Engineering Geoscience 13, 25–44. https://doi.org/10.2113/gseegeosci.13.1.25
Senanayake, S., Pradhan, B., Huete, A., Brennan, J., 2020. Assessing Soil Erosion Hazards Using Land-Use Change and Landslide Frequency Ratio Method: A Case Study of Sabaragamuwa Province, Sri Lanka. Remote Sensing 12, 1483. https://doi.org/10.3390/rs12091483
Shi, W., Zhang, M., Ke, H., Fang, X., Zhan, Z., Chen, S., 2020. Landslide recognition by deep convolutional neural network and change detection. IEEE Transactions on Geoscience and Remote Sensing 59, 4654–4672.
Shorten, C., Khoshgoftaar, T.M., 2019. A survey on Image Data Augmentation for Deep Learning. Journal of Big Data 6, 60. https://doi.org/10.1186/s40537-019-0197-0
Shrestha, D.P., Saepuloh, A., van der Meer, F., 2019. Land cover classification in the tropics, solving the problem of cloud covered areas using topographic parameters. International Journal of Applied Earth Observation and Geoinformation 77, 84–93.
Shu, H., Hürlimann, M., Molowny-Horas, R., González, M., Pinyol, J., Abancó, C., Ma, J., 2019. Relation between land cover and landslide susceptibility in Val d'Aran, Pyrenees (Spain): Historical aspects, present situation and forward prediction. Science of The Total Environment 693, 133557. https://doi.org/10.1016/j.scitotenv.2019.07.363
Soares, L.P., Dias, H.C., Grohmann, C.H., 2020. Landslide segmentation with u-net: Evaluating different sampling methods and patch sizes. arXiv preprint arXiv:2007.06672.
Soeters, R., Westen, C.J., 1996. Slope instability Recognition, analysis and zonation. In: Turner, A.K., Schuster, R.L. (Eds.), Landslide: Investigations and Mitigation. Special Report, vol. 247. Transportation Research Board, National Research Council, National Academy Press, Washington, D.C. 129–17.
Sreekumar, S., 2009. Techniques for slope stability analysis: Site specific studies from Idukki district, Kerala. J Geol Soc India 73, 813–820. https://doi.org/10.1007/s12594-009-0065-1
Srivastava, P.K., Han, D., Rico-Ramirez, M.A., Bray, M., Islam, T., 2012. Selection of classification techniques for land use/land cover change investigation. Advances in Space Research 50, 1250–1265. https://doi.org/10.1016/j.asr.2012.06.032
Steger, S., Brenning, A., Bell, R., Glade, T., 2016. The propagation of inventory-based positional errors into statistical landslide susceptibility models. Natural Hazards and Earth System Sciences 16, 2729–2745. https://doi.org/10.5194/nhess-16-2729-2016
Stumpf, A., Kerle, N., 2011. Object-oriented mapping of landslides using Random Forests. Remote sensing of environment 115, 2564–2577.
UNISDR, 2015. Science is used for disaster risk reduction: UNISDR Science and Technical Advisory Group report 2015.
van Westen, C.J., Castellanos, E., Kuriakose, S.L., 2008. Spatial data for landslide susceptibility, hazard, and vulnerability assessment: An overview. Engineering Geology, Landslide Susceptibility, Hazard and Risk Zoning for Land Use Planning 102, 112–131. https://doi.org/10.1016/j.enggeo.2008.03.010
van Westen, C.J., van Asch, T.W.J., Soeters, R., 2006a. Landslide hazard and risk zonation—why is it still so difficult? Bull Eng Geol Environ 65, 167–184. https://doi.org/10.1007/s10064-005-0023-0
van Westen, C.J., van Asch, T.W.J., Soeters, R., 2006b. Landslide hazard and risk zonation—why is it still so difficult? Bull Eng Geol Environ 65, 167–184. https://doi.org/10.1007/s10064-005-0023-0
Varnes, D.J., 1984. Landslide hazard zonation: a review of principles and practice. Natural Hazards.
Varnes, D.J., 1978. Slope movement types and processes. Special report 176, 11–33.
Verburg, P.H., Neumann, K., Nol, L., 2011. Challenges in using land use and land cover data for global change studies. Global Change Biology 17, 974–989. https://doi.org/10.1111/j.1365-2486.2010.02307.x
Wadhawan, S.K., Singh, B., Ramesh, M.V., 2020. Causative factors of landslides 2019: case study in Malappuram and Wayanad districts of Kerala, India. Landslides 17, 2689–2697. https://doi.org/10.1007/s10346-020-01520-5

Winter, M.G., Shearer, B., Palmer, D., Peeling, D., Peeling, J., Harmer, C., Sharpe, J., 2018. Assessment of the economic impacts of landslides and other climate-driven events.
Zebin, T., Scully, P.J., Peek, N., Casson, A.J., Ozanyan, K.B., 2019. Design and Implementation of a Convolutional Neural Network on an Edge Computing Smartphone for Human Activity Recognition. IEEE Access 7, 133509–133520. https://doi.org/10.1109/ACCESS.2019.2941836
Zotero, 2016.

APPENDIX

Annexure-1 - List of article used to for literature analysis.

Sr. No.	Authors	Title of the paper
1	Dai et al. (2001)	Assessment of landslide susceptibility on the natural terrain of Lantau Island, Hong Kong
2	Ercanoglu et al. (2002)	Assessment of landslide susceptibility for a landslide-prone area (north of Yenice, NW Turkey) by fuzzy approach
3	Santacana et al. (2003)	A GIS-based multivariate statistical analysis for shallow landslide susceptibility mapping in La Pobla de Lillet area (Eastern Pyrenees, Spain)
4	Lee et al. (2004)	Application of likelihood ratio and logistic regression models to landslide susceptibility mapping using GIS
5	Sarkar et al. (2004)	An integrated approach for landslide susceptibility mapping using remote sensing and GIS
6	Ercanoglu et al. (2004)	Landslide susceptibility zoning north of Yenice (NW Turkey) by multivariate statistical techniques
7	Tangestani et al. (2004)	Landslide susceptibility mapping using the fuzzy gamma approach in a GIS, Kakan catchment area, southwest Iran
8	Lee et al. (2005)	Application of logistic regression model and its validation for landslide susceptibility mapping using GIS and remote sensing data
9	Ayalew et al. (2005)	The application of GIS-based logistic regression for landslide susceptibility mapping in the Kakuda-Yahiko Mountains, Central Japan
10	Fall et al. (2006)	A multi-method approach to study the stability of natural slopes and landslide susceptibility mapping
11	Zhu et al. (2006)	GIS-based logistic regression method for landslide susceptibility mapping in regional scale
12	Yalcin et al. (2008)	GIS-based landslide susceptibility mapping using analytical hierarchy process and bivariate statistics in Ardesen (Turkey): comparisons of results and confirmations
13	Dahal et al. (2008)	GIS-based weights-of-evidence modelling of rainfall-induced landslides in small catchments for landslide susceptibility mapping
14	Yao et al. (2008)	Landslide susceptibility mapping based on support vector machine: a case study on natural slopes of Hong Kong, China
15	He et al. (2008)	GIS-based regional landslide susceptibility mapping: a case study in southern California
16	Frattini et al. (2008)	Assessment of rockfall susceptibility by integrating statistical and physically-based approaches
17	Yilmaz et al. (2009)	GIS based statistical and physical approaches to landslide susceptibility mapping (Sebinkarahisar, Turkey)
18	Oh et al. (2009)	Predictive landslide susceptibility mapping using spatial information in the Pechabun area of Thailand
19	Ozdemir et al. (2009)	Landslide susceptibility mapping of vicinity of Yaka Landslide (Gelendost, Turkey) using conditional probability approach in GIS
20	Pradhan et al. (2010)	Weights-of-evidence model applied to landslide susceptibility mapping in a tropical hilly area
21	Mancini et al. (2010)	GIS and statistical analysis for landslide susceptibility mapping in the Daunia area, Italy
22	Ray et al. (2010)	Landslide susceptibility mapping using downscaled AMSR-E soil moisture: A case study from Cleveland Corral, California, US
23	Chauhan et al. (2010)	Landslide Susceptibility Zonation through ratings derived from Artificial Neural Network
24	Pradhan et al. (2010)	Landslide Susceptibility Mapping by Neuro-Fuzzy Approach in a Landslide-Prone Area (Cameron Highlands, Malaysia)
25	Choi et al. (2011)	Landslide Susceptibility Mapping by Using an Adaptive Neuro-Fuzzy Inference System (anfis)

26	Ozdemir et al. (2011)	Landslide susceptibility mapping using Bayesian approach in the Sultan Mountains (AkAYehir, Turkey)
27	Oh et al. (2011)	Landslide susceptibility mapping on Panaon Island, Philippines using a geographic information system
28	Sujatha et al. (2011)	Landslide susceptibility mapping of Tevankarai Ar sub-watershed, Kodaikkanal taluk, India, using weighted similar choice fuzzy model
29	Armaş et al. (2012)	Weights of evidence method for landslide susceptibility mapping. Prahova Subcarpathians, Romania
30	Yilmaz et al. (2012)	GIS-based landslide susceptibility mapping using bivariate statistical analysis in Devrek (Zonguldak-Turkey)
31	Li et al. (2012)	Application and verification of fractal approach to landslide susceptibility mapping
32	Pourghasemi et al. (2012)	Landslide susceptibility mapping using index of entropy and conditional probability models in GIS: Safarood Basin, Iran
33	Kayastha et al. (2012)	Application of fuzzy logic approach for landslide susceptibility mapping in Garuwa sub-basin, East Nepal
34	Sujatha et al. (2012)	Landslide susceptibility analysis using Probabilistic Certainty Factor Approach: A case study on Tevankarai stream watershed, India
35	Kayastha et al. (2013)	Application of the analytical hierarchy process (AHP) for landslide susceptibility mapping: A case study from the Tinau watershed, west Nepal
36	Pourghasemi et al. (2013)	Landslide susceptibility mapping by binary logistic regression, analytical hierarchy process, and statistical index models and assessment of their performances
37	Solaimani et al. (2013)	Landslide susceptibility mapping based on frequency ratio and logistic regression models
38	Wang et al. (2013)	Landslide susceptibility analysis with logistic regression model based on FCM sampling strategy
39	Legorreta Paulin et al. (2013)	Landslide inventory mapping and landslide susceptibility modeling assessment on the SW flank of Pico de Orizaba volcano, Puebla-Veracruz, Mexico
40	Setayeshirad et al. (2013)	Landslide susceptibility assessment along the southern coast of the Caspian Sea, Iran
41	Trigila et al. (2013)	Landslide susceptibility mapping at national scale: the Italian case study
42	Chen et al. (2014)	Landslide susceptibility mapping based on GIS and information value model for the Chencang District of Baoji, China
43	Kavzoglu et al. (2014)	Landslide susceptibility mapping using GIS-based multi-criteria decision analysis, support vector machines, and logistic regression
44	Kim et al. (2014)	Landslide susceptibility mapping using a grid-based infiltration transient model in mountainous regions
45	Ding et al. (2014)	Susceptibility mapping of landslides in Beichuan County using cluster and MLC methods
46	Regmi et al. (2014)	Application of frequency ratio, statistical index, and weights-of-evidence models and their comparison in landslide susceptibility mapping in Central Nepal Himalaya
47	Kavzoglu et al. (2015)	An assessment of multivariate and bivariate approaches in landslide susceptibility mapping: a case study of Duzkoy district
48	Shahabi et al. (2015)	Landslide susceptibility mapping using GIS-based statistical models and Remote sensing data in tropical environment
49	Teixeira et al. (2015)	Physically based shallow translational landslide susceptibility analysis in Tibo catchment, NW of Portugal
50	Posner et al. (2015)	Normalized landslide index method for susceptibility map development in El Salvador
51	Youssef et al. (2015)	Landslide susceptibility mapping using ensemble bivariate and multivariate statistical models in Fayfa area, Saudi Arabia
52	Demir et al. (2015)	Landslide susceptibility mapping by frequency ratio and logistic regression methods: an example from Niksar-Resadiye (Tokat, Turkey)
53	Wang et al. (2015)	GIS-based assessment of landslide susceptibility using certainty factor and index of entropy models for the Qianyang County of Baoji city, China

54	Ahmed et al. (2015)	Landslide susceptibility mapping using multi-criteria evaluation techniques in Chittagong Metropolitan Area, Bangladesh
55	Braun et al. (2015)	Landslide Susceptibility Mapping with Data Mining Methods-a Case Study from Maily-Say, Kyrgyzstan
56	Myronidis et al. (2016)	Landslide susceptibility mapping based on landslide history and analytic hierarchy process (AHP)
57	Bronowski et al. (2016)	Landslide susceptibility mapping in the Beskid Niski Mts., Western Carpathians (Dukla commune, Poland)
58	Tsangaratos et al. (2016)	Landslide susceptibility mapping using a modified decision tree classifier in the Xanthi Perfection, Greece
59	Basharat et al. (2016)	Landslide susceptibility mapping using GIS and weighted overlay method: a case study from NW Himalayas, Pakistan
60	Wang et al. (2016)	Landslide susceptibility mapping at Gongliu county, China using artificial neural network and weight of evidence models
61	Basofi et al. (2016)	Landslides Susceptibility Mapping Using Fuzzy Logic: A Case Study in Ponorogo, East Java, Indonesia
62	Leonardi et al. (2016)	Landslide Susceptibility Mapping Using a Fuzzy Approach
63	Akgun et al. (2016)	Landslide susceptibility mapping by geographical information system-based multivariate statistical and deterministic models: In an artificial reservoir area at Northern Turkey
64	Kouhpeima et al. (2017)	Landslide susceptibility mapping using logistic regression analysis in Latyan catchment
65	Kanwal et al. (2017)	GIS based landslide susceptibility mapping of northern areas of Pakistan, a case study of Shigar and Shyok Basins
66	Huang et al. (2017)	Landslide susceptibility mapping based on self-organizing-map network and extreme learning machine
67	Lin et al. (2017)	Landslide susceptibility mapping on a global scale using the method of logistic regression
68	Dhianaufal et al. (2018)	Fuzzy Logic Method for Landslide Susceptibility Mapping in Volcanic Sediment Area in Western Bogor
69	Adineh et al. (2018)	Landslide susceptibility mapping using Genetic Algorithm for the Rule Set Production (GARP) model
70	Mokarram et al. (2018)	Landslide Susceptibility Mapping Using Fuzzy-AHP
71	Long et al. (2018)	Analysis and mapping of rainfall-induced landslide susceptibility in a Luoi District, Thua Thien Hue Province, Vietnam
72	Chen et al. (2018)	Landslide spatial susceptibility mapping by using deep belief network
73	Awawdeh et al. (2018)	Landslide susceptibility mapping using GIS and weighted overlay method: a case study from North Jordan
74	Yang et al. (2019)	Local-scale landslide susceptibility mapping using the B-GeoSVC model
75	Kaafarani et al. (2019)	Landslide susceptibility mapping based on triggering factors using a multi-modal approach
76	Park et al. (2019)	Landslide Susceptibility Mapping Based on Random Forest and Boosted Regression Tree Models, and a Comparison of Their Performance
77	Anis et al. (2019)	GIS-based landslide susceptibility mapping using bivariate statistical methods in North-western Tunisia
78	Chawla et al. (2019)	Landslide Susceptibility Zonation Mapping: A Case Study from Darjeeling District, Eastern Himalayas, India
79	Boualla et al. (2019)	GIS-based landslide susceptibility mapping in the Safi region, West Morocco
80	Park et al. (2019)	Assessment of rainfall-induced landslide susceptibility at the regional scale using a physically based model and fuzzy-based Monte Carlo simulation
81	Ciurleo et al. (2019)	Landslide susceptibility assessment by TRIGRS in a frequently affected shallow instability area
82	Palacio Cordoba et al. (2020)	Probabilistic landslide susceptibility analysis in tropical mountainous terrain using the physically based r. slope. stability model

83	Marin et al. (2020)	Physically-based landslide susceptibility analysis using Monte Carlo simulation in a tropical mountain basin
84	Zhou et al. (2020)	Nationwide susceptibility mapping of landslides in Kenya using the fuzzy analytic hierarchy process model
85	Wang et al. (2020)	Spatial prediction of landslide susceptibility based on GIS and discriminant functions
86	Wubalem et al. (2020)	Landslide susceptibility mapping using information value and logistic regression models in Goncha Siso Eneses area, northwestern Ethiopia
87	Pasang et al. (2020)	Landslide Susceptibility Mapping Using Statistical Methods along the Asian Highway, Bhutan
88	Medina et al. (2021)	Fast physically-based model for rainfall-induced landslide susceptibility assessment at regional scale
89	Arabameri et al. (2021)	Decision tree based ensemble machine learning approaches for landslide susceptibility mapping
90	Wubalem et al. (2021)	Landslide susceptibility mapping using statistical methods in Uatzau catchment area, northwestern Ethiopia
91	Qi et al. (2021)	AI-Based Susceptibility Analysis of Shallow Landslides Induced by Heavy Rainfall in Tianshui, China
92	Le et al. (2021)	Developing a Landslide Susceptibility Map Using the Analytic Hierarchical Process in Ta Van and Hau Thao Communes, Sapa, Vietnam
93	Harmouzi et al. (2021)	Landslide Susceptibility Mapping in the Vrancea-Buzau Seismic Region, Southeast Romania
94	Bostjancic et al. (2021)	Regional-Scale Landslide Susceptibility Mapping Using Limited LiDAR-Based Landslide Inventories for Sisak-Moslavina County, Croatia
95	Grozavu et al. (2021)	Mapping landslide susceptibility at national scale by spatial multi-criteria evaluation
96	Miao et al. (2022)	Integrating Data Modality and Statistical Learning Methods for Earthquake-Induced Landslide Susceptibility Mapping
97	Hussain et al. (2022)	Landslide Susceptibility Mapping using Machine Learning Algorithm
98	Hussain et al. (2022)	Landslide Susceptibility Mapping Using Machine Learning Algorithm Validated by Persistent Scatterer In-SAR Technique
99	Hussain et al. (2022)	Landslide Susceptibility Mapping Using Machine Learning Algorithm: A Case Study Along Karakoram Highway (KKH), Pakistan
100	Sincic et al. (2022)	Landslide susceptibility assessment of the City or Karlovac using the bivariate statistical analysis

Annexure-2 – Questionnaire and consent form for interview with end-user and producers.

End-users perspective on landslide susceptibility maps
1. Do you use landslide susceptibility maps? If yes, for which decisions you have to make in your work, it is essential to know which areas are dangerous due to landslides.
2. Do you consider three susceptibility classes enough? If yes, how do you decide in areas with medium landslide susceptibility zones? If not, what do you suggest otherwise, and why?
a. Safe (Low): no problems with landslides are expected
b. Dangerous (High): Problems expected
c. Intermediate (Medium): Maybe landslides are expected
3. How do you deal with the situation when landslides occur in areas where nothing is predicted?
4. How does a large area in a high susceptibility zone affect planning and governance?
5. What are the rule-of-thumb decisions taken in specific situations? For eg. Banning all types of construction within 50 meters from channels.
6. What information do you require regarding landslide prediction, e.g. when/where a landslide will occur? What is more important info- **When** or **Where**?

7. How does the map having only initiation information limit its applicability?
8. Should runout and initiation information both be in the hazard map?
9. What is the mapping unit of the map required for the governance/implementation? (Showing three different maps)
10. Generally, maps have grid cells as mapping units; how do you make a decision on that?
11. How do you communicate your idea/information to someone who will implement that at another level of governance?

Map producers on landslide susceptibility maps
1. Could you please give a short description of how the map was made?
2. What were input data used for the analysis and related uncertainties?
3. How was the map classified into different classes, and why were those threshold values?
4. What could one expect in these classes in terms of landslide numbers or damage etc.?
5. Did you consider the rainfall distribution while generating the map?
6. What was the purpose of the generation of this landslide susceptibility map for, e.g., information, statutory, engineering etc.?
7. Who is intended to use this map, and how can they use it?
8. Did you discuss with the end-users for their requirements (required information, use, detailing) with respect to the output map? If yes, what was required?
9. What were the biggest problems faced when generating the map?

Consent Form

Topic Tittle: Analysing the posterior predictive capability of landslide susceptibility maps

Researcher:
Tanuj Pareek
MSc student
Faculty of Geo-Information Science and Earth Observation
Natural hazards and disaster risk reduction
University of Twente

I am currently working on my Master's Thesis, which will examine the predictive capability of Landslide Susceptibility Maps (LSMaps). A component of the research is an examination of the usability of the LSMaps, in which we investigate map producers' perspectives on the purpose and applicability of the LSMaps. It seeks to comprehend the specific applications for which these maps are created, as well as the intended user of the maps. On the other hand, we investigate map users' perspectives on map usability for the purpose they require. The importance of this investigation is to better understand the needs of end users and the purposes for which they require them. The type and level of detail required for the various applications for which these maps are used.

Only a few studies have looked into the usability and end-user requirements of these maps. It would be more important to gain clarity on what exactly is required from these maps for their application on the ground, as well as identify areas where these maps fall short.

Satement of Consent :
I have read and understood the study information dated [28/02/2022], or it has been read to me. I understand that information I provide will be used for research. I understand that personal information collected about me that can identify me, such as [e.g. my name or where I live], will not be shared beyond the study team. The researcher ensures the privacy of the participants and protects any collected personal data. The researcher will follow General Data Protection Regulation (GDPR)(https://gdpr.eu/) from European Union (2019) and the Netherlands Code from Netherlands Enterprise Agency, RVO, (2021)
I consent to participate in the study.

Tick yes if you agree
Yes No

Annexure-3 –Sample test results of MsaU-Net model

Learning Rate	Batch Size	Filters	Gamma	Accuracy	Precision	Recall	F1-Score
0.001	8	32	0.8	0.9500	0.7598	0.7946	0.7760
0.001	8	32	0.85	0.9478	0.7505	0.7992	0.7730
0.001	8	32	0.9	0.9478	0.7689	0.7572	0.7622
0.001	8	16	0.8	0.9498	0.7693	0.7862	0.7766
0.001	8	16	0.85	0.9514	0.7801	0.7839	0.7807
0.001	8	16	0.9	0.9500	0.7595	0.8110	0.7836
0.001	8	8	0.8	0.9459	0.7534	0.7767	0.7631
0.001	8	8	0.85	0.9456	0.7358	0.8132	0.7711
0.001	8	8	0.9	0.9486	0.7797	0.7683	0.7731
0.001	16	32	0.8	0.9511	0.7810	0.7922	0.7851
0.001	16	32	0.85	0.9484	0.7504	0.8074	0.7769
0.001	16	32	0.9	0.9498	0.7693	0.7862	0.7766
0.001	16	16	0.8	0.9491	0.7750	0.7722	0.7728
0.001	16	16	0.85	0.9478	0.7546	0.7907	0.7707

Annexure-4 –Relative landslide density index (R-Index)

Overall Landslide Density Index using landslide points (P) & landslide polygon area (A)

GSI

No.	Susceptibility class	Landslides		Susceptibility class area (Km^2)	Ni	ni (P)	ni (A)	ni/Ni (P)	R-index (P)	ni/Ni (A)	R-index (A)
		Points	Area (Km^2)								
1	Low	180	0.41	766.52	43.48	20.83	23.86	0.48	13.68	0.55	14.96
2	Medium	418	0.68	693.72	39.35	48.38	40.06	1.23	35.11	1.02	27.76
3	High	266	0.61	302.75	17.17	30.79	36.08	1.79	51.20	2.10	57.28
	Total	864	1.70	1762.99			∑ ni/Ni (P)	3.50	∑ ni/Ni (A)	3.67	

***Ni**: % of susceptibility class area* ***ni**: % of landslides in the susceptibility class*

KU&MTU

No.	Susceptibility class	Landslides		Susceptibility class area (Km^2)	Ni	ni (P)	ni (A)	ni/Ni (P)	R-index (P)	ni/Ni (A)	R-index (A)
		Points	Area (Km^2)								
1	Low	264	0.54	835.24	47.36	30.56	31.92	0.65	15.81	0.67	16.73
2	Medium	278	0.49	397.43	22.53	32.18	29.00	1.43	34.98	1.29	31.96
3	High	307	0.65	338.77	19.21	35.53	38.28	1.85	45.31	1.99	49.48
4	No susceptibility	15	0.01	192.24	10.90	1.74	0.80	0.16	3.90	0.07	1.83
	Total	864	1.70	1763.68			∑ ni/Ni (P)	4.08	∑ ni/Ni (A)	4.03	

NCESS

No.		Landslides		Ni	ni (P)	ni (A)				

	Susceptibility class	Points	Area (Km^2)	Susceptibility class area (Km^2)				ni/Ni (P)	R-index (P)	ni/Ni (A)	R-index (A)
1	Low	0	0.00	11.31	0.64	0.00	0.00	0.00	0.00	0.00	0.00
2	Medium	157	0.36	391.94	22.08	18.17	21.06	0.82	23.64	0.95	22.26
3	High	189	0.56	224.36	12.64	21.88	33.14	1.73	49.72	2.62	61.20
4	No susceptibility	518	0.78	1147.46	64.64	59.95	45.80	0.93	26.64	0.71	16.54
	Total	864	1.70	1775.08			∑ ni/Ni (P)	3.48	∑ ni/Ni (A)	4.28	